

## INFORMATION TO USERS

This manuscript has been reproduced from the microfilm master. UMI films the text directly from the original or copy submitted. Thus, some thesis and dissertation copies are in typewriter face, while others may be from any type of computer printer.

**The quality of this reproduction is dependent upon the quality of the copy submitted.** Broken or indistinct print, colored or poor quality illustrations and photographs, print bleedthrough, substandard margins, and improper alignment can adversely affect reproduction.

In the unlikely event that the author did not send UMI a complete manuscript and there are missing pages, these will be noted. Also, if unauthorized copyright material had to be removed, a note will indicate the deletion.

Oversize materials (e.g., maps, drawings, charts) are reproduced by sectioning the original, beginning at the upper left-hand corner and continuing from left to right in equal sections with small overlaps. Each original is also photographed in one exposure and is included in reduced form at the back of the book.

Photographs included in the original manuscript have been reproduced xerographically in this copy. Higher quality 6" x 9" black and white photographic prints are available for any photographs or illustrations appearing in this copy for an additional charge. Contact UMI directly to order.

# UMI

A Bell & Howell Information Company  
300 North Zeeb Road, Ann Arbor MI 48106-1346 USA  
313/761-4700 800/521-0600



QUASI-OPTICAL TRANSMIT/RECEIVE LENS  
AMPLIFIER ARRAYS

by

STEIN HOLLUNG

M.S., University of Colorado, 1995

B.S., University of Colorado, 1994

Electrical Engineer, Oslo College of Engineering, 1992

A thesis submitted to the  
Faculty of the Graduate School of the  
University of Colorado in partial fulfillment  
of the requirements for the degree of  
Doctor of Philosophy  
Department of Electrical and Computer Engineering

1998

**UMI Number: 9827725**

---

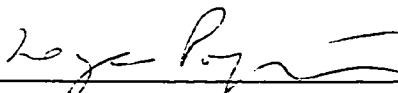
**UMI Microform 9827725**  
**Copyright 1998, by UMI Company. All rights reserved.**

**This microform edition is protected against unauthorized  
copying under Title 17, United States Code.**

---

**UMI**  
**300 North Zeeb Road**  
**Ann Arbor, MI 48103**

This thesis entitled:  
Quasi-Optical Transmit/Receive Lens Amplifier Arrays  
written by Stein Hollung  
has been approved for the Department of  
Electrical and Computer Engineering

  
\_\_\_\_\_  
Zoya B. Popović

  
\_\_\_\_\_  
Edward F. Kuester

Date 04/14/98

The final copy of this thesis has been examined by the  
signators, and we find that both the content and the form  
meet acceptable presentation standards of scholarly work in  
the above mentioned discipline.

Hollung, Stein (Ph.D., Electrical Engineering)

Quasi-Optical Transmit/Receive Lens Amplifier Arrays

Thesis directed by Associate Professor Zoya B. Popović

Quasi-optical power combiners offer an attractive means for realizing millimeter-wave front-ends for communication and radar systems. In this approach, potentially hundreds of solid-state devices are directly integrated into a radiating structure that functions as a power combiner, circuit element and antenna. These circuits can be fabricated monolithically in a compact module that offers broadband, reliable performance.

The emphasis of this research is to design and demonstrate quasi-optical lens amplifier arrays for both transmit and receive operation. Both microwave and millimeter-wave transmit/receive lens amplifier arrays are demonstrated. These front-ends are used to demonstrate several applications: a quasi-optical transceiver front-end; a quasi-optical AM receiver; multipath fading null reduction; a multi-user with frequency reuse FSK data link; and an angle diversity receiver. The feed losses of quasi-optical lens arrays are investigated in order to maximize the effective radiated power from these arrays. Several passive lens arrays are fabricated and tested to verify the theory. In large phased-arrays, it is found that a quasi-optical feed network can be less lossy and complex than a conventional feed network. Several other quasi-optical components for a new kind of transceiver architecture are also presented: a BPSK modulator; a linear-to-circular polarization converter; and an isolator. These components consist of several cascaded active and passive grids.

## DEDICATION

To Sandra, My Family and Friends.

If the day and the night are such that you greet them with joy, and life emits a fragrance like flowers and sweet-scented herbs, is more elastic, more starry, more immortal, —that is your success.

—H. D. Thoreau, *Walden*, 1854.

## ACKNOWLEDGMENTS

Most of all, I would like to thank my thesis advisor, Professor Zoya Popović, for her invaluable support, encouragement and guidance during my studies. From the moment I walked into her office looking for an advisor, she has always made me feel welcome and met my ideas and questions with an open mind.

I would also like to thank the past and present members of the Quasi-Optics Group for their friendship and support. It was a great experience to continue and build upon the work by Scott Bundy, Tom Mader, Jon Schoenberg, Wayne Shiroma, Jon Dixon and Milica Marković. Wayne Shiroma showed a tireless effort in explaining and clarifying my many questions during the first time in the group. The present group members: Eric Bryerton, Joe Tustin, Todd Marshall, Michael Forman, Jim Vian, Amanda Cox, Menoja Weiss, Shawn Stone and Slavko Djukić have all made the group a great place to work. Joe Tustin provided many days effort assisting and guiding me in the photolithography fabrication of the millimeter-wave array. Jim Vian and Amanda Cox both provided invaluable help and insight in the microwave array experiments. I would also like to thank Jason Lee for fabrication and testing of the passive lenses and Michael Forman for the pattern simulations of the millimeter-wave array.

Finally, I would like to thank our administrative assistant Helen Frey, who often went out of her way to make sure my circuit components would be there on time, and that our day-to-day operations ran smoothly.



## CONTENTS

### CHAPTER

1	INTRODUCTION AND BACKGROUND . . . . .	1
1.1	Requirements for Quasi-Optics in Wireless Communications . .	1
1.2	Quasi-Optical Transceiver Components . . . . .	5
1.2.1	Quasi-Optical Sources . . . . .	6
1.2.2	Quasi-Optical Transmit or Receive Amplifiers . . . . .	7
1.2.3	Other Quasi-Optical Components . . . . .	9
1.3	Organization of the Thesis . . . . .	9
2	DESIGN AND ANALYSIS OF LENS AMPLIFIER ARRAYS . . . . .	11
2.1	Feed Efficiency of Array Antennas . . . . .	11
2.1.1	Simulated Feed Loss . . . . .	15
2.1.2	Measured Feed Loss . . . . .	20
2.2	Constrained Lens Theory . . . . .	23
2.3	Design Constraints . . . . .	30
2.3.1	Feed Antenna and Feed Position . . . . .	31
2.3.2	Input and Output Antenna Arrays . . . . .	31
2.3.3	Amplifier Element . . . . .	37
2.3.4	Array Size and Layout . . . . .	38
2.3.5	Other Design Issues . . . . .	38
2.4	Figures of Merit . . . . .	40
2.4.1	Output Power . . . . .	40
2.4.2	Power Gain . . . . .	41
2.4.3	Power Combining Efficiency . . . . .	44

3	A MICROWAVE TRANSMIT/RECEIVE QUASI-OPTICAL LENS AMPLIFIER ARRAY . . . . .	45
3.1	Motivation . . . . .	45
3.2	Single Array Element . . . . .	47
3.3	Transmit/Receive Lens Amplifier Array . . . . .	49
3.4	Applications . . . . .	53
3.4.1	A Quasi-Optical Receiver . . . . .	53
3.4.2	Multipath Fading Reduction . . . . .	53
3.4.3	A Multi-User Application . . . . .	59
3.5	Conclusion . . . . .	59
4	A MILLIMETER-WAVE TRANSMIT/RECEIVE QUASI-OPTICAL LENS AMPLIFIER ARRAY . . . . .	62
4.1	Motivation . . . . .	62
4.2	Design . . . . .	62
4.3	Experiment . . . . .	68
5	A QUASI-OPTICAL ISOLATOR . . . . .	80
5.1	Motivation . . . . .	80
5.2	Design . . . . .	82
5.3	Experiment . . . . .	83
6	A QUASI-OPTICAL BPSK MODULATOR . . . . .	85
6.1	Motivation . . . . .	85
6.2	Design . . . . .	85
6.3	Experiment . . . . .	86
7	A QUASI-OPTICAL ANGLE DIVERSITY RECEIVER . . . . .	89
8	CONCLUSIONS AND FUTURE WORK . . . . .	93
8.1	Conclusions . . . . .	93
8.2	Future work . . . . .	95

8.2.1	Quasi-optical T/R lens front-ends . . . . .	95
8.2.2	Retrodirective Arrays . . . . .	97
8.2.3	High-speed Wireless Data Link . . . . .	97
8.2.4	Quasi-optical Angle Diversity Receiver . . . . .	98
BIBLIOGRAPHY . . . . .		99

## TABLES

## TABLE

2.1	Estimated feed loss due to spill-over loss and non-uniform illumination of various quasi-optical lens amplifier arrays with different F-numbers and feed antennas. . . . .	18
2.2	Estimated aperture efficiencies of various quasi-optical lens amplifier arrays. . . . .	32
4.1	Typical properties of the low-noise amplifier MMICs used for reception and the three-stage driver amplifier MMICs used for transmission at 28 GHz. . . . .	67
4.2	Typical parameters for the MMIC SPDT switches at 28 GHz. . . .	68

## FIGURES

### FIGURE

1.1	An example of a quasi-optical transceiver. . . . .	6
2.1	Schematic of a phased array. . . . .	12
2.2	Schematic of a quasi-optical lens array. . . . .	13
2.3	Estimated feed loss comparison for quasi-optically and circuit fed arrays. . . . .	14
2.4	Estimated feed loss due to spill-over loss and non-uniform illumination of a lens array. . . . .	16
2.5	H-plane radiation pattern of an E-plane feed horn. . . . .	18
2.6	Estimated feed loss due to spill-over loss, non-uniform illumination and aperture efficiency of a lens array. . . . .	19
2.7	Estimated feed loss due to spill-over loss and non-uniform illumination of a lens array for several different feed antennas. . . . .	20
2.8	Layout of the 30-element passive lens array. . . . .	21
2.9	Measured feed loss for three different lens arrays. . . . .	23
2.10	Measured and simulated E- and H-plane radiation patterns for the 30-element passive lens at 9.9 GHz. . . . .	24
2.11	Measured loss due to non-uniform illumination of a lens array. . . . .	25
2.12	Geometry of a planar constrained lens with one degree of freedom. . . . .	27
2.13	Focal surfaces for different F-number lenses with one degree of freedom. . . . .	28
2.14	Minimized path length errors versus scan angle for different F-number one degree of freedom lens designs. . . . .	28

2.15 Measured beam-steering patterns for the three X-band passive 14-element lenses with a waveguide feed. . . . .	29
2.16 Simulated directivity of four arrays with 37 and 21 elements in a rectangular layout and 37 and 24 elements in a triangular layout versus element spacing. . . . .	35
2.17 Simulated antenna gain (including feed loss) of a 37- and a 21-element rectangular array and a 37- and a 21-element triangular array with patch antennas versus element size. . . . .	36
2.18 Measured antenna gain of the 14-element active lens amplifier array with and without a metallic enclosure. . . . .	39
3.1 A quasi-optical T/R module consisting of a transmit/receive amplifier and a grid oscillator/mixer. . . . .	46
3.2 A transmit/receive X-band quasi-optical array amplifier element. . . . .	46
3.3 Circuit schematic of the unit cell. . . . .	47
3.4 Measured and simulated return loss for a single slot antenna. . . . .	48
3.5 Measured radiation patterns for a single antiresonant slot antenna at 10 GHz. . . . .	49
3.6 Measured gain of the transmit and receive amplifier in a unit cell. . . . .	50
3.7 Photograph of the circuit side of the 24-element transmit/receive amplifier array. . . . .	51
3.8 Measured absolute gain of the 24-element active and passive array in transmit and receive mode, with polarizers at input and output. . . . .	54
3.9 Measured antenna gain of the 24-element active and passive array in transmit and receive mode, with polarizers at input and output. . . . .	55
3.10 Measured and simulated E- and H-plane radiation pattern for the receive amplifier at 10.1 GHz. . . . .	56

3.11 A 10-kHz square-wave signal received by a quasi-optical receiver front-end and demodulated. . . . .	57
3.12 Test set-up for the multipath experiment. . . . .	57
3.13 Measured maximum multipath fading nulls of a 10.1-GHz carrier signal. . . . .	58
3.14 Beam-scanning in E-plane for the 24-element lens array. . . . .	60
3.15 Test set-up for the multi-user experiment. . . . .	60
3.16 Received and FSK demodulated multi-user signals. . . . .	61
4.1 Schematic of the folded feed used for the $Ka$ -band array. . . . .	63
4.2 Layout and return loss of a $Ka$ -band patch antenna . . . . .	65
4.3 Layout of a $Ka$ -band slot coupler. . . . .	66
4.4 Simulated reflection and transmission coefficients of a slot coupler. . . . .	67
4.5 Layout of the $Ka$ -band feed- and front-side unit cells. . . . .	69
4.6 Layout of the feed and front side of the 36-element $Ka$ -band transmit/receive lens amplifier array. . . . .	70
4.7 Measured absolute gain for the passive 36-element array . . . . .	72
4.8 Measured absolute gains for the $Ka$ -band array in transmit mode versus number of elements populated. . . . .	73
4.9 Measured absolute gains for the $Ka$ -band array in receive mode versus number of elements populated. . . . .	74
4.10 Measured antenna gains for the $Ka$ -band array fed from an open waveguide section in transmitting and receiving modes. . . . .	74
4.11 Measured antenna gains for the $Ka$ -band array fed from a patch antenna located in the center of the feed-side array in transmitting and receiving modes. . . . .	75
4.12 Measured E- and H-plane radiation patterns for the $Ka$ -band array in transmit mode at 28.3 GHz. . . . .	76

4.13	Simulated radiation patterns versus device failure. . . . .	78
4.14	Measured temperature profile of the <i>Ka</i> -band array in transmit mode with and without air cooling. . . . .	79
5.1	The isolator system consists of a linear-to-circular polarization converter and an absorbing surface. . . . .	81
5.2	Experimental set-up of the isolator system. . . . .	83
5.3	Measured results of the quasi-optical isolator at 8.83 GHz. . . . .	84
6.1	Quasi-optical transmission-type BPSK grid modulator. . . . .	85
6.2	Measured phase shift for the BPSK quasi-optical transmission-type grid modulator. . . . .	87
6.3	Measured relative amplitude for the BPSK quasi-optical transmission-type grid modulator. . . . .	88
7.1	A quasi-optical angle diversity receiver. . . . .	90
7.2	Measured IF power levels in a quasi-optical angle diversity receiver. . . . .	91
7.3	Measured RF power levels in a quasi-optical angle diversity receiver. . . . .	92
8.1	Example of a full duplex transmit/receive lens amplifier front-end. . . . .	96



## CHAPTER 1

### INTRODUCTION AND BACKGROUND

#### 1.1 Requirements for Quasi-Optics in Wireless Communications

Transmission lines are generally the preferred choice of transmission medium for high-speed data communication systems. There are however a variety of network scenarios where wired connectivity solutions are impractical, expensive or slow to implement and where wireless solutions are more attractive. Current microwave wireless communication systems are unable to handle the broad channel bandwidth needed for high data rate communications. While the microwave frequency band is relatively congested, the millimeter-wave spectrum offers a large amount of available bandwidth. Given the channel bandwidth and power restrictions from FCC today, the maximum data rate for spread spectrum wireless Local Area Networks (LANs) is 25 Mbps in the microwave band, while data rates in excess of 5000 Mbps are possible in the millimeter-wave portion of the spectrum [1].

The millimeter-wave spectrum corresponds to frequencies between 30 GHz and 300 GHz. These wavelengths generally allow for smaller and lighter components than their microwave counterparts. This is especially important in space-borne applications, as well as mobile communication systems where size and weight are prime concerns. Atmospheric attenuation of millimeter waves is lower than optical wavelengths in the "transmission window" spectrum that lies between water vapor and oxygen absorption peaks, where millimeter-wave cameras and radar systems are effective in penetrating clouds, smoke and haze unlike their optical counterparts [2].

The large atmospheric absorption at 60 GHz, forms a natural cell-boundary, which has been utilized in indoor and short-range outdoor communications such as wireless LANs [3, 4], satellite cross-links and secure battlefield communications. Several automotive radar systems exist at 77 GHz [5].

For a communication system to be lightweight, compact and reliable, it is preferable to use solid-state devices to tube sources. However, vacuum devices are capable of producing significantly greater power levels than their solid-state counterparts. Electron tubes such as klystrons and gridded tubes can generate several kilowatts of RF power in the microwave spectrum [6, 7]. Gyrotrons can produce tens of kilowatts in the millimeter-wave spectrum, and Traveling-Wave Tubes (TWTs) are capable of 100 watts at 100 GHz [8, 9, 10]. The size and weight of the required high voltage DC power supplies increase the cost and limits the usefulness of these sources. Electron tubes are costly, have limited lifetimes and systems relying on them are subject to catastrophic failure. Solid-state devices have low cost, can offer decreased size and weight, improved reliability and require low-voltage power supplies [11, 12]. Therefore, it would be advantageous to use solid-state devices to achieve medium and high power levels at microwave and millimeter-wave frequencies.

However, at these frequencies solid-state devices have very limited power generating capability. IMPATT diodes can produce several watts at 100 GHz, but the noise generated by the avalanche multiplication process limits their usefulness. Gunn diodes offer improved noise performance, but can only generate a few hundred milliwatts at 100 GHz [8, 10]. The low DC-to-RF conversion efficiency of these devices generates unwanted heat that must be dissipated with large and heavy heat sinking. Devices such as MESFETs, PHEMTs, HBTs, and HFETs offers better DC-to-RF efficiency and good noise performance. At X-band, the maximum output power of these devices found in the literature or manufacturers' specification sheets are presently: 33 dBm for HBTs, 39 dBm for PHEMTs, and 40 dBm for HFETs [13,

14]. Because the output power from these devices are approximately proportional to  $1/f^2$ , the available power at millimeter-wave frequencies are much lower. To obtain the required power levels for communication using solid-state devices at millimeter-wave frequencies, it is necessary to combine the output powers from several devices.

A review of microwave and millimeter-wave power-combining techniques can be found in [14, 15, 16]. Several types of power combiners have been developed, such as resonating cavity and distributed circuit combiners. Both resonant cavity and circuit combiners tend to be lossy for large scale power combining due to conductor losses in the waveguide walls and distributed feed networks.

In a quasi-optical transmitter, the output power of many solid-state devices are combined in free-space to overcome these limitations and obtain the required power levels. Quasi-optical components can hence provide lightweight, compact, less expensive and reliable front-ends to millimeter-wave communication systems. An antenna-based power-combining circuit was reported by Staiman *et al.*[17] as early as 1968. The active array consisted of a 100-element array of dipole antennas above a ground plane. Each dipole antenna was fed by a solid-state amplifier. The array demonstrated 100 watts of output power at 410 MHz. Durkin *et al.* [18] demonstrated a 35 GHz radar transmitter using IMPATT amplifiers driving a printed slot array. Mink later suggested to use an array of millimeter-wave devices as a "gain medium" within a Fabry-Perot resonator as means of large-scale power combining [19]. The power can be distributed over a larger number of devices than in waveguide combiners, because the quasi-optical combining structure can be many wavelengths across.

The term *quasi-optical* is used to describe power combining that uses traditionally optical techniques and components. Quasi-optical components such as Fabry-Perot resonators, grids and polarizers have their optical analogues. Optical

techniques such as reflection, focusing, and polarization isolation or rotation are utilized in quasi-optical components. However, the operating wavelength is comparable to the size of most quasi-optical components, so diffraction plays an important role and the quality factors of quasi-optical resonators are much lower than their optical counter-parts.

Since these first demonstrations of spatial power-combining, a significant amount of research has been done in the field. Several excellent books and review articles discuss a variety of quasi-optical power-combining components [14, 16].

While most of the quasi-optical circuits presented to date have been designed for either transmit or receive operation, a few transceiver applications have been demonstrated. Birkeland *et al.* [20] used an *X*-band quasi-optical oscillator as both a transmitter and a self-oscillating mixer in reception. The receiver output is the mixing product of the transmitted signal and a received signal. A simple Doppler radar application was demonstrated using this circuit. Using the same technique, a two-element active microstrip patch array was used to demonstrate a Doppler radar with azimuth tracking capabilities [21] at 6.5 GHz. An active integrated antenna transceiver [22] was used to demonstrate two-way communications at 6 GHz. Cross-polarization separates the transmit and receive functions in this transceiver. Full duplex operation was demonstrated using orthogonal polarization to isolate transmit and receive signals in an active two-element patch antenna array [23]. The array has a transmitted power of 5.4 dBm, and a gain of 8.2 dB at 4.05 GHz in reception.

A possible application for quasi-optical front-ends is base-station antennas for mobile communications such as cellular and PCS. These transceivers require high transmitted power of about 100 W [24] and more than 10 dB antenna gain (depending on the number of sectors). Solid-state power amplifiers with 1 W of output power in each element of a 100-element quasi-optical front-end can be used to achieve the required power level and antenna gain for this system. By using the beam-steering

properties of a lens array, several sectors can simultaneously be addressed from the same front-end. Other communication systems where quasi-optical front-ends can be used are the LMDS (Local Multipoint Distribution Service) master transmitters and repeaters, which require about 60 W transmitted power in the 27-30 GHz range. These systems currently use traveling-wave tube sources with either omni-directional antennas or horns, and typically weigh between 150 and 500 pounds. A quasi-optical front-end can decrease the size and weight as well as improve the reliability of these systems.

Radar is another interesting application for quasi-optical transmit/receive front-ends. An example is Synthetic Aperture Radars (SAR) such as the Shuttle Imaging Radar (SIRC) which operate at 5 GHz. In this radar, several hundred T/R modules produce a total power of 1.5 kW peak with a 5 % duty cycle. To cover a look angle of 25-50 degrees in the azimuth direction, 5-10 beams with a 5° beamwidth are required. A transmit/receive lens array with 5-10 feed antennas along the focal arch can provide the necessary power and beam-steering requirements without using phase shifters. Existing automotive radars at 77 GHz use passive Rotman lenses with several discrete beams [25, 5]. By including solid-state T/R modules in each array element, higher dynamic range in reception and high EIRP in transmission can be achieved. Another example is missile seekers at *Ka*-band, where a transmitted power of tens of watts is required. Current systems are bulky and beam steering of about 30 degrees is performed mechanically. A transmit/receive lens front-end, can provide the required output power while decreasing weight and size as well as improving the functionality of the system.

## 1.2 Quasi-Optical Transceiver Components

Several quasi-optical components such as the ones presented here, can be

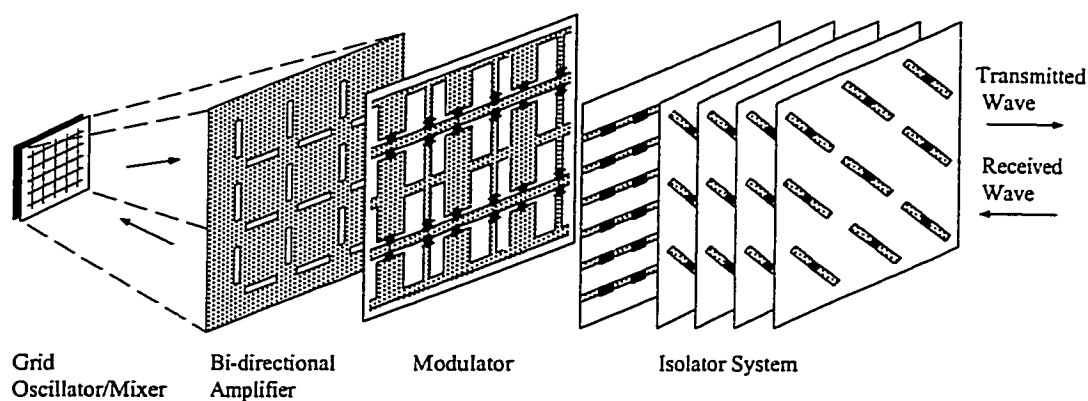


Figure 1.1. An example of a quasi-optical transceiver. The transceiver consists of an oscillator / self-oscillating mixer, a transmit/receive lens amplifier, a modulator and an isolator.

combined to form a complete quasi-optical T/R module for millimeter-wave communications. A conceptual example of a quasi-optical transceiver consisting of several different cascaded components is shown in Figure 1.1. The main functions of a quasi-optical transceiver are signal generation, amplification, reception and modulation/demodulation. The following Sections 1.2.1-1.2.3 give an overview of these quasi-optical components.

### 1.2.1 Quasi-Optical Sources

The source in a quasi-optical transceiver can be a grid oscillator [26, 27] or an oscillator antenna array [28]. A single active antenna or an antenna connected to a separate oscillator can also be used, but these sources would not include combining at the source level. In a grid oscillator, a metal grating is loaded with two- or three-terminal solid-state devices. The grating is printed on a dielectric substrate and has a period much smaller than a free-space wavelength. The radiators connected to each of the active devices are thus strongly coupled in these grids. A mirror is placed behind the grid to provide the positive feedback necessary for oscillation. A partially transparent reflector is often placed in front of the grid, analogous to a Fabry-Perot

cavity laser, where the active grid serves as the gain medium. In these oscillators the radiated power from many devices are combined in free-space, to produce an effective radiated power of several watts. Details of the first demonstrations of grid oscillators at the California Institute of Technology are described in [26], while a summary of all grid oscillators reported in the literature to date are found in [27].

In an oscillator antenna array, the radiating elements are spaced by half a wavelength or more and coupling between the individual elements are thus relatively low. The individual oscillators are often coupled through a transmission line. The oscillator arrays generally have lower phase-noise than the grid oscillators, but the power density and total radiated power is also lower. Functions such as beam steering without using phase-shifters have been demonstrated for these arrays [14].

### 1.2.2 Quasi-Optical Transmit or Receive Amplifiers

A large number of transmission mode quasi-optical amplifiers have been presented to date. Similar to the oscillators, the quasi-optical amplifiers can be divided into grid amplifiers and array amplifiers. The first quasi-optical amplifier was a grid structure [29]. Since the first demonstration, several grid amplifiers with more elements and more output power have been developed [30]. Because stability is hard to achieve in these planar grid amplifiers due to strong coupling between the individual elements, antenna array amplifiers with larger unit cells have been developed [31, 32].

In these arrays, input and output antennas in each element of the array are interconnected by a solid-state amplifier. The input and output antennas are often orthogonally polarized to improve isolation. The amplifier circuit in each cell can be designed for high power [33], high efficiency [34], low noise [13], high gain [35] or broad bandwidth [36]. Schoenberg *et al.* demonstrated X-band amplifier arrays using Class-A amplifiers for high effectively radiated power (EIRP) in transmission, and

low-noise/high gain two-stage amplifiers to achieve high dynamic range in reception. A high power hybrid design reports a saturated output power of 2 W at  $Ka$ -band [33]. For a high power design, heat sinking becomes a problem due to the large amount of heat generated by the devices. In a portable system, power consumption should be kept at a minimum to increase the operating time and weight. It is therefore desirable to use amplifiers with high efficiency. Mader *et al.* demonstrated a C-band Class-E power amplifier antenna array with 2.4 W of output power and 64 % power-added efficiency. While most of these arrays are designed at microwave or low millimeter-wave frequencies, several quasi-optical amplifier arrays have been developed using monolithic design techniques at millimeter-wave frequencies [37, 38, 39].

Many of these quasi-optical amplifiers suffers from large feed losses often exceeding the amplifier gain, because a far-field source is required to provide a uniform phase-front to the array. To overcome this spill-over loss, external lenses [37] and oversize waveguides have been used [40]. To reduce the feed loss without using external lenses, lens amplifier arrays have been developed [41, 13]. By incorporating lensing delay lines in each array element, the amplifier array can be fed from a focal point in the near field, and thus minimize spill-over loss. Focusing also allows for other functions such as beam steering in transmission and adaptive signal processing in reception. A 10-element linear lens-fed array using a dielectric slab to guide the waves from the feed to the individual antenna elements in the input array demonstrate reduced spill-over loss of linear lens amplifier arrays [42].

While these amplifier arrays operate either in transmission or reception, bi-directional amplifier arrays such as the ones presented here, have been developed for added functionality [43, 44]. In a quasi-optical transceiver, a transmit/receive lens amplifier array is located in front of an oscillator to provide high-power amplification in transmission and low-noise amplification in receive mode. The transmit/receive amplifier arrays presented to date must be electronically switched from transmit to



receive mode. Hence, full duplex operation can not be achieved with these arrays. To obtain a stable full duplex amplifier array, the problem of isolating the transmitted signals from the received signals must be resolved. The transmit/receive amplifier array presented in [43] uses orthogonal polarizations to isolate the transmit and receive signals, but the isolation was found to be insufficient for stable full duplex operation.

### 1.2.3 Other Quasi-Optical Components

Several X-band digital phase modulators have been demonstrated [45]. In a quasi-optical transceiver, a QPSK transmission mode modulator can be placed in front of the amplifier for data transmission. An X-band BPSK modulator using *p-i-n* diodes is presented in Chapter 6. Most transmitters have isolators to protect them. Quasi-optical arrays are not compatible with standard waveguide or coaxial isolators. To protect the quasi-optical transmit amplifier from high-level reflected waves, a quasi-optical isolator is designed [46]. The isolator presented in Chapter 5 also provides a circularly polarized wave at the output. In a communication system, the use of circular polarization has been shown to reduce multipath fading, because odd-number reflections rotate in the opposite direction of the direct signal and are not received by the antenna. In satellite communications, circular polarization is preferred to save power lost due to Faraday rotation if linear polarization is used. Other quasi-optical components such as mixers [47, 48, 49], VCOs [50], filters [51], multipliers [52, 53, 54], switches [55, 56], and phase shifters [57] have also been developed.

## 1.3 Organization of the Thesis

This thesis introduces several microwave and millimeter-wave components for quasi-optical transceivers. The emphasis of the thesis is the design of quasi-optical

microwave and millimeter-wave transmit/receive lens amplifier front-ends. The motivation for using quasi-optical components in a wireless communication system, as well as a short description of previous work in this field, are presented in Chapter 1.

Chapter 2 describes the design and analysis of quasi-optical lens amplifier arrays. Some early work on lens amplifier arrays as well as an overview of constrained lens theory is presented. The different loss mechanisms of lens arrays are investigated.

In Chapter 3, an *X*-band transmit/receive lens amplifier array is presented. Experimental results and several applications of the array are discussed: a quasi-optical transceiver front-end; a quasi-optical AM receiver; multipath fading null reduction; and a multi-user system with frequency reuse application.

A *Ka*-band transmit/receive lens amplifier array is demonstrated in Chapter 4. The design and experimental results are presented.

Other quasi-optical components such as an isolator and a modulator are presented in Chapter 5 and Chapter 6, respectively. In Chapter 7 a quasi-optical angle diversity receiver using a lens amplifier array and three grid oscillators is demonstrated.

Finally, Chapter 8 gives a summary of the thesis and some suggestions for future work on quasi-optical T/R front-ends.

## CHAPTER 2

### DESIGN AND ANALYSIS OF LENS AMPLIFIER ARRAYS

#### 2.1 Feed Efficiency of Array Antennas

Large phased arrays are often used as the front-end in a transceiver system to meet the desired directivity and beam-steering requirements. A phased array consists of an array of radiating elements fed with a corporate power collection/distribution network as shown in Figure 2.1. In a transmitting phased array, many power dividers and long lengths of transmission lines are required to distribute the power from a transmitter to the individual antenna elements. Phase shifters and power amplifiers are often included in each element to achieve beam-steering control and high EIRP. In a receiving array, power combiners are used to combine the received power from the antenna elements to a receiver. Low-noise amplifiers and phase shifters in each element are often used to improve the dynamic range and add beam-forming capability to a phased array.

The insertion loss of the power dividers and transmission lines increase as a function of array size, and can be greater than 16 dB for large arrays [58]. For the large phased arrays often used in military radar systems [59, 60], several thousand transmission lines and DC control lines are needed. The corporate feed network thus becomes very complex and expensive. However, by using a corporate feed structure it becomes relatively simple to obtain uniform phase and amplitude at all the array elements. The feed loss for an N-element phased array with uniform phase and amplitude distribution and using two-way power dividers, is given by

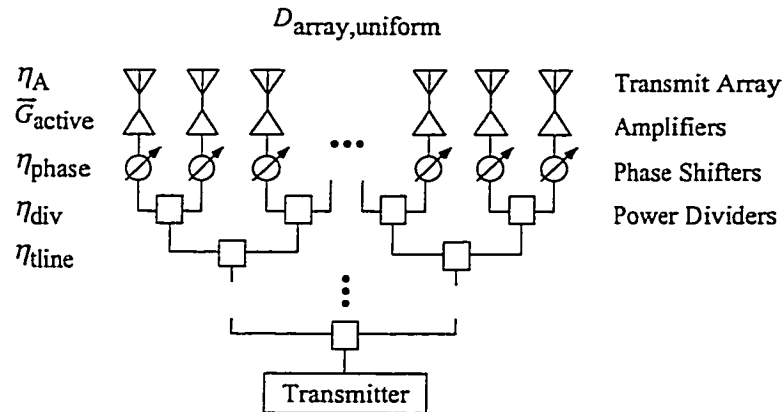


Figure 2.1. General corporate feed structure of an active phased array. Phase shifters and transmit amplifiers in each element allow for high EIRP and beam-steering control in transmission.

$$G_{\text{antenna}} = D_{\text{array,uniform}} \eta_A (\eta_{\text{div}} \eta_{\text{tline}})^{\frac{\log N}{\log 2}} (\eta_{\text{phase}})^N \overline{G_{\text{active}}}, \quad (2.1)$$

where  $D_{\text{array,uniform}}$  is the directivity of the antenna array and  $\eta_A$  is the aperture efficiency of the array including loss in the antenna elements. The loss in each power divider and phase shifter is  $\eta_{\text{div}}$  and  $\eta_{\text{phase}}$ , respectively. The transmission-line loss for the transmission-line section in each power divider is  $\eta_{\text{tline}}$  and  $\overline{G_{\text{active}}}$  is the average amplifier gain. Notice that for a large number of elements  $N$  the loss due to the power dividers and transmission lines becomes large. A quasi-optical feed structure can be used to reduce the feed loss and complexity of large phased arrays.

The feed structure for a transmit-mode quasi-optical lens amplifier array is shown in Figure 2.2. In a quasi-optical lens amplifier array, a feed antenna connected to the transmitter is used to distribute the power in free-space to the individual elements in an input antenna array. The signals received are then amplified and reradiated from the radiating elements in the output array. Because the array is fed from the near field, lensing delay lines must be used to achieve a uniform phase distribution at the output elements. The theory and design equations for constrained lenses are presented in Section 2.2.

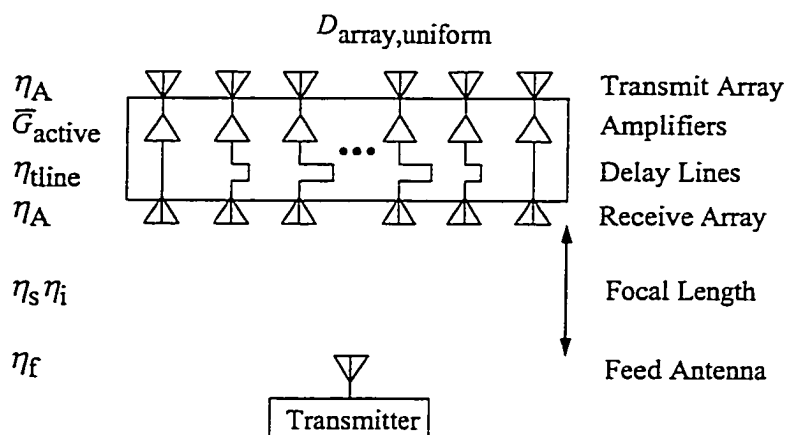


Figure 2.2. A general quasi-optical lens amplifier array. The corporate feed structure is replaced by a spatial feed.

The feed loss associated with the transmission lines and power dividers in the corporate feed network of a phased array are thus eliminated in a quasi-optically fed array. The feed loss in a quasi-optically fed array can be divided into: feed antenna loss,  $\eta_f$ ; spill-over loss,  $\eta_s$ ; reduction in directivity due to non-uniform amplitude distribution of the elements,  $\eta_i$ ; and aperture loss,  $\eta_A$ , including loss in the antenna elements in the input and output arrays. The gain of a quasi-optical lens amplifier front-end, assuming uniform phase distribution of the output array, and the same aperture efficiency for the input and output array is given by

$$G_{antenna} = D_{array,uniform} \eta_f \eta_s \eta_i \eta_A^2 \eta_{line} \overline{G}_{active}. \quad (2.2)$$

These losses will be discussed in more detail in Section 2.1.1. The minimum feed loss for circuit and quasi-optically fed phased arrays as a function of number of array elements is shown in Figure 2.3. The feed loss of a quasi-optically fed array can be as low as 5 dB, as shown in Section 2.1.1. The feed loss of a circuit fed array with two-way power dividers for several different divider/transmission-line losses are shown. While the feed losses in circuit-fed phased arrays increase with the number of elements in the array, the feed losses in a quasi-optically fed array

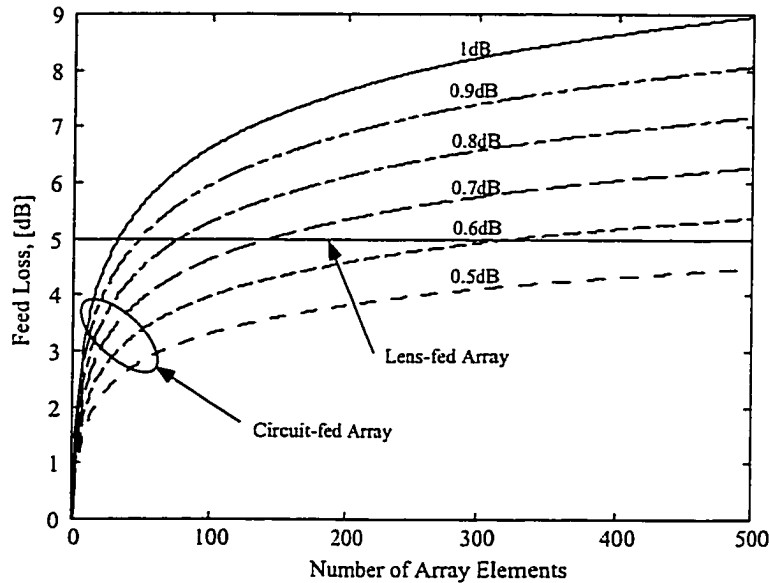


Figure 2.3. Estimated feed loss of circuit and quasi-optically fed arrays versus array size. The feed losses for circuit fed arrays with two-way dividers/combiners are shown for different divider and transmission-line losses. The feed loss of quasi-optical arrays is estimated to be 5 dB as calculated in Section 2.1.1.

are constant assuming a constant  $F/D$  ratio. So for large arrays the feed losses of phased arrays will exceed the feed losses of quasi-optically fed lens arrays. While phased arrays often use frequency dependent phase shifters to achieve beam steering, the delay lines in a constrained lens array represents a true time delay and are thus frequency independent. Broadband beam-steering applications requiring a constant phase distribution over a wide frequency band are thus possible with a quasi-optical lens-fed array.

For a far-field fed quasi-optical array without lensing delay-lines or external dielectric lenses, the spill-over loss and loss due to non-uniform phase and amplitude distribution in Equation 2.2 is found from the Friis transmission formula:

$$\eta_s \eta_i = G_f D_{\text{array,uniform}} \left( \frac{\lambda}{4\pi R} \right)^2, \quad (2.3)$$

where  $G_f$  is the directive gain of the feed antenna,  $D_{\text{array,uniform}}$  is the directivity

of the input array and  $R$  is the distance from the feed antenna to the input array. While the loss due to non-uniform amplitude distribution can be neglected, the spill-over loss becomes very large because the feed horn must be in the far field of the input array ( $R > \frac{2D^2}{\lambda}$ ). External lenses can be used to reduce the spill-over loss, but they add complexity, cost and weight to the system. The Gaussian beams provided by these external lenses also increase the loss due to a non-uniform amplitude distribution.

### 2.1.1 Simulated Feed Loss

The various feed losses in a quasi-optically fed lens array were identified in Section 2.1. However, to design a lens with minimal loss it is desirable to determine the dominant losses and understand how they can be minimized. Two methods based on geometrical optics and the Friis formula have been used to estimate the spill-over loss of lens arrays.

The Friis formula method calculates the power received by each individual antenna element in the input array and compares it to the total input power to the feed antenna. It is assumed that: the feed antenna and the individual antenna elements are in the far field of each other; the elements are non-coupled; and no standing waves (or multiple reflections) between the feed antenna and the input array exist. Knowing the gain pattern of the feed antenna and of the individual elements in the input array as well as the distances between them, the Friis formula can be applied to each element in the array. The spill-over loss is found by adding the powers received by all the elements and comparing this power to the feed antenna input power. Using the gain pattern and amplitudes of the output array elements, the directivity of the output array with non-uniform amplitude distribution is estimated. The non-uniform illumination efficiency is then found by comparing this directivity with the ideal directivity when all array elements have unity amplitude.

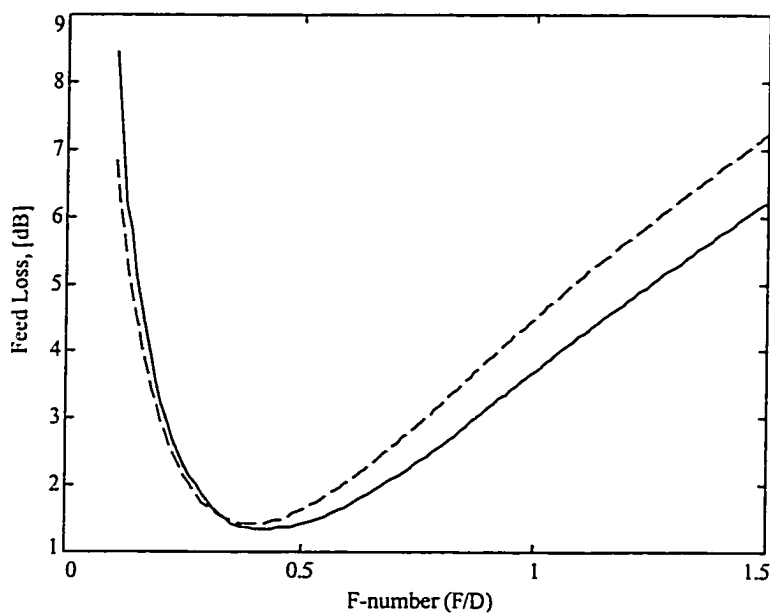


Figure 2.4. Estimated feed loss due to spill-over loss and reduction in directivity due to non-uniform amplitude as a function of F-number for a lens amplifier array. The loss calculated using the Friis formula method is shown in solid line and the one found using the geometrical optics method is shown in dashed line. An E-plane horn with 9 dB directive gain was used as a feed antenna for these calculations.

The 14-element lens array presented in [61], was used as an example. An E-plane horn with 9-dB directive gain is used as a feed antenna in these calculations. The simulated feed loss due to spill-over loss and reduction in directivity of the output array due to non-uniform illumination is shown in Figure 2.4. The effective area of each element in the input array is set equal to the physical area (seen from the angle of incidence) of the individual element for comparison purposes. By instead using the radiation pattern of the individual elements, the aperture efficiency of the input array is also included in the calculations. Simulations of a 30-element array predicts almost identical feed loss.

The geometrical optics method is based on the feed efficiency calculations of reflector antennas presented in [62]. For a planar circular aperture lens array, the equations for non-uniform illumination efficiency and spill-over efficiency can be derived as given by Equations 2.4 and 2.5 below. The method assumes 100 %



aperture efficiency of the input array.

$$\eta_i = \frac{4F^2}{\pi D^2} \frac{\left( \int_0^{2\pi} \int_0^{\Phi/2} \sqrt{g(\theta, \phi)} \frac{\sin \theta}{(\cos \theta)^{3/2}} d\theta d\phi \right)^2}{\int_0^{2\pi} \int_0^{\Phi/2} g(\theta, \phi) \sin \theta d\theta d\phi} \quad (2.4)$$

$$\eta_s = \frac{\int_0^{2\pi} \int_0^{\Phi/2} g(\theta, \phi) \sin \theta d\theta d\phi}{\int_0^{2\pi} \int_0^{\pi} g(\theta, \phi) \sin \theta d\theta d\phi} \quad (2.5)$$

where  $g(\theta, \phi)$  is the gain of the feed antenna,  $\theta$  is the angle from the optical axis at the feed ( $\theta = \Phi$  at the edge of the array.), and  $\phi$  is the polar angle in the plane of the array. If the directive gain of the feed antenna is assumed to be independent of  $\phi$ , the combined feed efficiency reduces to

$$\eta_s \eta_i = \frac{4F^2}{D^2} \left( \int_0^{\Phi/2} \sqrt{g(\theta)} \frac{\sin \theta}{(\cos \theta)^{3/2}} d\theta \right)^2. \quad (2.6)$$

The radiation pattern of a feed horn can be approximated by

$$g(\theta) = \begin{cases} 2(n+1)(\cos \theta)^n & \text{if } \theta \in (0, \pi/2) \\ 0 & \text{otherwise} \end{cases}, \quad (2.7)$$

where  $n$  is a fitting parameter. The measured radiation pattern for the E-plane horn used to feed the X-band lenses presented here, agree well with the gain function in Equation 2.7 with  $n=3$  (9 dB directive gain) as shown in Figure 2.5. With these approximations, a closed form expression for the feed efficiency can be found:

$$\eta_s \eta_i = \frac{32F^2}{D^2} \frac{n+1}{(n-1)^2} \left( 1 - 2 \left( \cos \frac{\Phi}{2} \right)^{\frac{n-1}{2}} + \left( \cos \frac{\Phi}{2} \right)^{n-1} \right) \quad (2.8)$$

The resulting feed loss calculated using Equation 2.8 is plotted in Figure 2.4. The estimated feed loss is within 1 dB for the two methods, and a minimum feed loss is estimated for a lens with F-number around 0.4. For F-numbers less than 0.4 loss due to non-uniform illumination is dominating, while for F-numbers greater

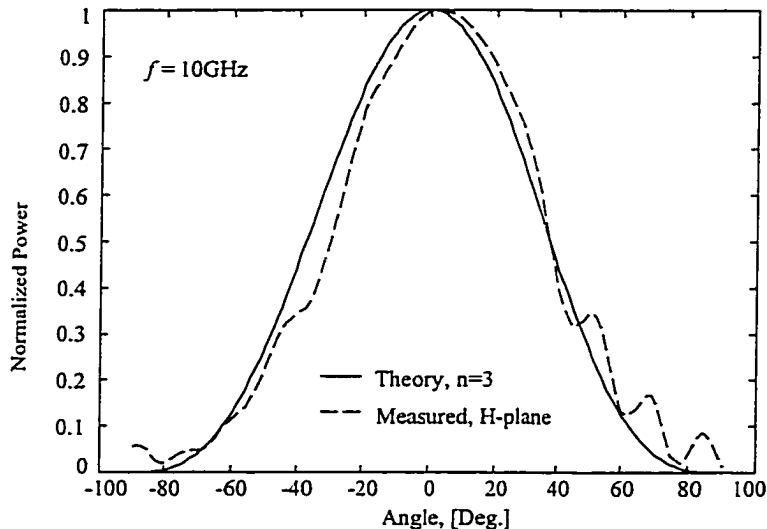


Figure 2.5. Theoretical (solid line) and measured (dashed line) H-plane radiation pattern for the E-plane horn used to feed the arrays presented.

than 0.4 spill-over loss is dominating. Most lens arrays presented to date have F-numbers between 1 and 1.5 and thus suffer from unnecessarily high feed loss. A summary of the lenses presented to date, their F-number and estimated feed loss due to spill-over loss and non-uniform illumination is given in Table 2.1. It is important to emphasize that both of these simulations have strong limitations, and are only shown to predict the general behavior of a lens array. These estimates does not account for the aperture efficiency of the input array, losses due to coupling between the array elements, non-uniform phase across the output array, losses in the array elements and feed antenna, as well as losses in the delay line sections.

Quasi-Optical Lens	F-number	Feed Antenna	$\eta_s \eta_i$
Schoenberg [35]	2.0	E-plane Horn	10 dB
Schoenberg [32]	1.2	E-plane Horn	5.5 dB
Berg [61]	0.75	E-plane Horn	3 dB
Hollung [44]	1.5	E-plane Horn	7.25 dB
Hollung, Chapter 4	0.6	Open Waveguide	4 dB

Table 2.1. Estimated feed loss due to spill-over loss and non-uniform illumination of various quasi-optical lens amplifier arrays with different F-numbers and feed antennas.

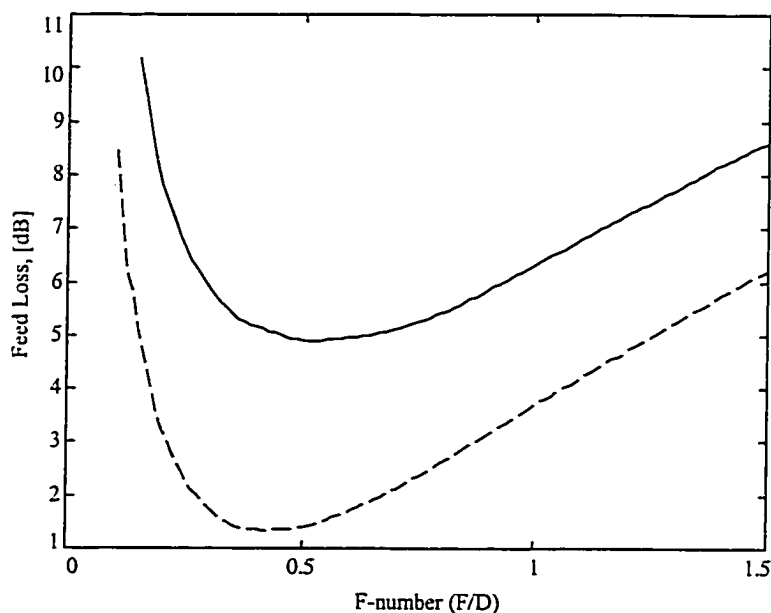


Figure 2.6. Estimated feed loss (solid line) due to spill-over loss, aperture efficiency of the input array, and reduction in directivity due to non-uniform amplitude as a function of F-number for the 14-element lens amplifier array. The estimated feed loss without including the aperture efficiency of the array is also shown (dashed line). The feed loss is calculated using the Friis formula method.

If the measured gain pattern of the patch antennas are included in the simulations, the feed-loss including the aperture efficiency of the input array is estimated as shown in Figure 2.6. Notice how the minimum feed loss now occurs for a slightly higher F-number lens (0.5) due to a less uniform amplitude distribution across the array.

While these calculations have assumed a feed antenna gain of 9 dB, it is of interest to investigate the effect of feed antenna directivity on the feed loss. The estimated feed loss for several different feed antennas using the geometrical optics method are shown in Figure 2.7. It is evident that a more directive feed antenna can reduce the spill-over loss for a given lens array. Because the lens should be located in the far field of the feed antenna, a more directive feed with a longer far-field distance may require a larger diameter lens for a given F/D ratio.

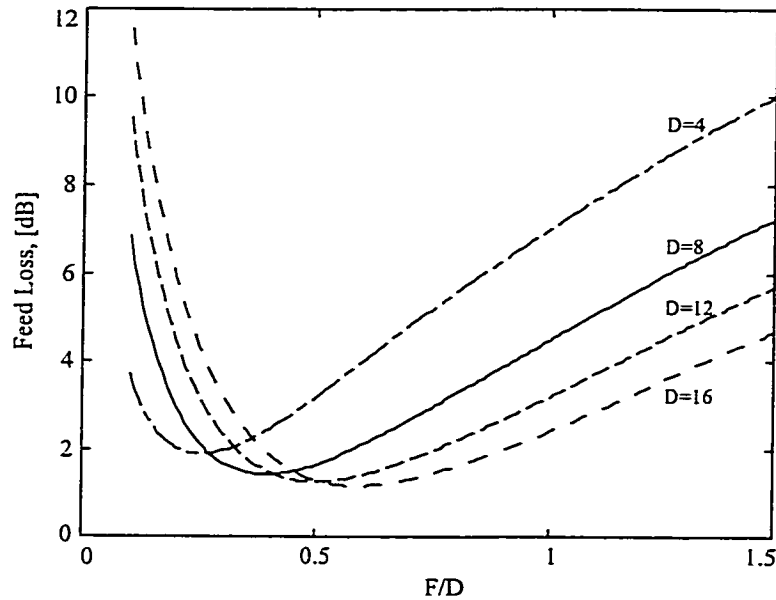


Figure 2.7. Estimated feed loss due to spill-over loss and non-uniform illumination of a lens array for several different feed antennas. The feed loss is calculated using the geometrical optics method.

### 2.1.2 Measured Feed Loss

Several passive  $X$ -band lens amplifier arrays were fabricated to investigate how different  $F/D$  ratios affects the feed loss and beam-steering performance of a lens array. The 14-element lens amplifier design presented in [61], was used with the amplifier stages replaced by through lines. Passive lenses with  $F$ -numbers 0.75, 1.0 and 1.5 as well as an array without lensing was designed and fabricated. A 30-element array based on the same unit cell was fabricated as shown in Figure 2.8. The array was designed to minimize the feed loss, with an  $F$ -number of 0.6 ( $F=7.5$  cm).

The passive array with equal delay-line lengths interconnecting the input and output antennas was first used to determine the aperture efficiency,  $\eta_A$  of the input and output antenna arrays as well as the loss in the patches,  $\eta_{\text{patch}}$  and transmission lines,  $\eta_{\text{line}}$  connecting them. The array was placed in the plane of an aperture in absorbing material. Two co-polarized  $E$ -plane horns located in the far field in front of the array and connected to an HP 70820A microwave transition analyzer, were

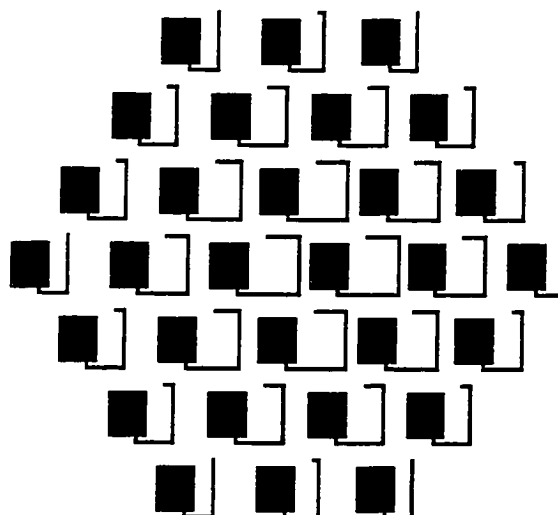


Figure 2.8. Layout of the 30-element passive lens array. The F-number for this lens is 0.6 corresponding to a focal length  $F=7.5$  cm. The unit cell size is  $0.63 \times 0.83 \lambda$ .

used to measure the aperture efficiency. An aperture efficiency,  $\frac{\eta_A}{\eta_{\text{patch}}}$  (not including radiation efficiency of the patches) of 90 % is measured for both the input and output arrays by comparing the received power reflected from the array to a measurement with the array replaced by a metallic mirror.

A transmission measurement with one horn located in the far field in front of the array, and the other horn oppositely polarized and located in the far field behind the array, was performed to determine the loss in the patches and the transmission line section. The transmitted power through the array was compared to a measurement without the array inserted in the aperture and with the horns co-polarized. Knowing the aperture efficiency of the input array, a loss of -3.36 dB was calculated for the two patches and transmission line sections connecting them. The patch loss was estimated to be 1 dB (80 % efficiency). The transmission line loss including the via connection and return loss of the patches is then 1.36 dB.

To investigate how the total feed loss of lens amplifier arrays depends on the feed antenna gain, the four passive lenses were measured using two different feed antennas: an E-plane horn (9-dB directive gain); and an open WR-90 waveguide

(6-dB directive gain).

The measured antenna gain  $G_{\text{antenna}}$  of a passive lens front-end can be factored and expressed in terms of several loss factors and the directivity  $D_{\text{array,uniform}}$  of a uniformly fed output array:

$$G_{\text{antenna}} = \frac{EIRP}{P_{\text{in}}} = \eta_f \eta_s \eta_A^2 \eta_{\text{tline}} \eta_i D_{\text{array,uniform}} \quad (2.9)$$

A feed efficiency  $\eta_{\text{feed}}$  can then be defined as:

$$\eta_{\text{feed}} = \eta_f \eta_s \eta_A \eta_{\text{tline}} \eta_i \quad (2.10)$$

The measured feed loss for the different lenses and feed antennas is plotted in Figure 2.9. The theoretical feed loss is calculated by adding the measured loss due to the transmission lines to the simulated feed loss using the Friis formula method described in the previous section. The measured gain pattern of the open waveguide was used in the simulations with a maximum directive gain of 6 dB. Good agreement is seen between the simulated and measured feed loss. As expected from simulations, the feed loss can be reduced by using a more directive antenna and a lower F-number lens. The difference between the theory and measurement can be due to coupling between the antenna elements.

To investigate the non-uniform illumination efficiency of the passive lenses, the E- and H-plane radiation patterns are measured, and the array directivity  $D_{\text{array}}$  is estimated from the measured patterns using Equation 2.22. The measured and simulated radiation patterns for the 30-element passive lens array are shown in Figure 2.10. The simulated patterns are calculated from a measured patch pattern and the calculated array factor. From these radiation patterns, it is evident that the measured directivity of these lenses is lower than the theoretical.

The reduction in directive gain,  $\eta_i$ , due to non-uniform amplitude and phase of the output array elements is then estimated by comparing the measured directivity

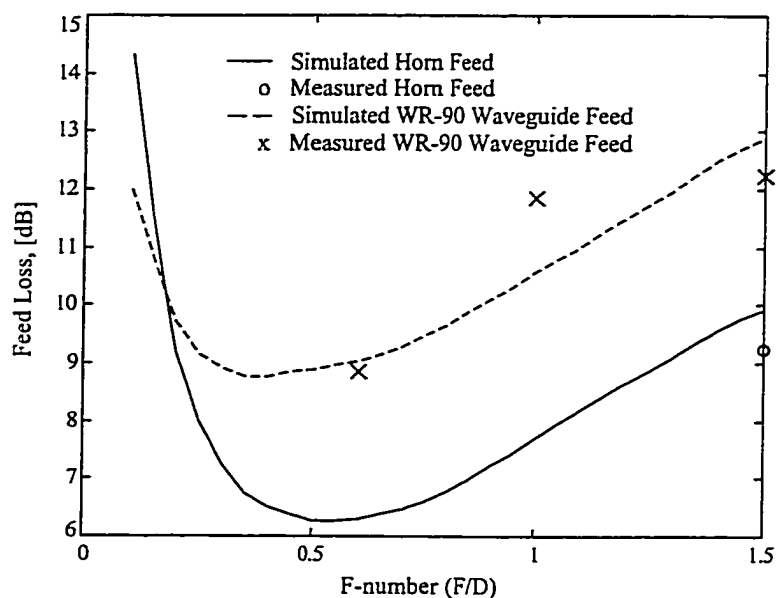
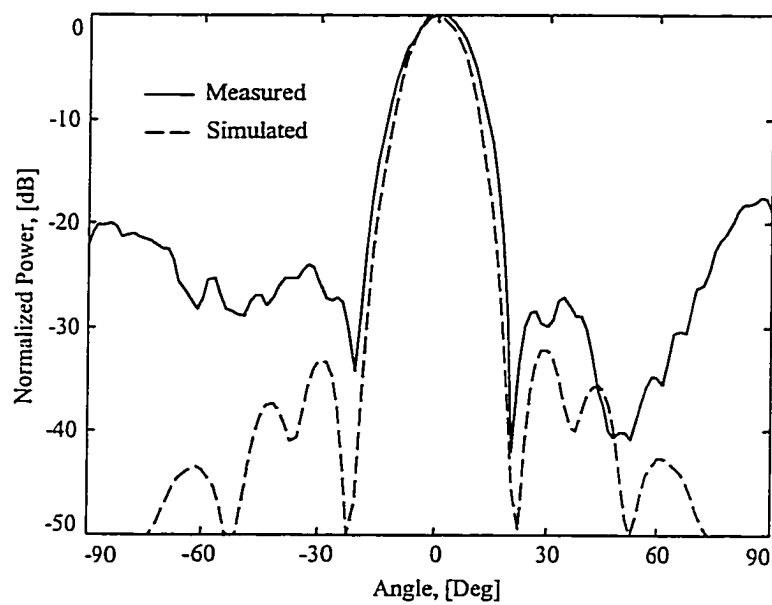


Figure 2.9. Measured and theoretical feed loss for lenses with different F-numbers and fed by different antennas. The theoretical feed efficiency for an E-plane horn feed is shown by a solid line, and for a waveguide feed with a dotted line. The measured feed efficiencies for the passive lenses with three different F-numbers are shown for a horn feed (o) and a waveguide feed (x).

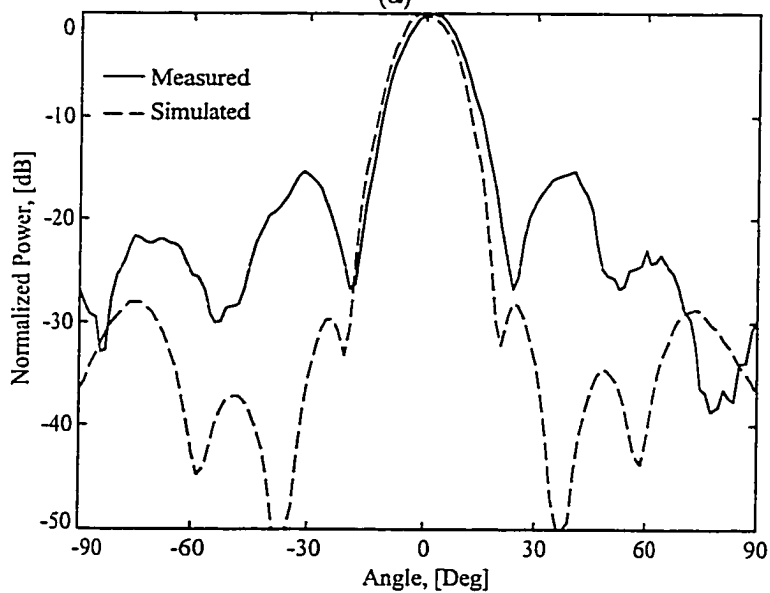
to the theoretical directivity of a uniformly fed array as shown in Figure 2.11. The simulations assumes uniform phase across the array. As expected, the measured non-uniform illumination loss is higher than the theoretical due to a less uniform amplitude and phase distribution across the array. The E-plane horn feed is only used for the  $F=12$  cm lens array, because the shorter focal length arrays would not be in the far field of this horn.

## 2.2 Constrained Lens Theory

Geometrical optics principles can be successfully applied in many microwave and millimeter-wave design problems. Several good books discuss this topic [63, 62]. The geometrical optics principles follow from Maxwell's equations in the infinite frequency limit. To use the approximations of geometrical optics, one must be aware of the limitations of this technique. The medium's refractive index or surface curvature



(a)



(b)

Figure 2.10. (a) Measured (—) and simulated (---) E-plane radiation patterns for the passive 30-element lens at 9.9 GHz. (b) Measured (—) and simulated (---) H-plane radiation pattern for the passive 30-element lens at 9.9 GHz. The theoretical patterns were calculated using the measured antenna pattern of a single patch antenna.



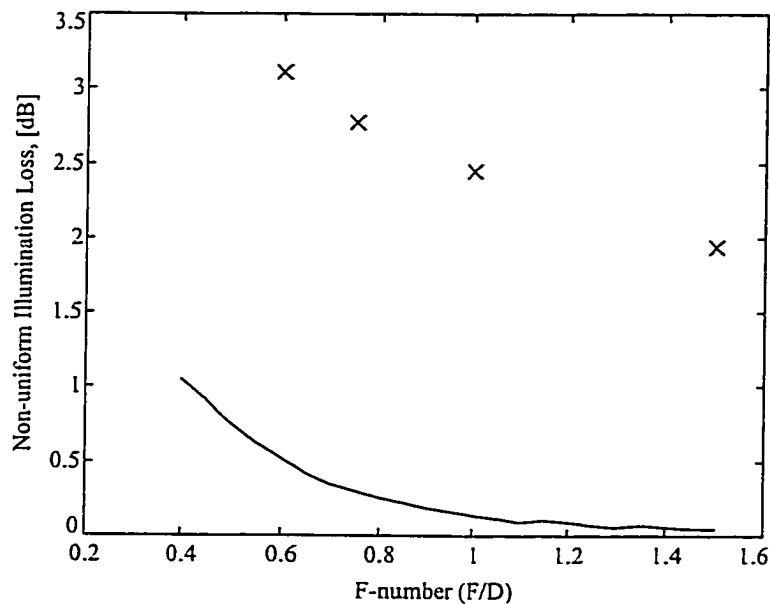


Figure 2.11. Measured (x) and theoretical (solid line) loss due to non-uniform amplitude and phase distribution of the output array elements for the three passive lenses with different F-numbers and with a waveguide feed.

must be a slowly varying function of spatial coordinate relative to a wavelength. The following discussion describes the applicability of the geometrical optics principles to discrete microwave lenses.

The first constrained lens antenna array (the "Bootlace" Aerial) was developed by Gent in 1957 [64]. This passive lens array consisted of pairs of folded dipole radiators separated by a ground plane, and interconnected by parallel wire transmission lines. The transmission-line lengths connecting the antenna pairs were carefully chosen to collimate an incident spherical wave front from a focal point behind the aerial. While the bootlace aerial only had one perfect focal point, a lens design satisfying the path-length equality conditions for three perfect focal points was demonstrated by Rotman [65]. By displacing the input and output elements relative to each other as well as curving the input element surface, Rotman obtained the three geometrical degrees of freedom needed to solve for the three focal points. The fabricated Rotman lens array with the three focal points located along a focal

arch was used to demonstrate beam steering in one plane from -30 to +30 degrees without much amplitude variation. Today, Rotman lenses are used in a wide variety of applications such as automotive radar [25, 5], missile seekers, tank radars, aircraft landing systems and communications equipment [66].

As many as four perfect focal points can be achieved by curving the output surface and thus adding a fourth degree of freedom. These four focal points can be located on a straight line [67] or on a circle [68]. While the quadrifocal lenses are hard to fabricate due to the curved surfaces at the input and output, a planar constrained lens design using microstrip transmission lines was suggested by McGrath [69]. A planar design is preferred at millimeter-wave frequencies, where printed circuit fabrication is necessary due to the small dimensions. Because the input and output surfaces are planar, the only two geometrical degrees of freedom available are the placement of the input and output antenna elements relative to each other and the transmission line length interconnecting them.

A simple one degree of freedom design using two identical input and output antenna arrays with different delay line lengths connecting the antenna elements as shown in Figure 2.12 can be used. The design equation for the delay line lengths  $W(r)$  satisfying the path length equality condition for a focal point on the optical axis at a distance  $F$  behind the lens is given by:

$$W(r) = \sqrt{F^2 + \left(\frac{D}{2}\right)^2} - \sqrt{F^2 + r^2} \quad (2.11)$$

where  $D$  is the diameter of the lens and  $r$  is the radial length from the optical axis to the individual antenna element as shown in Figure 2.12. Such a lens is the discrete-element ("constrained") analog to an optical "thin lens" since Equation 2.11 is the same as the "thickness" function for a spherical thin lens [70].

The path length error for an element located at  $(r, \phi)$  on the array and a given scan angle  $\theta$  is given by Equation 2.12. Where the focal surface minimizing

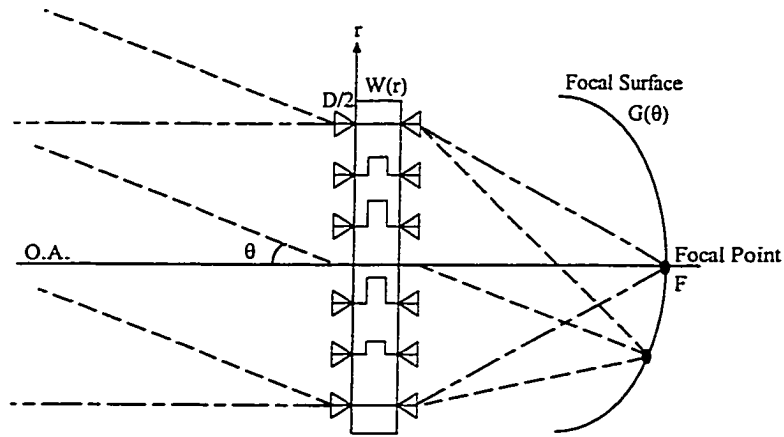


Figure 2.12: Geometry of a planar constrained lens with one degree of freedom.

the path length error,  $\epsilon_i(r, \theta, \phi)$  is given by  $G(\theta)$ . Notice that the path length error only arises for  $\theta \neq 0$ . The normalized RMS path length error for an  $N$ -element array is then given by Equation 2.13.

$$\epsilon_i(r, \theta, \phi) = \sqrt{\left( (G \sin \theta + r \cos \phi)^2 + G^2 \cos^2 \theta \right) + r^2 \sin^2 \theta} - \sqrt{G^2 + r^2} - r \cos \phi \sin \theta \quad (2.12)$$

$$\left( \frac{\epsilon}{F} \right)_{\text{RMS}} = \sqrt{\frac{1}{N_{\text{elements}}} \sum_i \left( \frac{\epsilon_i}{F} \right)^2} \quad (2.13)$$

The focal surface  $G(\theta)$  minimizing the path length error for a one degree of freedom lens design can be numerically calculated for lenses with different F-numbers as shown in Figure 2.13. The minimized path length errors associated with each of these focal surfaces are plotted in Figure 2.14. Notice how the path length error increase for lower F-number lenses.

Beam steering of about  $25^\circ$  was measured for the three passive 14-element  $X$ -band lenses with different F-numbers and fed by a WR-90 waveguide as shown in Figure 2.15. A broader main beam as well as higher side lobe levels were expected as an effect of the increased path length error [69]. The measured patterns show no noticeable degradation in beam steering between these lenses, and no conclusion

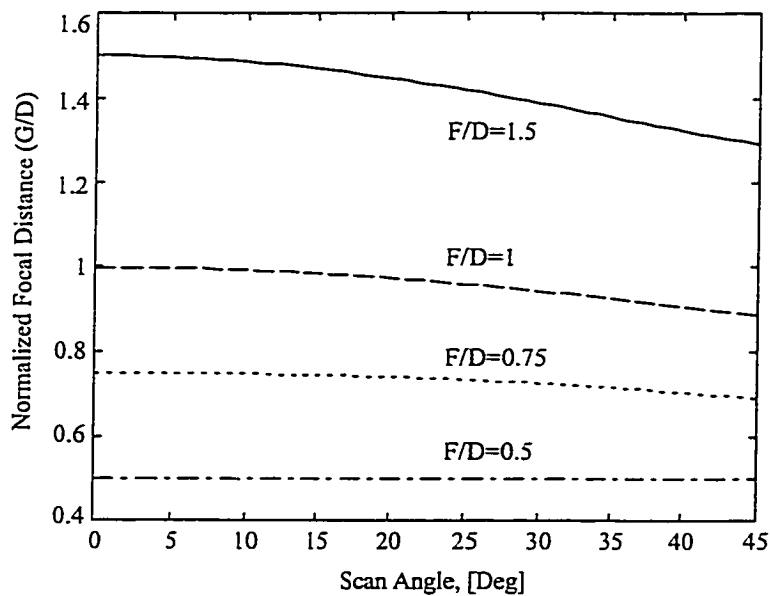


Figure 2.13. Focal surfaces for different F-number lenses with one degree of freedom, as calculated for the 14-element lens.

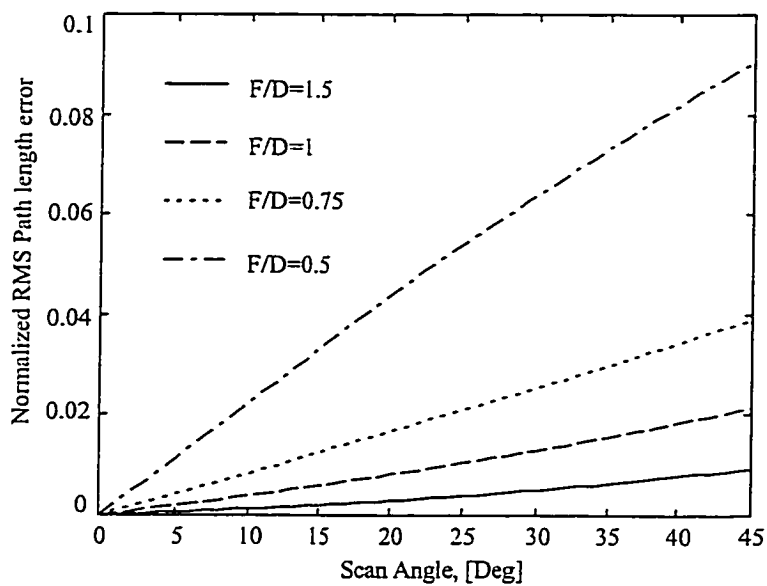


Figure 2.14. Minimized path length errors versus scan angle for different F-number lens designs of a one degree of freedom lens.

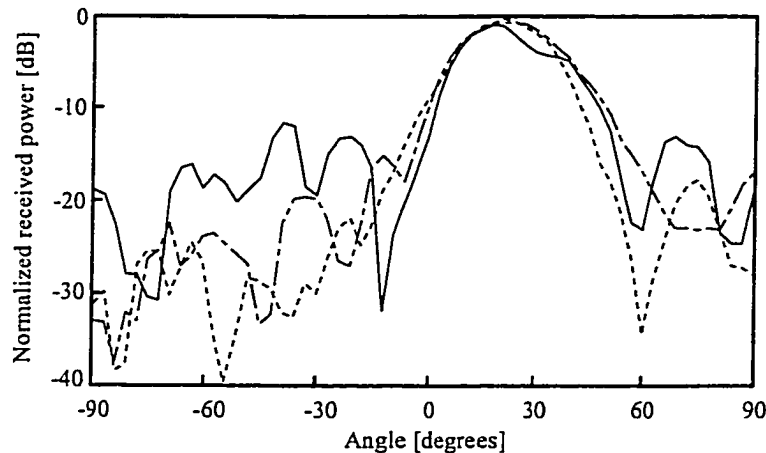


Figure 2.15. Measured beam-steering patterns with a waveguide feed for the three X-band passive 14-element lenses with  $F=12$  cm (solid line),  $F=8$  cm (dashed-dotted line) and  $F=6$  cm (dotted line). The measured patterns are normalized to the maximum power received when the feed is located on the optical axis behind the lenses.

to the effect of increased path length errors can be made. The maximum received power is about 1 dB below the measured power levels with  $0^\circ$  beam steering for the three lenses. The reduced gain is expected from the increased spill-over loss at the feed side, a less uniform amplitude distribution across the array, as well as a lower directivity (or effective area) of the output array when the feed is moved off-axis.

It was found in [69] that the path length errors of a one degree of freedom lens are mostly cubic functions of  $r$  or "Coma" aberrations. By moving the feed closer to the lens (refocusing), the path length errors can be slightly reduced. To reduce the path length errors and improve the beam-steering capabilities of planar lens arrays further, a second degree of freedom can be utilized by displacing the input and output elements relative to each other. This design allows for either two perfect focal points or a "cone of best focus" placed at an angle  $\theta_0$  from the optical axis and a distance  $F$  from the lens array. It has been shown that the path length errors for this design are mostly second-order "focusing" aberrations which can be significantly reduced by "refocusing" (moving the feed closer or farther away from the lens). The two degree of freedom errors are significantly lower than the one degree of freedom

errors. However, even with refocusing, the path length errors for the two degrees of freedom lens are far greater than for a similar Rotman lens which employ three degrees of freedom. The chief advantage to the one and two degree of freedom lenses is the potential ease of fabrication.

The design equations for the input and output array antenna locations ( $r, \rho$ ) as well as the delay line lengths ( $W$ ) connecting them for a two degree of freedom lens are given by:

$$\rho = r \sqrt{\frac{F^2 - r^2 \sin^2 \theta_0}{F^2 - r^2}} \quad (2.14)$$

$$W = F + W_0 - \frac{1}{2} \sqrt{F^2 + \rho^2 - 2\rho F \sin \theta_0} - \frac{1}{2} \sqrt{F^2 + \rho^2 + 2\rho F \sin \theta_0} \quad (2.15)$$

The focal surfaces and associated path length errors for this design are explained in [69, 13]. While Schoenberg *et al.* demonstrated lenses with two degrees of freedom, the simpler one degree of freedom lens design with identical feed and front side arrays is used for the lenses presented here.

### 2.3 Design Constraints

The first step in designing a lens amplifier array is to determine certain design specifications such as gain, bandwidth, output power, noise-figure, directivity, size, cost, and functionality (e.g. beam steering). Once these parameters are specified, one can optimize several design parameters to achieve these goals. The design parameters in a lens design are feed antenna type and position, array size and layout, input and output antenna elements and amplifier elements. The following sections describe these design parameters in more detail.

### 2.3.1 Feed Antenna and Feed Position

The feed antenna used for most lens amplifiers presented to date has been an E-plane horn due to its relatively high directivity. To provide a spherical wave to the input side of the array, it is essential to use a feed antenna with a far-field distance shorter than the focal length of the lens array. Open waveguide sections, microstrip patch or slot antennas can also be used, but with increased spill-over loss due to the lower directivity of these antennas. However, a more directive feed antenna results in a less uniform amplitude distribution which lowers the directivity of the output array. Dielectrically-loaded horns and multi-mode horns, often used to optimize the spill-over and illumination loss of reflector antennas, seem attractive for feeding a constrained lens [71].

The feed location or focal length of the lens array should also be chosen to minimize the spill-over loss, while maintaining relatively uniform amplitude distribution and satisfactory focal length phase error for beam-steering applications. While F-numbers of less than one can be used to minimize the spill-over loss as indicated in Figure 2.4, larger F-number lenses might be desirable for beam-steering applications with low side-lobe levels. Figure 2.14 shows the simulated phase error for lens arrays with different F-numbers. Ideally, the feed antenna should also be designed to minimize standing waves between the feed antenna and the lens array. While it is almost impossible to remove these reflections entirely, the focal length can be set to a multiple of half-wavelengths to maximize the gain.

### 2.3.2 Input and Output Antenna Arrays

The aperture loss of an antenna array corresponds to the power incident on the array area that is reflected instead of coupled into the antenna elements. The aperture efficiency is a function of element size  $A_{\text{element}}$  and gain of the radiating elements  $G_{\text{element}}$  as given below:

Quasi-Optical Lens Amplifier	Unit Cell Size	Aperture Efficiency, $\eta_A$
Schoenberg [35]	$0.75 \times 0.9 \lambda$	0.6
Schoenberg [32] (w/polarizers)	$0.75 \times 0.9 \lambda$	0.21 (0.42)
Berg [61]	$0.63 \times 0.83 \lambda$	0.75
Hollung [44] (w/polarizers)	$1.17 \times 1.23 \lambda$	0.1 (0.2)
Hollung, Chapter 4	$1 \times 1 \lambda$	0.3

Table 2.2. Estimated aperture efficiencies of various quasi-optical lens amplifier arrays.

$$\eta_A = \frac{A_{\text{effective}}}{A_{\text{physical}}} = \frac{G_{\text{element}} \lambda^2}{4\pi A_{\text{element}}} \quad (2.16)$$

While Equation 2.16 predicts the aperture efficiency of the front side array, it can not be applied to the feed side array. To accurately predict the aperture efficiency of the feed side array, the gain of each radiating element in the direction of the feed must be used in the calculations.

$$\eta_{A,\text{feed}} = \frac{1}{N_{\text{elements}}} \sum_i \frac{G_{\text{element}}(\theta_i, \phi_i) \lambda^2}{4\pi A_{\text{element}}} \quad (2.17)$$

While the aperture loss is minimal for the 14-element lens described in Section 2.1.2, the aperture loss is dominating the total feed loss in other arrays. The estimated aperture efficiencies including antenna efficiencies for the lens amplifiers presented to date, are summarized in Table 2.2. It is evident that the aperture efficiency can be a dominating loss factor in lenses with large unit cells. The aperture efficiency of the lens array presented in Chapter 3 is as low as 20% (7-dB loss).

To obtain a high aperture efficiency and hence reduce the feed loss of the lens array, the unit-cell size should be minimized. A high permittivity substrate can be used to reduce the size of the antennas as well as the circuits. In addition to scaling the antenna size, the choice of substrate material also affects several other antenna characteristics such as radiation efficiency, bandwidth, and input impedance. A higher dielectric constant material is likely to add loss due to increased excitation



of substrate modes or surface waves. Multiple substrate layers [72, 61] or tiles of substrates [28] can be used to achieve a smaller unit cell.

A wide variety of planar antennas have been used in quasi-optical amplifier arrays to date. Some of the antennas used are microstrip fed patches [32, 72, 61], CPW fed second resonant slots [13], multiple slot antennas [73] and tapered slots [40]. Other planar antennas such as bow-tie antennas and dielectric resonator antennas can also be used. Second-resonant slot antennas offer relatively high bandwidth, but they are larger than resonant antennas and thus results in a lower aperture efficiency. The radiation patterns of the center-fed second-resonant slot antennas often have nulls in the broadside direction, which will reduce the broadside antenna gain of an array. These antennas also requires the use of polarizers at the input and output of the array to achieve high gain. Microstrip patch antennas have been used in several quasi-optical amplifiers, but they require double-layer substrates [72] or alternating ground planes [35] to operate in transmission mode. Microstrip patches also suffer from limited bandwidth. To avoid substrate mode excitations from a patch, the following design criterion for the substrate thickness should be satisfied [74]:

$$h < \frac{c}{4f_u \sqrt{\epsilon_r - 1}}, \quad (2.18)$$

where  $h$  and  $\epsilon_r$  are the substrate thickness and dielectric constant,  $c$  is the speed of light, and  $f_u$  is the highest operating frequency.

Ideally one would make the unit cells as small as possible to achieve good aperture efficiency and low side-lobe levels. There are however limitations to how small a unit cell can be made. As the unit-cell size is reduced, coupling between the antennas increases. For a stable design, the coupling between the input and output antenna elements should always be less than the gain of the amplifier connecting them. In designing arrays with strong coupling, special care must be taken when

designing the individual array elements. The edge elements in the array are coupled less than the center elements and thus behave differently.

To maximize the directivity and thus the EIRP of an array, it is of interest to see how the unit-cell size affects the directivity. The directivity of two lens designs with 21 and 37 elements in a rectangular layout as well as two lens designs with 24 and 37 elements in a triangular layout are plotted versus element size in Figure 2.16. The directivities are calculated using the measured radiation pattern of a single patch antenna. A rectangular layout is used for the 20- and 36-element arrays presented in Chapter 4, and a triangular layout is used for the 24-element array presented in Chapter 3. For a given number of elements, the directivity of a rectangular layout is maximized for a unit-cell size of about  $0.9 \lambda$  by  $0.9 \lambda$ . For a triangular layout, the maximum directivity occurs for a slightly larger unit-cell size of  $\lambda$  by  $\lambda$ .

While the directivity increase as a function of array area for an element separation of less than  $0.9 \lambda$ , the feed loss also increase as a function of element size due to the reduced aperture efficiency of the feed side array. In order to maximize the antenna gain of these lens arrays, the effect of both the feed loss and directivity combined must be investigated. The simulated antenna gains for the same 21- and 37-element rectangular arrays as well as the 24- and 37-element triangular arrays are plotted in Figure 2.17. An E-plane horn is used for the feed antenna, and the F-number is kept constant at 0.5 for all unit-cell sizes. The patches are assumed to be 80% efficient and have 6-dB directive gain. No loss is included for the delay lines and a uniform phase distribution is assumed. Notice how the antenna gains are almost constant for a unit-cell spacing smaller than  $0.8\lambda$ . For a high antenna gain design, the element size should therefore be chosen less than 0.8 wavelengths square. A slightly larger unit cell can be used if a triangular layout is used. For a patch array with a unit-cell size of about 0.8 wavelengths square, the aperture efficiency is typically around 75% (or -1.3 dB).

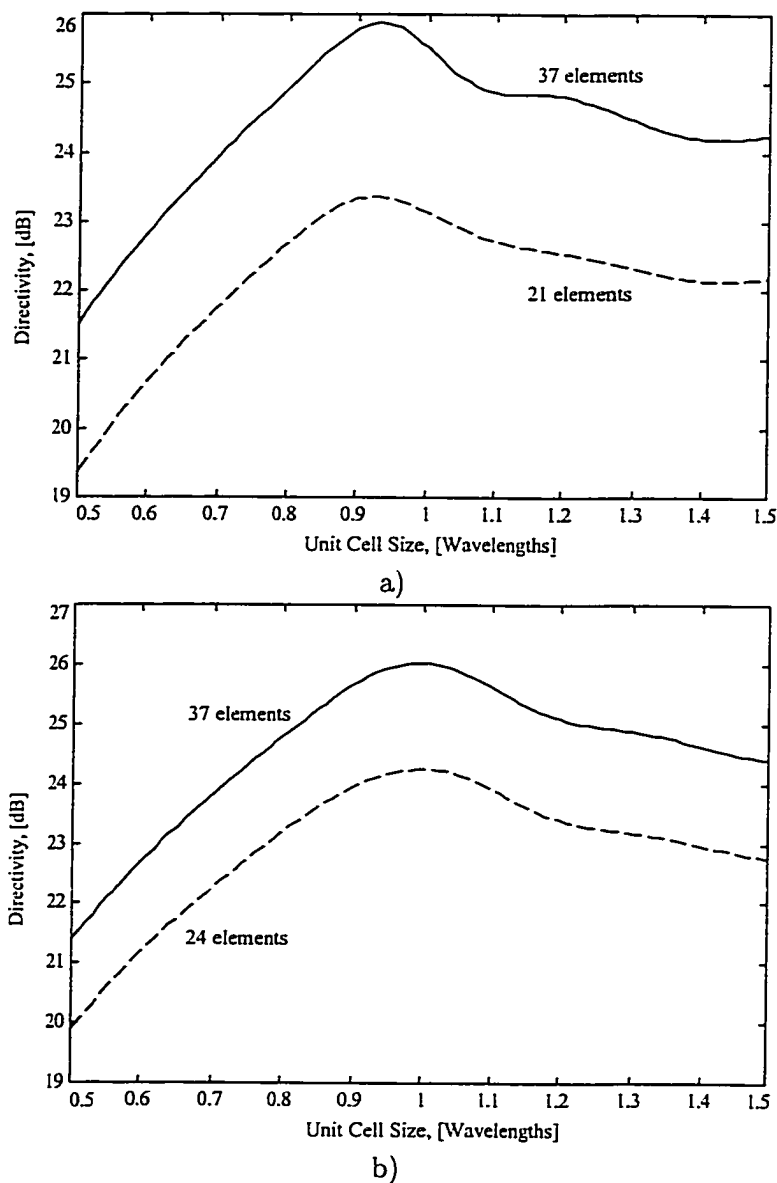
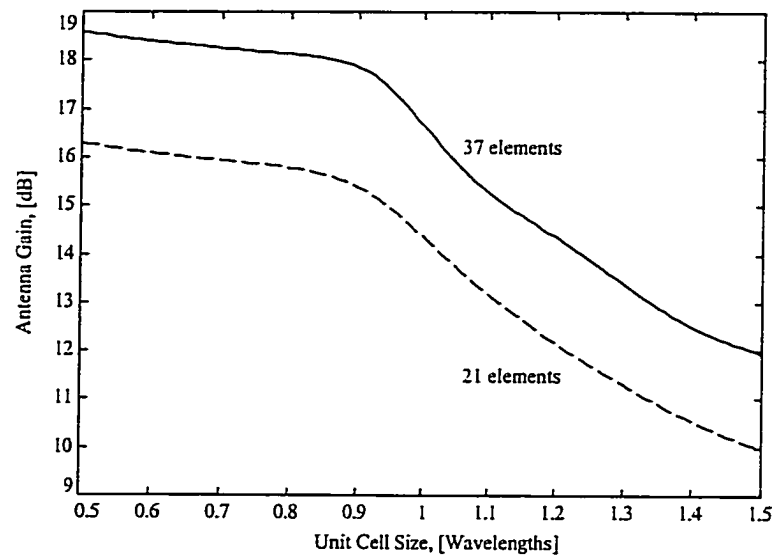
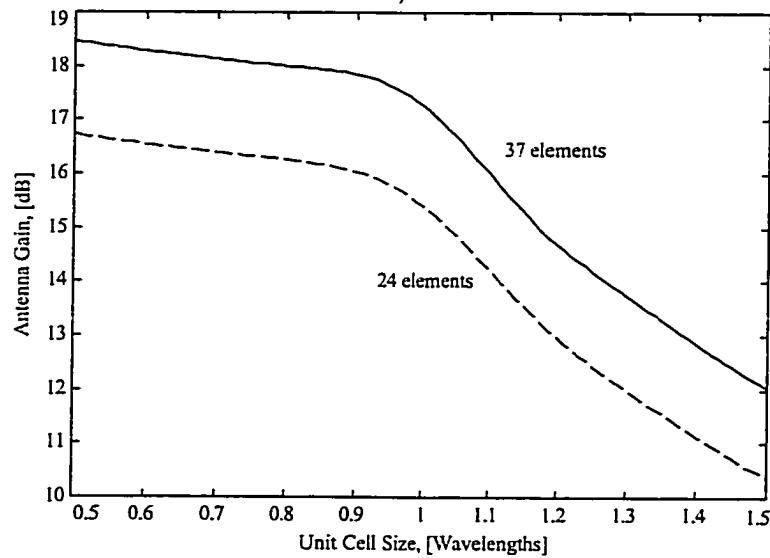


Figure 2.16. a) Simulated directivity of a 37- (solid line) and a 21-element (dashed line) array with rectangular layout versus element size in wavelengths. b) Simulated directivity of a 37- (solid line) and a 24-element (dashed line) array with triangular layout versus element size in wavelengths. Uniform amplitude and phase distribution across the array is assumed, and the measured pattern of a patch antenna are used in the simulations.



a)



b)

Figure 2.17. a) Simulated antenna gain (including feed loss) of a 37- (solid line) and a 21-element (dashed line) array with rectangular layout versus element size in wavelengths. b) Simulated antenna gain (including feed loss) of a 37- (solid line) and a 24-element (dashed line) array with triangular layout versus element size in wavelengths. The F-number of the array is set to 0.5, and an E-plane horn feed is used. The patches are assumed to be 80% efficient and have 6-dB directive gain. No loss is included for the delay lines.

As the unit-cell size decrease, the heat from the amplifiers per area also increases. For high-power amplifier arrays this becomes a limiting factor. It is therefore important to investigate the thermal properties of the circuit when deciding on a circuit geometry, substrate materials and antenna elements.

### 2.3.3 Amplifier Element

To overcome the feed loss of a quasi-optical amplifier it is important to use an amplifier stage with sufficient gain. At millimeter wavelengths, the gain from a single solid state amplifier stage is limited. Several amplifier stages have been used to achieve sufficient gain. To obtain a small unit cell, a relatively small amplifier circuit is essential. At high millimeter-wave frequencies, monolithic design techniques must be used to achieve a compact design [37]. In the microwave and low millimeter-wave bands, hybrid design techniques using MMIC amplifiers can be used [33]. The maximum gain of the amplifier stage is determined by the isolation between the input and output antenna elements for a stable design. Because the input impedance of the antenna elements often varies dramatically with frequency, the amplifier stage should be unconditionally stable to ensure a stable circuit.

In a receive array, a low-noise amplifier element can be used to achieve high dynamic range. In a transmit array, a power amplifier stage can be used to achieve high effectively radiated power. The operating bandwidth of a quasi-optical array is usually limited to a few percent due to the bandwidth of the radiating elements. The bandwidth of the amplifier elements can thus be designed to be relatively narrow. If a broadband antenna such as a bow-tie is used for the radiating elements, a broadband amplifier design should also be used. To reduce the generated heat from the active circuits, high efficiency amplifiers have been developed [36, 75, 34].

### 2.3.4 Array Size and Layout

The optimum number of elements is determined by the desired effective isotropic radiated power (EIRP) from the array. Because heat generated in the array elements are mostly dissipated from the edges of the array, cooling can become a problem for large arrays. For certain applications a compact and less complex design can be desired. The array can be designed in a rectangular or triangular layout. The triangular layout reduces the grating-lobe levels and can therefore be used to improve the beam-steering capabilities of an array [13]. A rectangular layout can however reduce coupling between the individual antennas [76]. To further improve beam steering, a lens design with two degrees of freedom can be used to minimize the path length error for large scan angles. A rectangular design often leads to a reduced unit-cell size and simpler design, because it is easier to layout the necessary DC bias lines to each unit cell. The bias lines should be as thin as possible to minimize coupling in the array, while being sufficiently wide to reduce ohmic loss and provide uniform DC bias to the array elements. The widths of the bias lines used in the arrays presented in Chapters 3 and 4 are 0.3 and 0.2 mm, respectively. For a given F-number and feed antenna, the array size must be sufficiently large for the focal length to be longer than the far-field distance of the feed antenna. However, the delay-line lengths increase with array size, and can become hard to fit in a small unit cell for large arrays.

### 2.3.5 Other Design Issues

In certain applications (e.g. satellite communications) a compact design is important. Optical techniques such as folding can be used as shown in Chapter 4 to reduce the size of the lens system. In a practical application, the lens front-end would be placed in a metallic enclosure. To investigate the effect on the lens performance, a metallic horn-like enclosure was added on the feed side as shown in

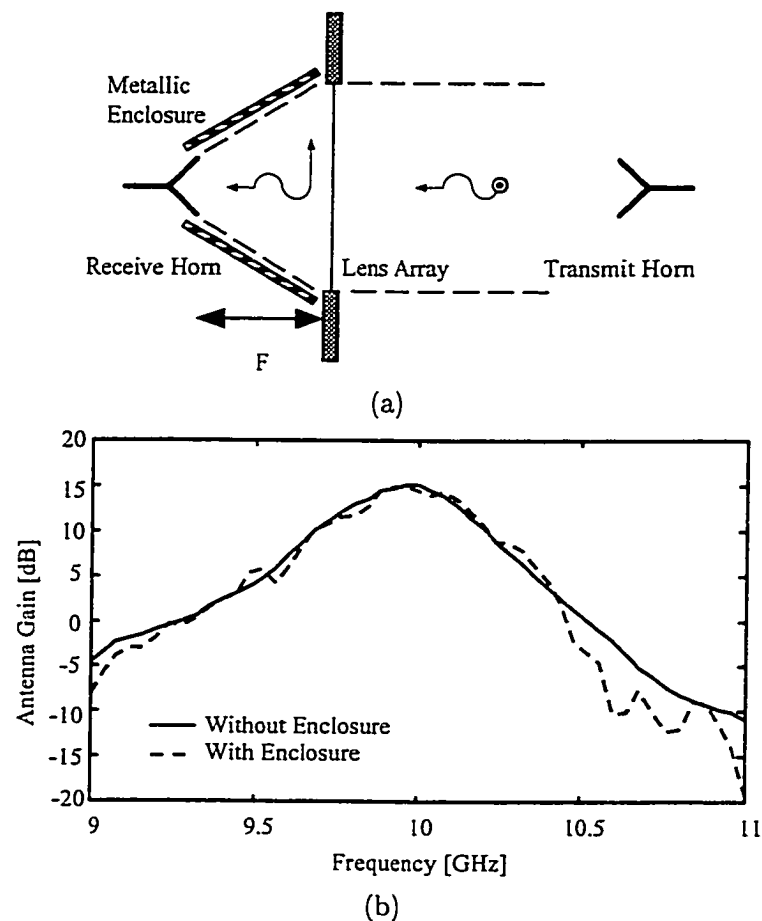


Figure 2.18. (a) Experimental set-up for the 14-element array with the feed side enclosed in a metallic enclosure. (b) Measured antenna gain of the active lens amplifier array presented in [61]. Solid lines shows the results without an enclosure and the dashed lines shows the results for the lens in a setup with a metallic enclosure.

Figure 2.18. The measured antenna gain in Figure 2.18 and radiation patterns show minimal degradation due to the metallic enclosure when fed by the E-plane horn. If a less directive feed antenna such as an open ended WR-90 waveguide is used, the radiation pattern is more distorted.

For a high power design, it is necessary to implement a layout that can dissipate the heat generated by the active circuits [77]. A test fixture using Fluorinert FC-43 coolant liquid can be used to reduce the heat [33]. Substrate materials with high thermal conductivity such as sapphire, diamond and aluminum nitride can also

be used to remove the heat.

## 2.4 Figures of Merit

A variety of gain, efficiency and output power definitions for quasi-optical amplifiers are presented in the literature. This often makes it difficult or even impossible to compare the reported results. Some work toward developing standard figures of merit for power-combining arrays has been published by Gouker [78]. Because the different power-combining circuits are designed with different applications in mind, it is hard to agree on a set of standard evaluation criteria and calibration techniques. The following sections describes and compares some of the different definitions that are used to describe quasi-optical amplifier arrays.

### 2.4.1 Output Power

The only unambiguous measurement for a transmitting array is the effectively isotropic radiated power (EIRP or ERP). The EIRP is defined as the product of the transmitted power  $P_t$  and the directive gain of the output antenna array  $G_t$ . Using the Friis transmission formula, the measured power  $P_{\text{meas}}$  received by a receive antenna with gain  $G_{\text{meas}}$  at a distance  $R$  in the far field in front of the array is related to the transmitted power as shown below.

$$P_{\text{meas}} = P_t G_t G_{\text{meas}} \left( \frac{\lambda}{4\pi R} \right)^2 \quad (2.19)$$

The EIRP can then be calculated from the received power.

$$EIRP = P_t G_t = \frac{P_{\text{meas}}}{G_{\text{meas}}} \left( \frac{4\pi R}{\lambda} \right)^2 \quad (2.20)$$

The total radiated RF power  $P_{\text{rad}}$  from the array is important for estimating the DC-to-RF efficiency, system gain, and combining efficiency. This power can



be approximated by integrating over the experimentally determined 3D radiation pattern. Notice that the total radiated power  $P_{\text{rad}}$  is lower than the transmitted power  $P_t$  due to losses in the output array accounted for in the previous equation by using the gain  $G_t$  instead of the directivity  $D_t$ . The total radiated power can now be calculated from the measured EIRP.

$$P_{\text{rad}} = \frac{EIRP}{D_t} \quad (2.21)$$

The directivity of the transmit array (unlike the gain) can be calculated relatively accurately from the radiation pattern by using Equation 2.22. For a uniformly excited array the directivity can be estimated from the physical aperture.

$$D_t = \frac{4\pi |E(\theta, \phi)|_{\text{max}}^2}{\int_0^{2\pi} \int_0^\pi |E(\theta, \phi)|^2 \sin\theta d\theta d\phi} \quad (2.22)$$

Where  $E(\theta, \phi)$  is the radiated electric field pattern in the far field in front of the array given by the product of the array factor and the pattern of a single element.

#### 2.4.2 Power Gain

Once the radiated power is estimated, one can define the system gain  $G_{\text{system}}$  of a transmitting array as

$$G_{\text{system}} = \frac{P_{\text{rad}}}{P_{\text{in}}}, \quad (2.23)$$

where  $P_{\text{in}}$  is the power delivered to the feed horn. This gain definition includes the feed loss from the feed antenna to the active elements as well as the gain contributed by the array. While this definition requires the directivity of the transmit array to be estimated, an antenna gain,  $G_{\text{antenna}}$ , including the directivity of the transmit array can be defined:

$$G_{\text{antenna}} = \frac{EIRP}{P_{\text{in}}} = G_{\text{system}} D_t \quad (2.24)$$

For quasi-optical amplifier arrays fed from the far field, the feed loss at the input can be much greater than the active gain of the array [13]. It is therefore essential to use dielectric lenses or use a near-field feed with lensing to achieve real gain.

Notice that most far-field fed quasi-optical amplifier arrays often calibrate out the feed loss at the input side and reports the effective power gain  $G_{\text{eff}}$  contributed only by the active elements in the array. First, a calibration is performed without the quasi-optical amplifier array between the transmitting and receiving horns. The array is next inserted and the received power measured  $P_{\text{meas}}$ . The effective isotropic power gain (EIPG) are then defined as given below.

$$EIPG = G_r G_{\text{active}} G_t = \frac{P_{\text{meas}}}{P_{\text{cal}}} \frac{(r_1 + r_2)^2}{r_1^2 r_2^2} \left( \frac{4\pi}{\lambda} \right)^2 \quad (2.25)$$

By calculating the directivities of the receiving and transmitting arrays as indicated in the previous section, the effective power gain can be estimated.

$$G_{\text{eff}} = \frac{EIPG}{D_r D_t} \quad (2.26)$$

In grid amplifier arrays [30, 29], the directivities are often estimated by the physical aperture of the array. Then the effective gain becomes:

$$G_{\text{eff}} = \frac{EIPG}{A_{\text{phys}}^2} \left( \frac{\lambda^2}{4\pi} \right)^2 \quad (2.27)$$

The definition of absolute gain was introduced by Schoenberg [13]. Where *absolute* is used to describe an increase in the EIRP of a source due to using a quasi-optical amplifier array in a transmitter. The active array is placed at the plane of an aperture cut out of a large absorbing sheet. A through measurement without the

array inserted is first performed as a calibration. The quasi-optical amplifier array is next inserted, and the received power measured. The absolute gain is then defined as

$$G_{\text{abs}} = \frac{P_{\text{meas}}}{P_{\text{cal}}}. \quad (2.28)$$

Both the absolute gain definition and the antenna gain definition are used in Chapters 3 and 4. For a quasi-optical lens with a small F-number, the absolute and antenna gains can be related as follows:

$$P_{\text{meas}} = P_{\text{in}} G_{\text{antenna}} G_{\text{meas}} \left( \frac{\lambda}{4\pi R} \right)^2 = G_{\text{abs}} P_{\text{cal}} \quad (2.29)$$

where

$$P_{\text{cal}} = P_{\text{in}} G_{\text{f}} G_{\text{meas}} \left( \frac{\lambda}{4\pi(R+F)} \right)^2 \quad (2.30)$$

then

$$G_{\text{antenna}} = \frac{G_{\text{abs}} G_{\text{f}} (R+F)^2}{R^2} \quad (2.31)$$

where  $G_{\text{f}}$  is the gain of the feed antenna. In these equations, it is assumed that the focal length is short and the aperture does not affect the through calibration of the absolute power gain.

A passive array with the active elements replaced by through lines is often used to accurately measure the average gain of the active elements in the array  $\overline{G_{\text{active}}}$ . The average active gain is then simply given by the ratio

$$\overline{G_{\text{active}}} = \frac{G_{\text{abs,active}}}{G_{\text{abs,passive}}} = \frac{G_{\text{antenna,active}}}{G_{\text{antenna,passive}}}. \quad (2.32)$$

### 2.4.3 Power Combining Efficiency

The combining efficiency describes how effectively the combiner is summing the available power from the individual devices. In a quasi-optical array the combining efficiency can be defined as the ratio of the total radiated power to the sum of the maximum possible power available from each of the devices in the array.

$$\eta_{\text{comb}} = \frac{P_{\text{rad}}}{\sum_i^N P_{i,\text{avail}}} \quad (2.33)$$

If the loss in the transmitting antenna elements is not included in the combining efficiency, another combining efficiency can be defined as

$$\eta_{\text{comb}} = \frac{\overline{G_{\text{active}}}}{G_{\text{active,element}}} \quad (2.34)$$

where  $G_{\text{active,element}}$  is the measured power gain of a single circuit amplifier. This combining efficiency will always be higher than the efficiency based on the previous definition.

## CHAPTER 3

### A MICROWAVE TRANSMIT/RECEIVE QUASI-OPTICAL LENS AMPLIFIER ARRAY

#### 3.1 Motivation

Several transmission-mode plane-wave fed quasi-optical amplifiers for microwave and millimeter-wave power combining have been presented to date [30, 73, 31]. Each of these amplifiers is fed with a plane wave from a source in the far field as was discussed in Chapter 2. In order to improve feed efficiency without using external lenses, lens amplifier arrays were developed [35, 41]. In a transmission-mode lens amplifier, the feed is placed in the near field along the focal surface, thereby minimizing diffraction loss. In transmission, a lens amplifier can provide high effective radiated power. A lens amplifier can also be used in reception, offering high dynamic range because the noises contributed from the individual amplifiers are uncorrelated [13]. In reception, a plane wave is received, amplified and focused onto a mixer [49]. The transmit and receive functions of a lens amplifier can be combined to form a quasi-optical T/R module as shown in Figure 3.1. In this chapter a 24-element bi-directional quasi-optical lens amplifier with a unit cell as shown in Figure 3.2 is presented. Section 3.2 describes the unit cell, Section 3.3 discusses the array, and Section 3.4 describes some applications for this lens array.

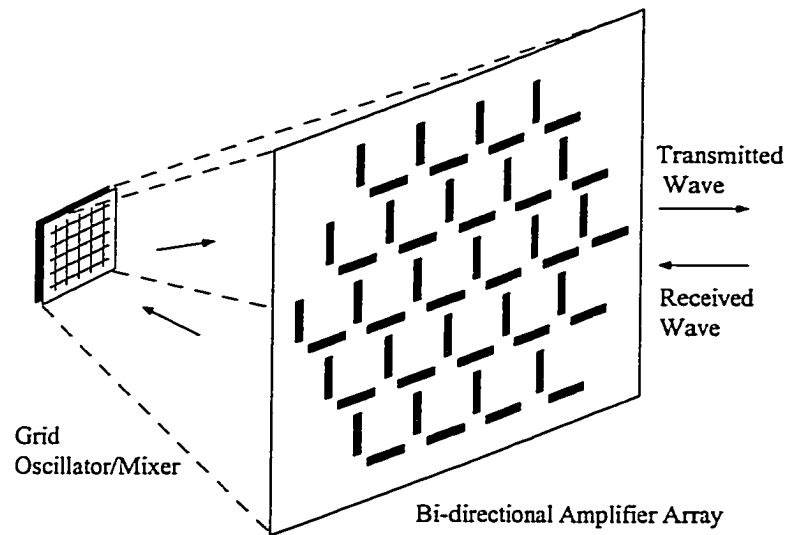


Figure 3.1. A quasi-optical T/R module consisting of a transmit/receive amplifier and a grid oscillator/mixer.

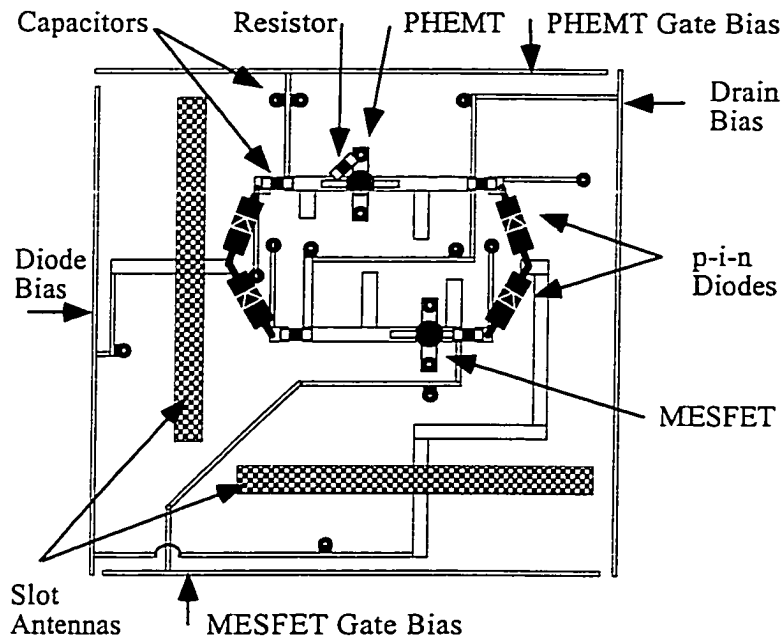


Figure 3.2. A transmit/receive X-band quasi-optical array amplifier element. The slot antennas are 2.5 cm long and 2 mm wide, and the unit cell dimensions are 3.5 by 3.7 cm.

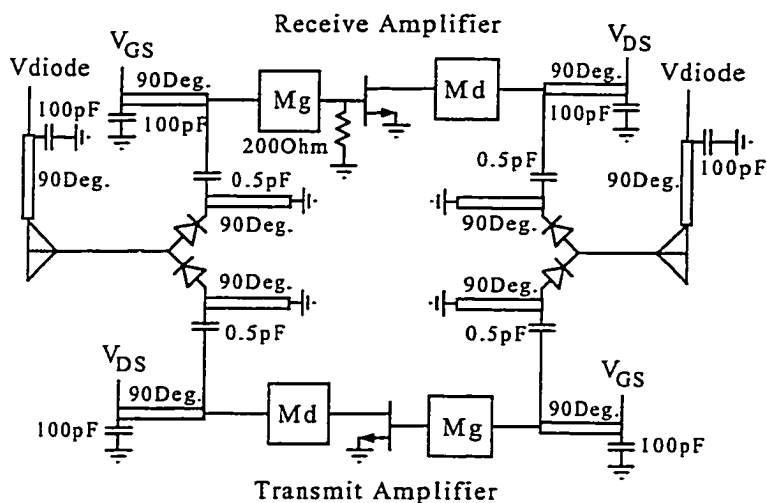


Figure 3.3. Circuit schematic of the unit cell. Both amplifiers are matched for gain with matching circuits  $M_g$  at the gates and  $M_d$  at the drains.

### 3.2 Single Array Element

A bi-directional transmission amplifier element, designed to operate around 10 GHz, was fabricated on a 0.507-mm-thick Duroid substrate with  $\epsilon_r = 2.2$ . A circuit schematic of the array element is shown in Figure 3.3. Orthogonally polarized antiresonant slot antennas were used at the input and output because of their wide bandwidth and ease of fabrication with microstrip feed lines. Figure 3.4 shows the measured and simulated return loss for a single slot antenna. A 2:1 VSWR bandwidth of about 40 % was measured. The measured E- and H-plane radiation patterns for a single slot antenna are shown in Figure 3.5. The H-plane pattern shows a null in the boresight direction as expected for a center-fed second resonance slot. Both the characteristic impedance of the microstrip and the antenna input impedance are  $65 \Omega$ , to avoid additional matching sections for the antennas. Two SPDT switches are used to switch between a general-purpose MESFET amplifier stage for transmit mode and a PHEMT amplifier stage for receive mode. Both amplifiers are matched for gain in this unit cell. The receive amplifier is stabilized with a 200- $\Omega$  chip resistor from gate to source. Two *p-i-n* diodes are used for each switch. The DC bias for

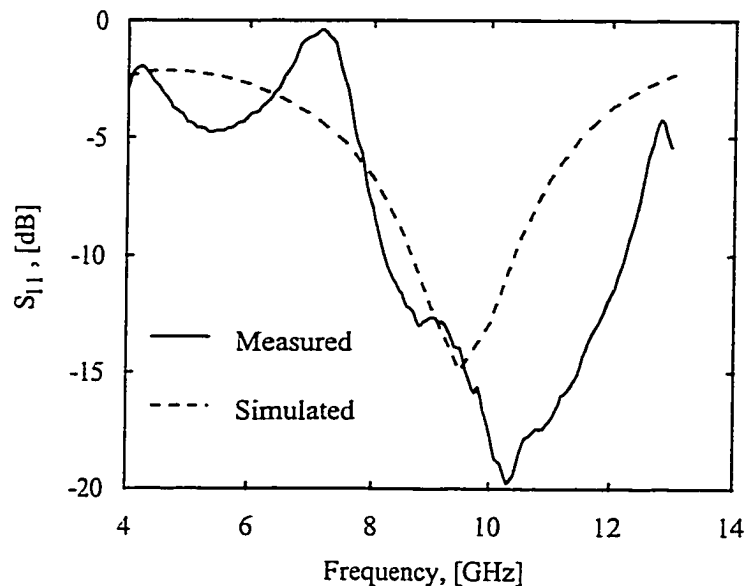


Figure 3.4. Measured (-) and simulated (--) return loss for a single slot antenna. The simulations were performed with the CAD package *Ensemble*.

the diodes is supplied through the slot antenna feed-lines. Both transistors share the same drain bias to reduce the number of bias lines.

Measurements for the unit cell are conducted using E-plane horns placed in the far field and connected to an HP 70820A microwave transition analyzer. In transmission, an incoming plane wave from a vertically polarized horn is amplified by the transmit amplifier, reradiated as a horizontally polarized plane wave, and received by a horizontally polarized horn. In reception, an incoming plane wave from the horizontally polarized horn is amplified by the receive amplifier, reradiated as a vertically polarized plane wave, and received by the vertically polarized horn. Polarizers are inserted at a half wavelength on each side of the unit cell to improve the gain. The received power is measured for both the transmit and receive amplifiers over a range of frequencies. The gains contributed by the amplifiers are approximately calculated from the Friis formula and plotted in Figure 3.6. A gain of 5.5 dB for the slot antennas with polarizers was used for the calculations, based



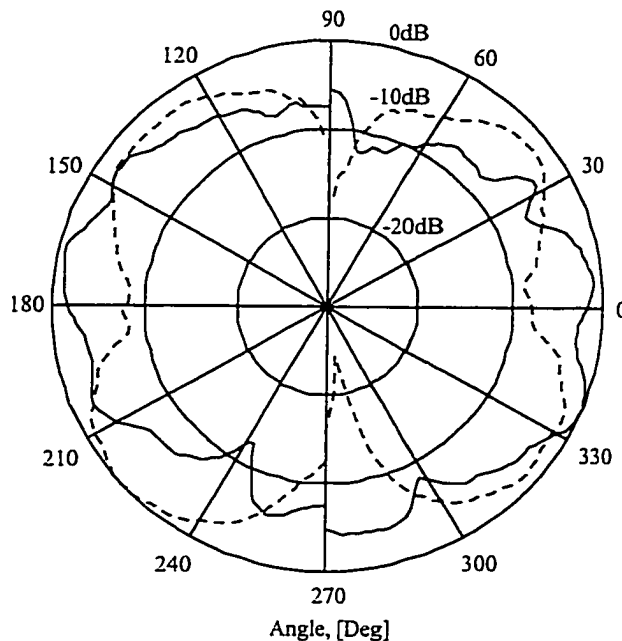


Figure 3.5. Measured radiation patterns for a single antiresonant slot antenna at 10 GHz.  $0^\circ$  represents the circuit side and  $180^\circ$  represents the ground plane. E-plane(-) and H-plane (- -).

on the measurement shown in Figure 3.5. The transmit amplifier has a maximum measured gain of 10 dB at 11 GHz. The receive amplifier has a measured gain of 7.5 dB at 10.8 GHz. Measured ON/OFF isolation of about 10 and 20 dB are seen for the receive and transmit amplifiers, respectively.

### 3.3 Transmit/Receive Lens Amplifier Array

The transmit/receive lens amplifier array consists of 24 elements in a triangular lattice with four elements in the first and fifth row, five elements in the second and fourth row, and six elements in the third row as shown in Figure 3.2. Lensing delay lines are incorporated between the antenna pairs in each unit cell. The delay line lengths were calculated using the design equations for a lens with one degree of freedom [69]. The focal distance of the array is 27.5 cm and the corresponding F-number is 1.5. Each element in the array measures  $3.5 \times 3.7$  cm. The gate bias lines

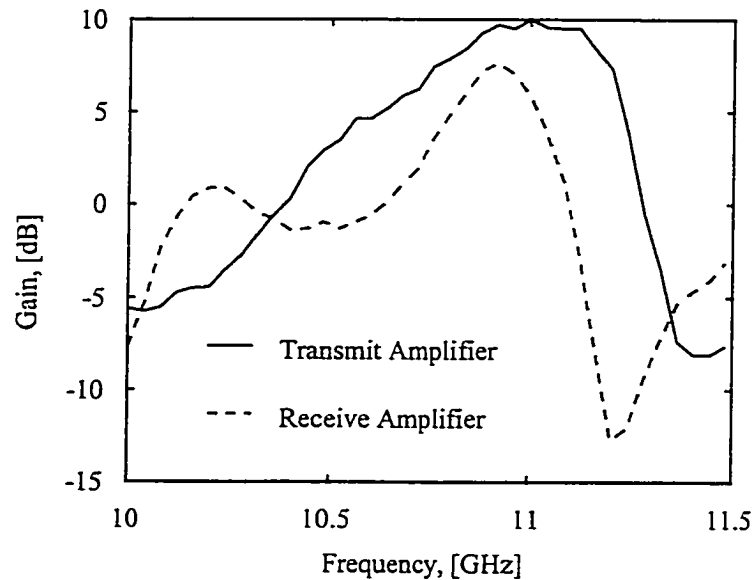


Figure 3.6. Measured gain of the transmit (-) and receive (--) amplifier in a unit cell.

are horizontal, while the drain and diode bias lines are distributed diagonally. An identical passive array, with the amplifiers replaced by  $65\text{-}\Omega$  through lines between the two slots, is used for calibration.

For reception, a transmit horn antenna, located in the far field of the array, provides a horizontally polarized incident plane wave to the array. The array receives, amplifies and reradiates a vertically polarized wave to a receive horn located at the focal point. For transmission, the signal path is reversed. Two polarizers are inserted at a half-wavelength distance on each side of the array. The passive array is measured to provide a reference for the measurements. The measurements are normalized to a through measurement with the transmit and receive horns co-polarized. A  $22 \times 26$  cm aperture cut out of absorbing material is used for this calibration.

Measurements were first performed with the 10 central elements populated. A measured ON/OFF isolation of 25 dB for both receive and transmit modes with 10 elements is seen. In receive mode, a maximum active power gain of about 10 dB relative to the passive array with 10 elements connected is measured at 9.4 GHz. In

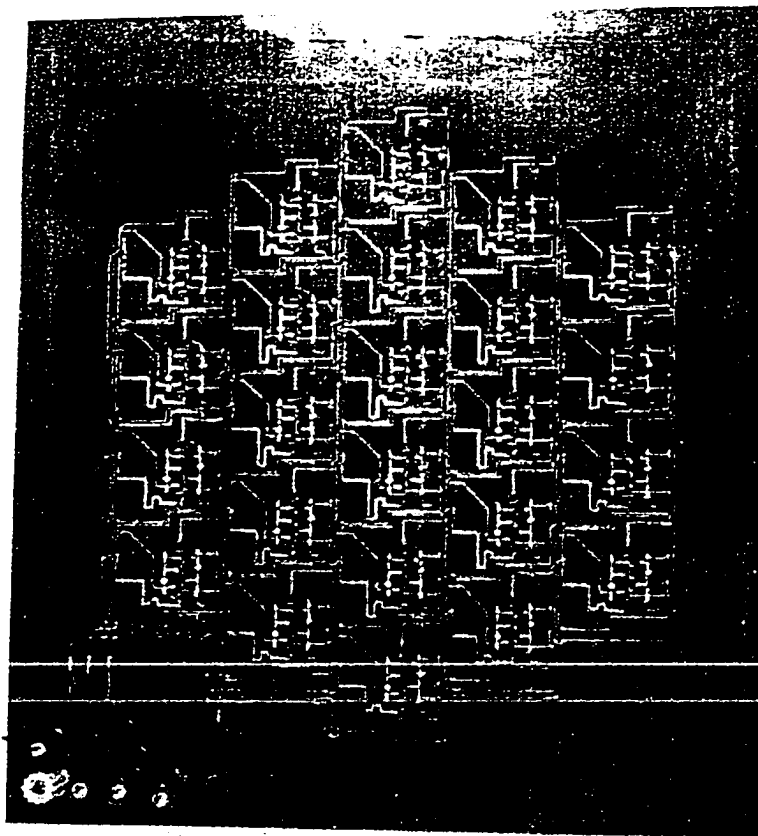


Figure 3.7. Photograph of the circuit side of the 24-element transmit/receive amplifier array. Orthogonally polarized slot antennas are located in the ground plane as indicated in Figure 3.2.

transmit mode, the measured active power gain is about 5 dB at 10.2 GHz.

These measurements were repeated with the 24 elements populated; the results are plotted in Figure 3.8. In receive mode, a maximum active power gain of 5.5 dB relative to the passive array with all 24 elements connected is measured at 10.1 GHz. The corresponding bias point for the array in receive mode is:  $V_{d,lna} = 1.5$  V,  $I_{d,lna} = 400$  mA, and  $I_{diodes} = 700$  mA. In transmit mode, the measured active power gain is 2.0 dB at 10.2 GHz. The optimum bias point for the array in transmit mode is:  $V_{d,pow} = 1.75$  V,  $I_{d,pow} = 500$  mA, and  $I_{diodes} = 700$  mA.

A possible explanation for reduction in gain when increasing the size of the array from 10 to 24 elements is increased non-uniformity of the amplifiers across the array. This could be due to fabrication, unmatched devices, coupling between unit cells, as well as a larger fraction of edge elements in the 24-element array as compared to the 10-element array. The absolute power gain relative to the rectangular aperture is 3.9 dB in reception and 0.9 dB in transmission. Measured ON/OFF isolation ratios of about 15 dB in receive mode, and more than 20 dB in transmit mode are seen. Notice that the physical area of the active antenna array only covers 55% of the aperture, so the absolute power gains are expected to be higher than those measured. Also note due to the limited performance bandwidth of the amplifiers, the active array is lossy compared to the passive array outside the amplifier gain range. The measured antenna gains shown in Figure 3.9 are 8.5 dB in reception and about 5 dB in transmission when the array is fed from an E-plane horn.

The 24-element lens amplifier has a measured beamwidth of about 10 degrees in both E and H-plane, with side-lobe levels of less than -10 dB as shown in Figure 3.10. The theoretical patterns were calculated using the measured radiation pattern of a single slot antenna. From the measured radiation patterns a directivity of about 25 dB is estimated for the output array. Using an antenna gain of about 3 dB from Figure 3.9 for the passive array, a relatively high feed loss of around 22 dB

for this lens amplifier array is calculated. The high feed loss for this array is largely due to the low aperture efficiency of about 20 % and large spill-over loss due to the high F-number of 1.5. A hybrid design with MMIC amplifiers/switches and a substrate with a higher dielectric constant can be used to reduce the unit-cell size and increase the aperture efficiency. A more directive feed and shorter focal length can be used to improve the spill-over loss.

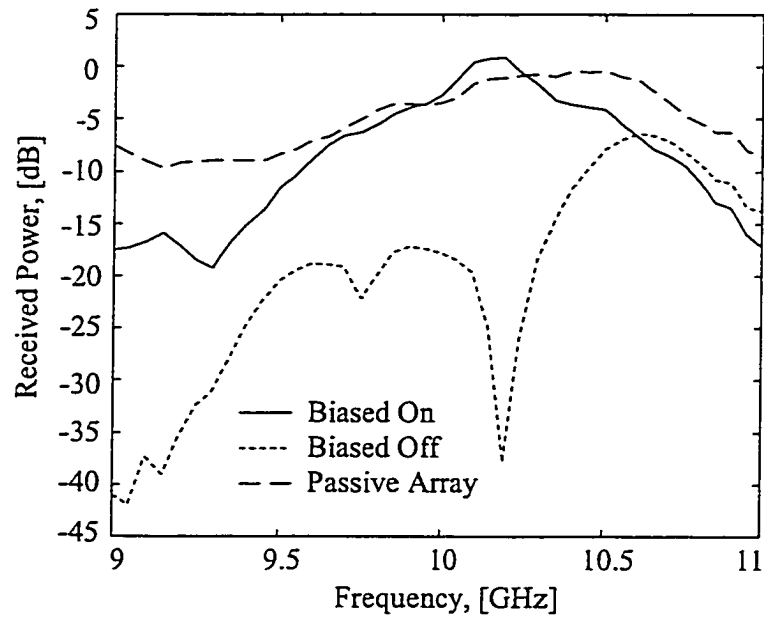
### **3.4 Applications**

#### **3.4.1 A Quasi-Optical Receiver**

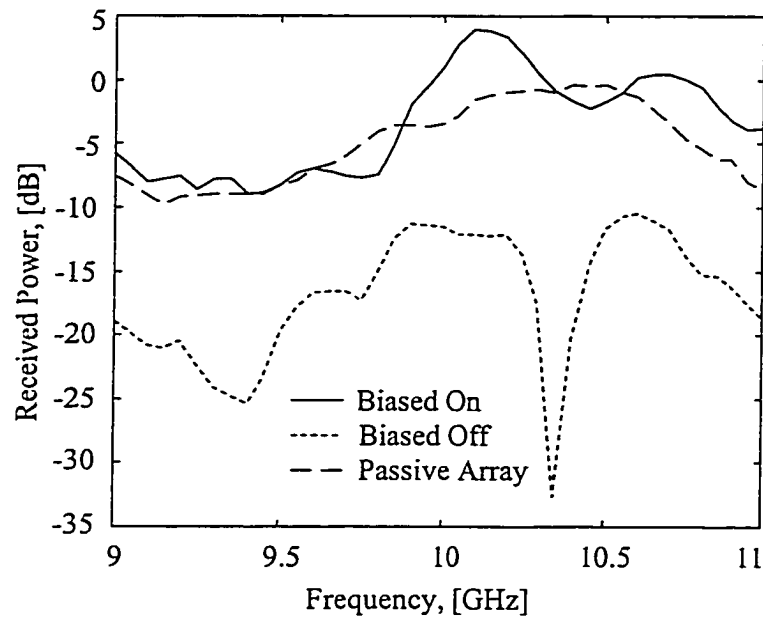
A complete quasi-optical receiver front end can be formed by cascading the lens amplifier with a 10.39-GHz grid oscillator/mixer as shown in Figure 3.1. A transmitted 10.10 GHz carrier, amplitude modulated with a 10-kHz square wave, is amplified and focused by the 10-element lens amplifier towards the self-oscillating mixer located at the focal point. The 290-MHz IF present on the bias-lines of the grid oscillator is demodulated using an HP 89441A Vector Signal Analyzer. The recovered 10-kHz square wave is shown in Figure 3.11. The quasi-optical grid oscillator is just one example of a feed type. Possible advantages of using a grid oscillator are: power combining at the source level; reduced phase noise as more devices in the grid lock [14]; and self-oscillating fundamental or harmonic mixing in reception [49].

#### **3.4.2 Multipath Fading Reduction**

Reduction of multipath fading using a lens amplifier array can be demonstrated by a simple measurement. A 45×30 cm metallic mirror located parallel to the optical axis in front of the amplifier array was translated in 3-mm steps perpendicular to the optical axis as shown in Figure 3.12. For each step, the mirror was rotated through a set of angles. The received power was measured for all mirror

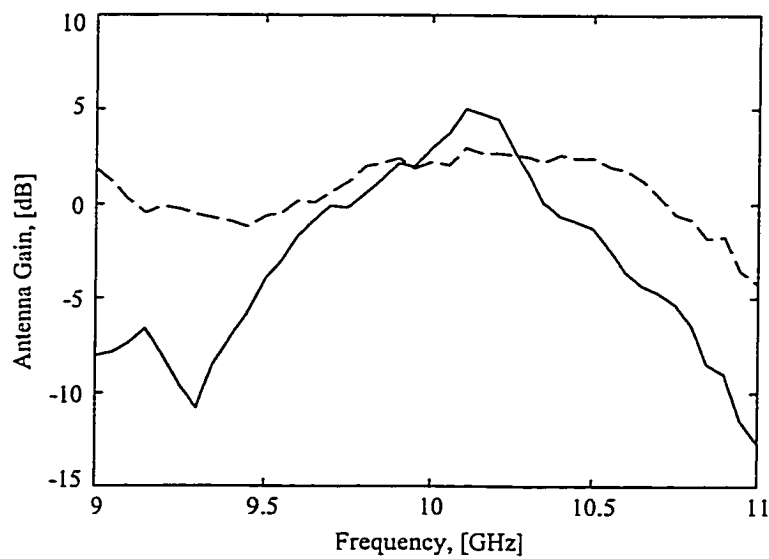


(a)

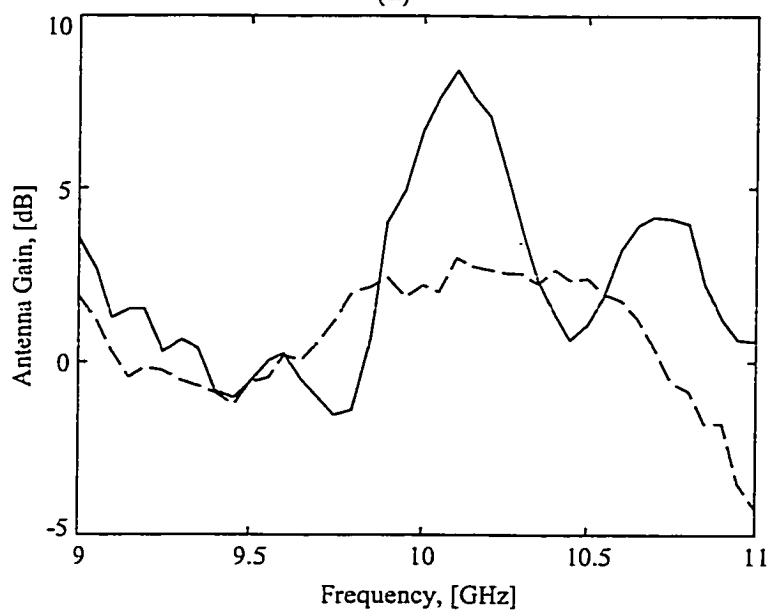


(b)

Figure 3.8. (a) Measured absolute gain of the 24-element active and passive array in transmit mode, with polarizers at input and output. (b) Measured absolute gain of the 24-element active and passive array in receive mode, with polarizers at input and output. The measurements are normalized to a through measurement with a rectangular aperture surrounded by absorbing material. The solid lines represents the biased on state, the dotted lines the biased off state, and the dashed lines shows the measured results for the passive array.

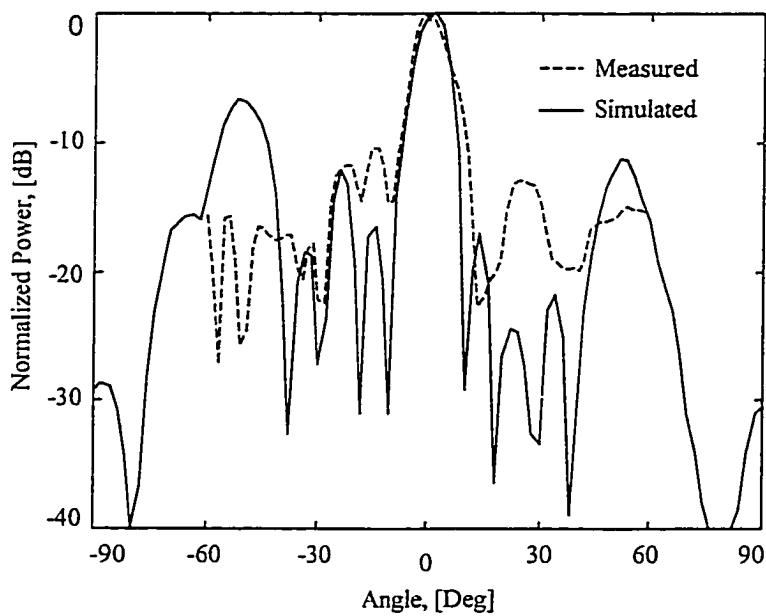


(a)

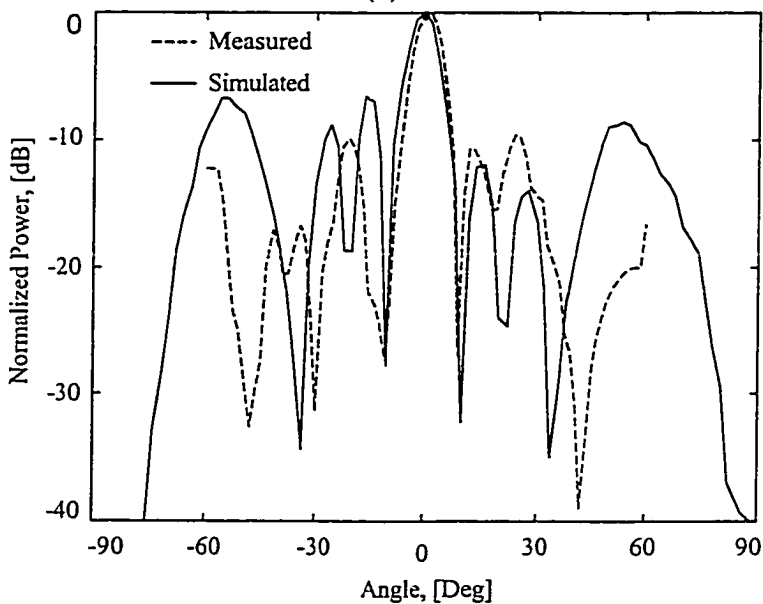


(b)

Figure 3.9. (a) Measured antenna gain of the 24-element active and passive array in transmit mode, with polarizers at input and output. (b) Measured antenna gain of the 24-element active and passive array in receive mode, with polarizers at input and output. The solid lines represents the biased on state and the dashed lines shows the measured results for the passive array.



(a)



(b)

Figure 3.10. (a) Measured (—) and simulated (---) H-plane radiation pattern for the receive amplifier at 10.1 GHz. (b) Measured (—) and simulated (---) E-plane radiation pattern for the receive amplifier at 10.1 GHz. The theoretical patterns were calculated using the measured antenna pattern of a single slot antenna.



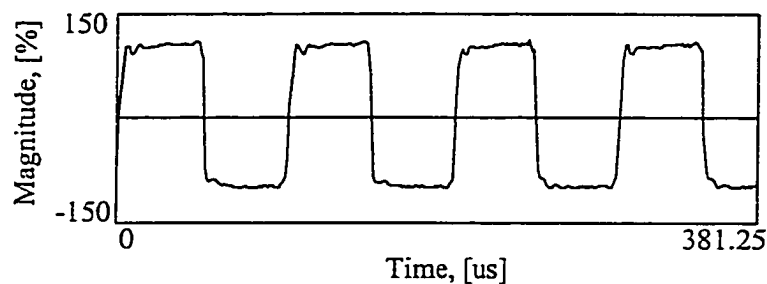


Figure 3.11. A 10-kHz square-wave signal received by a quasi-optical receiver front-end and demodulated. A transmitted amplitude modulated 10.1 GHz carrier is received, mixed to a 290-MHz IF and demodulated using a vector signal analyzer.

positions with and without the lens amplifier.

The measured maximum fades of a 10.1-GHz carrier signal, with and without the 24-element lens amplifier, and normalized to the received signal without the mirror inserted, are shown in Figure 3.13. Maximum fading nulls of less than -4 dB and more than -50 dB were measured with and without the lens amplifier, respectively. This simple measurement show that a lens amplifier can also provide a significant improvement of multipath fading effects due to the increased directivity of the receiver [79].

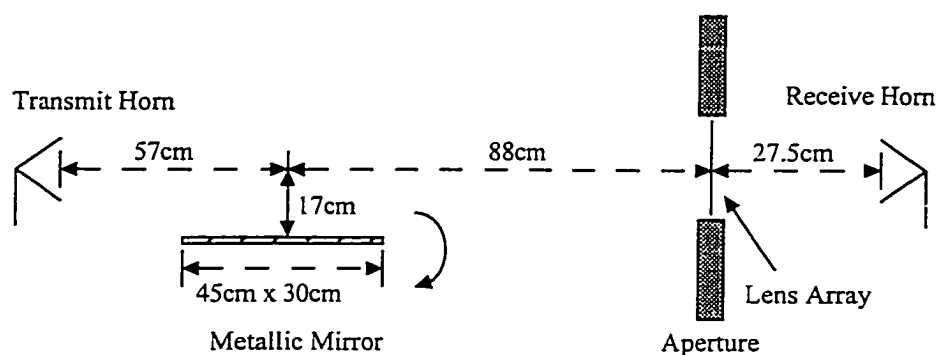


Figure 3.12. Test set-up for the multipath experiment. A 45×30 cm metallic mirror located parallel to the optical axis in front of the 24-element lens amplifier is translated in 3-mm steps from the axis. For each step, the mirror was rotated through a set of angles.

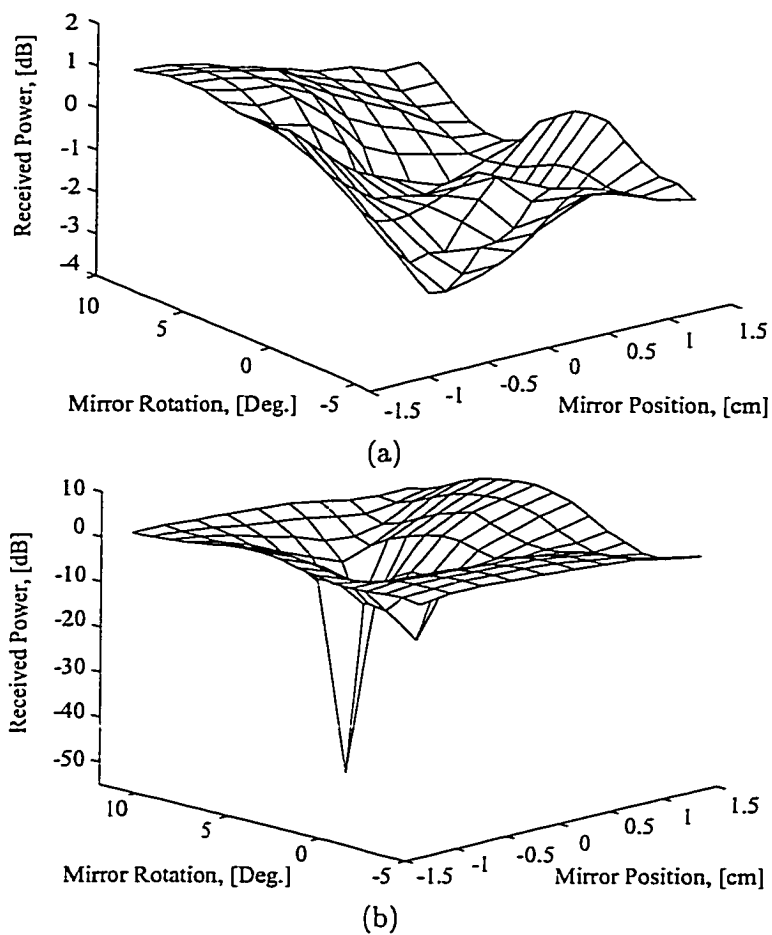


Figure 3.13. Measured maximum multipath fading nulls of a 10.1-GHz carrier signal. The received power is normalized to through measurements without the mirror inserted. With (a) and without (b) the 24-element lens amplifier array inserted. Notice the different vertical scales.

### 3.4.3 A Multi-User Application

A multi-user frequency reuse experiment demonstrates how two separate signals incident from different angles can be received independently at different locations along the focal surface of the 24-element lens amplifier array. Beam-steering patterns are measured at 10.1 GHz for receive locations at -20, 0 and +20 degrees along the focal surface in the E-plane of the array as shown in Figure 3.14. The normalizing power levels of the main lobes are within 2 dB. The measured sidelobe levels for the 0 and 20-degree receive locations are below -10 dB. A multi-user experiment, with two incident signals at 0 and 20 degrees and with the same incident power levels, is performed as shown in Figure 3.15. The received power of an interfering signal originating 20 degrees from the desired signal has a measured relative power of about -10 dB in this set-up. Square-wave signals at  $f_A = 50$  kHz and  $f_B = 150$  kHz are frequency modulated on a 10.1-GHz carrier and incident from 0 and 20 degrees, respectively. The demodulated signals received at the 0 and 20-degree positions on the focal surface are shown in Figure 3.16. The interfering signal appears as an additional ripple in the demodulated signal.

### 3.5 Conclusion

A transmit/receive quasi-optical lens amplifier array is presented. In transmit mode, the vertically polarized antiresonant slot antennas receive an input wave from a focal point and SPDT switches route it through transmit amplifiers to the horizontally polarized output slots. In reception, the horizontally polarized slots couple the input signal through the receive amplifiers to the vertically polarized slots. Amplifier gains of 5.5 dB at 10.1 GHz in receive mode, and 2.0 dB at 10.2 GHz in transmit mode are measured. The functionality of this quasi-optical approach is demonstrated with several examples: (1) a quasi-optical T/R module; (2) a quasi-optical AM receiver; (3) significant multipath fading null reduction; and (4) a multi-user with

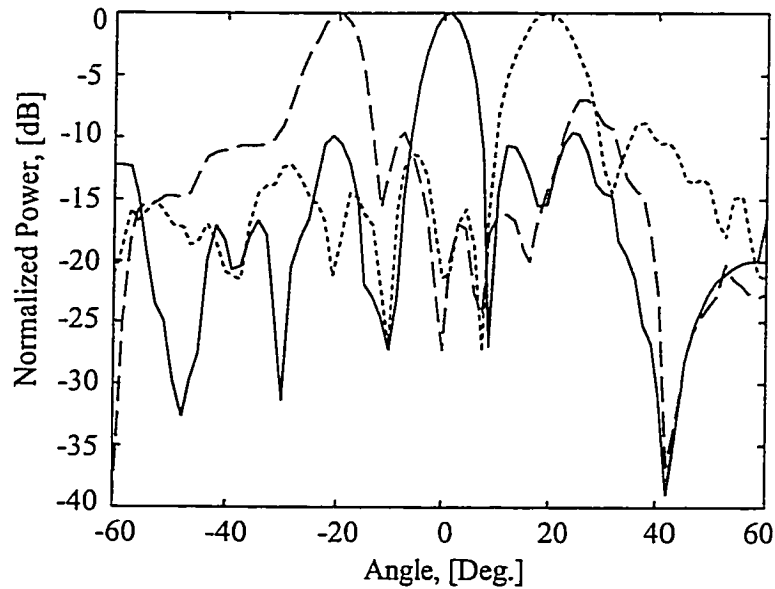


Figure 3.14. Beam-scanning in E-plane at 10.1 GHz for the 24-element lens amplifier array in receive mode. Receive horn at (-) 0, (- -) -20 and (...) 20-degree locations are shown. The normalizing power levels of the main lobes are within 2 dB.

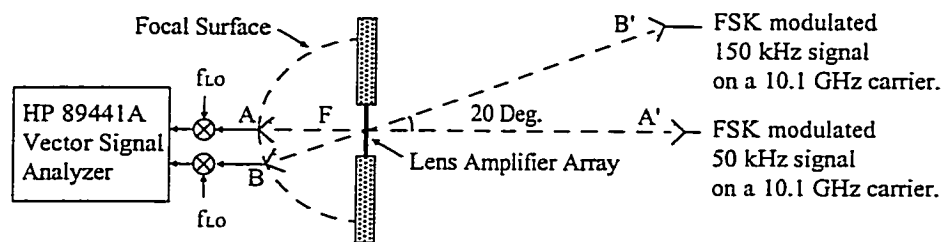
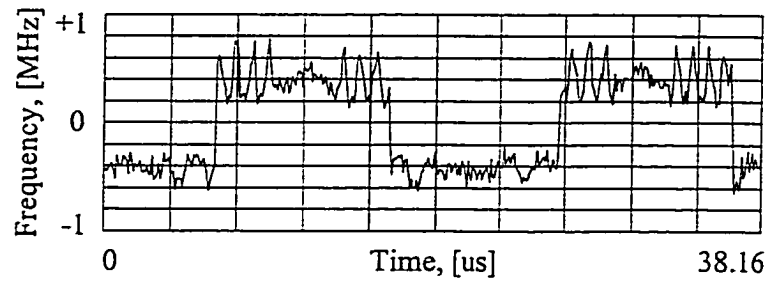
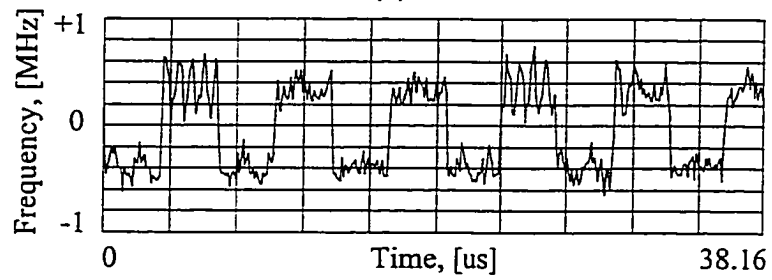


Figure 3.15. Test set-up for the multi-user experiment. Square-wave signals at  $f_A = 50$  kHz and  $f_B = 150$  kHz are frequency modulated on a 10.1-GHz carrier and input at 0 and 20 degrees from the optical axis, respectively. The two signals are received by horns located on the focal surface behind the 24-element lens amplifier array, and demodulated using a vector signal analyzer.



(a)



(b)

Figure 3.16. (a) Received and FSK demodulated 50-kHz signal for a receiver located at 0 degrees. (b) Received and FSK demodulated 150-kHz signal for a receiver located at 20 degrees. The signals are demodulated using a vector signal analyzer.

frequency reuse FSK data link.

## CHAPTER 4

### A MILLIMETER-WAVE TRANSMIT/RECEIVE QUASI-OPTICAL LENS AMPLIFIER ARRAY

#### 4.1 Motivation

While solid-state devices are capable of producing a few watts at microwave frequencies, the output power from a single device in the millimeter-wave band is limited. Due to the large available bandwidths in the millimeter-wave band, many applications use these frequencies despite the limited available power. Examples of such applications are satellite communications, automotive radar, remote sensing, imaging and military applications such as missile seekers. A T/R quasi-optical lens amplifier can provide a front-end with a relatively high EIRP in transmission and high dynamic range in reception for these kinds of applications. A millimeter-wave front-end is also more compact and lighter weight as compared to its microwave counterpart. The lens amplifier presented in this chapter is designed for *Ka*-band. The following Section 4.2 presents the design of this active antenna array, while some experimental results for the lens array are given in Section 4.3.

#### 4.2 Design

For a compact design and a relatively small unit cell, the *Ka*-band lens amplifier array uses a hybrid design technique with MMIC amplifiers and switches. While the *X*-band lens amplifier array was fabricated on a single substrate, two  $7.62 \times 7.62$  cm substrates mounted back-to-back are used for this array to double the

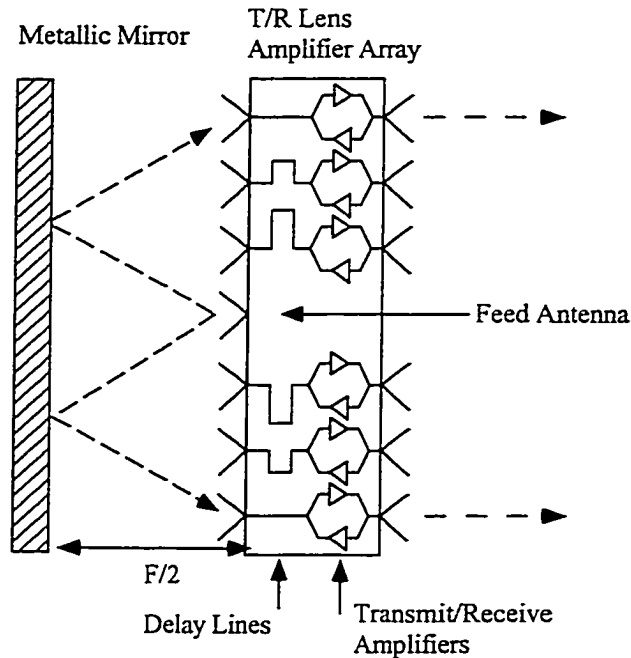


Figure 4.1. Schematic of the folded feed used for the  $Ka$ -band array. The lens array is fed from the center element in the feed side array with a metallic mirror located at half the focal distance of the lens.

circuit area of each unit cell. Both a passive 36-element design and a 20-element active array were fabricated. The 36-element passive design has an F-number of 0.63 to minimize the feed loss. In the active array, the center 20-elements of the array are populated with a corresponding F/D ratio of 0.89.

The center element in these lens arrays is reserved for a feed element. By feeding the feed-side array from this element with a metallic mirror located at half the focal distance in front of the array, a more compact folded system is achieved as shown in Figure 4.1. The feed-side array can also be fed from a separate feed antenna located at the focal distance in front of the array. This configuration allows for beam forming and beam steering by adding several feed antennas along the focal surface. Beam steering can be performed mechanically with the folded feed, by moving the metallic mirror along the arch at half the distance to the focal surface. The mirror must also be simultaneously rotated to face the beam-steering direction.

The heat produced by the amplifiers in the 20-element transmit array, is in excess of 15 W. A substrate with good thermal properties is therefore desirable. To reduce the size of the radiating elements, 0.38-mm-thick Rogers TMM10 substrates with a relatively high  $\epsilon_r=9.2$  were chosen. This substrate material exhibits low loss at  $Ka$ -band, allows for drilling of the holes necessary to mount the MMIC amplifiers, and has fair thermal conductivity of 0.73 W/mK. A design using an aluminum nitride substrate with thermal conductivity 170 W/mK on the feed side and a TMM10 substrate on the front side was first made for improved thermal properties, but it was found during fabrication that the different thermal expansion coefficients of the two substrates caused the TMM10 substrate to crack. Two aluminum nitride substrates could be used, but special fabrication equipment would be needed to drill the holes for the MMICs. The substrate thickness was chosen sufficiently thin to avoid substrate modes and as thick as possible for heat sinking and a less brittle design. The substrates are clad with 12- $\mu\text{m}$ -thick copper to reduce the amount of over-etching of the circuits during the photolithography. A 0.25-mm diameter hole is first drilled in each corner of the two substrates to facilitate alignment of the circuit layout on both sides of the feed- and front-side substrates.

Patch antennas were chosen for the radiating elements, because they do not require external polarizers and are easy to fabricate with microstrip feed lines. The patch antennas were first designed using *RP-Design* [80] and then optimized using *Ensemble* as shown in Figure 4.2. The simulated return loss for a 30-GHz patch design is shown in Figure 4.2. A 2:1 VSWR bandwidth of about 1 GHz (or 3%) is seen.

An initial passive array design operating at 30.5 GHz indicated over-etching of the circuits. All circuit dimensions of the final design were increased by 20- $\mu\text{m}$  in the mask layout to account for this effect. The operating frequency of the final design presented here, shifted to 28.5 GHz due to less over-etching during the fabrication



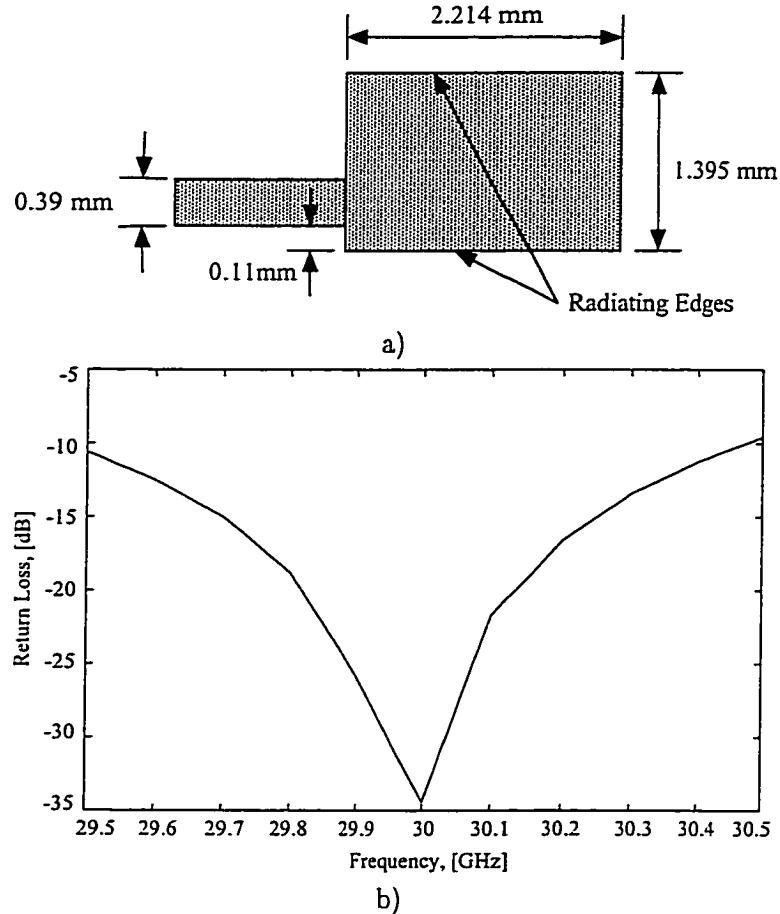


Figure 4.2. a) Layout of a  $Ka$ -band patch antenna on a 0.38-mm-thick TMM10 substrate. b) Simulated return loss for the patch antenna. The simulations were performed using *Ensemble*.

process.

Both the patch input impedance and the characteristic impedance of the microstrip lines are  $50\ \Omega$ , to avoid additional matching sections for the antennas and MMICs. The width of the bias lines is  $200\ \mu\text{m}$  to reduce ohmic losses while minimizing coupling.

Rectangular slots cut out in the ground planes of the two substrates are used to connect the microstrip lines on the feed- and front-side substrates as shown in Figure 4.3. The slots are 2 mm long and 0.56 mm wide, and the microstrip lines extend 0.49 mm over the slots. The simulated reflection and transmission coefficients

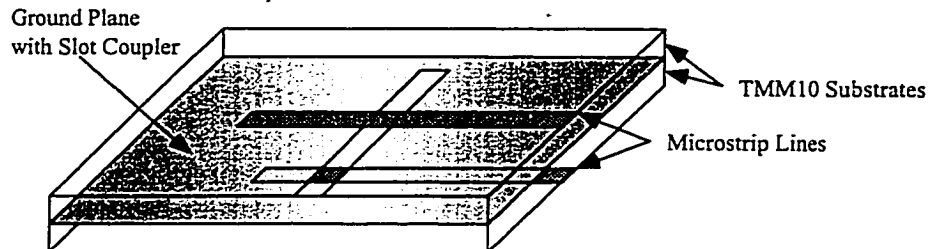


Figure 4.3. Layout of a  $Ka$ -band slot coupler. Two microstrip lines on two separate 0.38-mm-thick TMM10 substrates are coupled through a 2 mm long and 0.56 mm wide slot cut out in the common ground plane.

of a slot coupler are shown in Figure 4.4. The simulated transmission loss is less than 0.5 dB from 25 GHz to 35 GHz. The bandwidth of this lens array is hence limited by the bandwidth of the patch antennas. Ohmic losses in the microstrip lines accounts for most of the 0.25-dB loss at 30 GHz. The slot polarization is chosen orthogonal to the patch polarization in the front-side array, to minimize feedback between the input and output of the amplifiers and thus prevent oscillations.

An Alpha MMIC AA028N1 low-noise amplifier and an AA028P3 driver amplifier are chosen for the receiving and transmitting amplifiers. Two reflective MMIC SPDT switches (Alpha AP640R2) are used to switch between the amplifiers. The MMICs are mounted on the ground plane of the feed-side substrate in holes milled out of the front-side substrate. The amplifiers allow for a compact unit cell, because they are self-biased and thus require only a single bias line. A total of four bias lines are needed for the MMICs in each element. The DC bias to the amplifiers and switches is supplied through 47-pF blocking capacitors. A series 30- $\Omega$  resistor is added in each arm of the switches for better control of the DC current to the  $p$ - $i$ - $n$  diodes. The three-stage transmit and receive amplifiers have relatively high gains of 19 dB and 14 dB at 28 GHz to overcome the feed loss of the lens array. To ensure stability, 2-ns SPDT switches with more than 28-dB isolation and less than 1.1-dB insertion loss are used. Some important properties of the MMIC amplifiers and switches selected for the active array are summarized in Table 4.1 and 4.2.

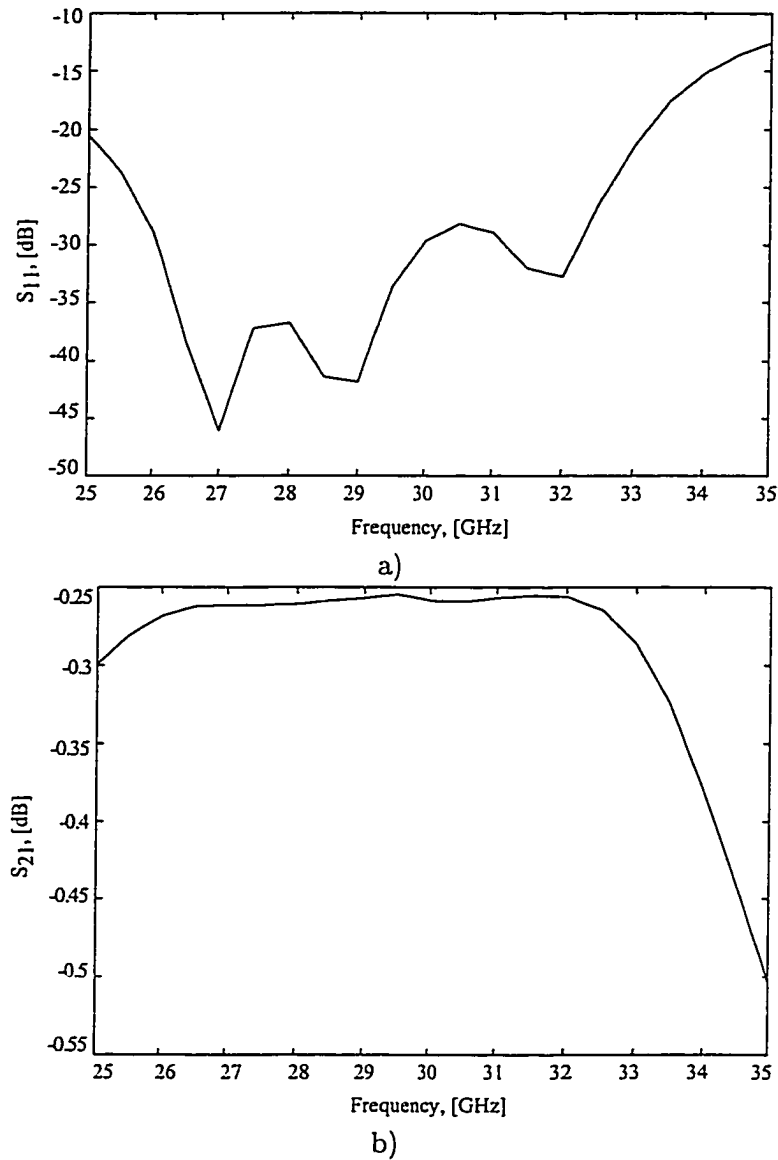


Figure 4.4. Simulated a) reflection coefficient and b) transmission coefficient of a slot coupler. The simulations were performed using *Ensemble*.

Parameter	Receive Amplifier	Transmit Amplifier
Frequency Band	24-30 GHz	27.5-29.5 GHz
Small Signal Gain	14 dB	19 dB
Noise Figure	2.8 dB	—
Output Power at 1 dBc	7 dBm	16 dBm
Saturated Output Power	—	18.5 dBm

Table 4.1. Typical properties of the low-noise amplifier MMICs used for reception and the three-stage driver amplifier MMICs used for transmission at 28 GHz.

Parameter	SPDT Switches
Frequency Band	26-40 GHz
Insertion Loss	< 1.1 dB
Isolation	> 28 dB
Switching Speed	< 2 ns
Power Capability	33 dBm

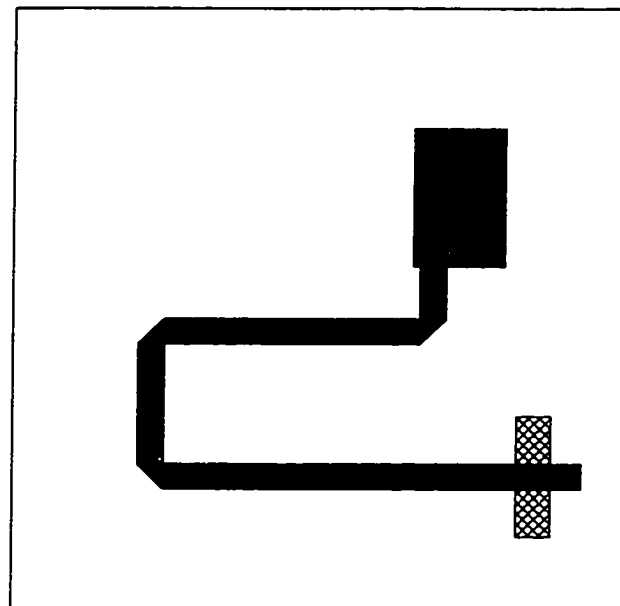
Table 4.2: Typical parameters for the MMIC SPDT switches at 28 GHz.

The layouts of the unit cells in the front- and feed-side arrays are shown in Figure 4.5. The unit-cell size is  $\lambda \times \lambda$ . While a slightly smaller unit cell would reduce grating lobes and increase the directivity of the array, concerns for coupling in the array and possibility for oscillations prevented the design of a smaller unit cell to be made.

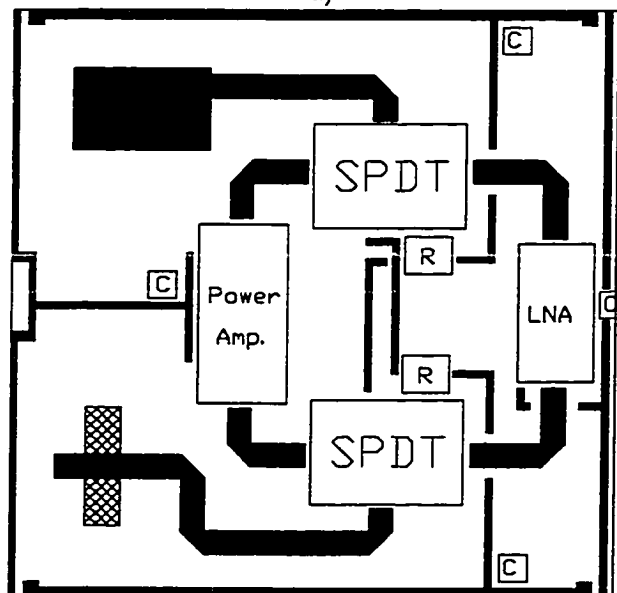
The delay lines located on the feed-side array, were designed using the design equations for a one degree of freedom lens with a perfect focal point on the optical axis [69]. The focal length is 4 cm ( $4\lambda$ ) for this lens. The layout of the feed- and front-side arrays are shown in Figure 4.6. A rectangular lattice was used to ease the layout of the bias lines and reduce the unit-cell size. Both the feed- and front-side arrays avoid the corners of the square substrates where a uniform photo resist layer is difficult to achieve during the photolithography process. This layout was also chosen to match the radiation pattern of the feed antenna to achieve a more uniform illumination of the array elements.

### 4.3 Experiment

A passive 36-element array was first fabricated and measured to check if the patch antennas and slot couplers operate at the desired frequency. A through calibration is first made on a HP 8510C network analyzer with an open  $Ka$ -band WR-28 waveguide located at the focal point, and a co-polarized  $Ka$ -band 25-dB standard gain horn located in the far field (125 cm) of the lens. The horn polarization is then



a)



b)

Figure 4.5. Layout of the a) feed- and b) front-side unit cell of the  $Ka$ -band transmit/receive lens amplifier array. The unit cell is  $10 \times 10$  mm. The MMICs, capacitors and resistors are mounted on the ground plane of the feed-side substrate in holes milled out of the front-side substrate.

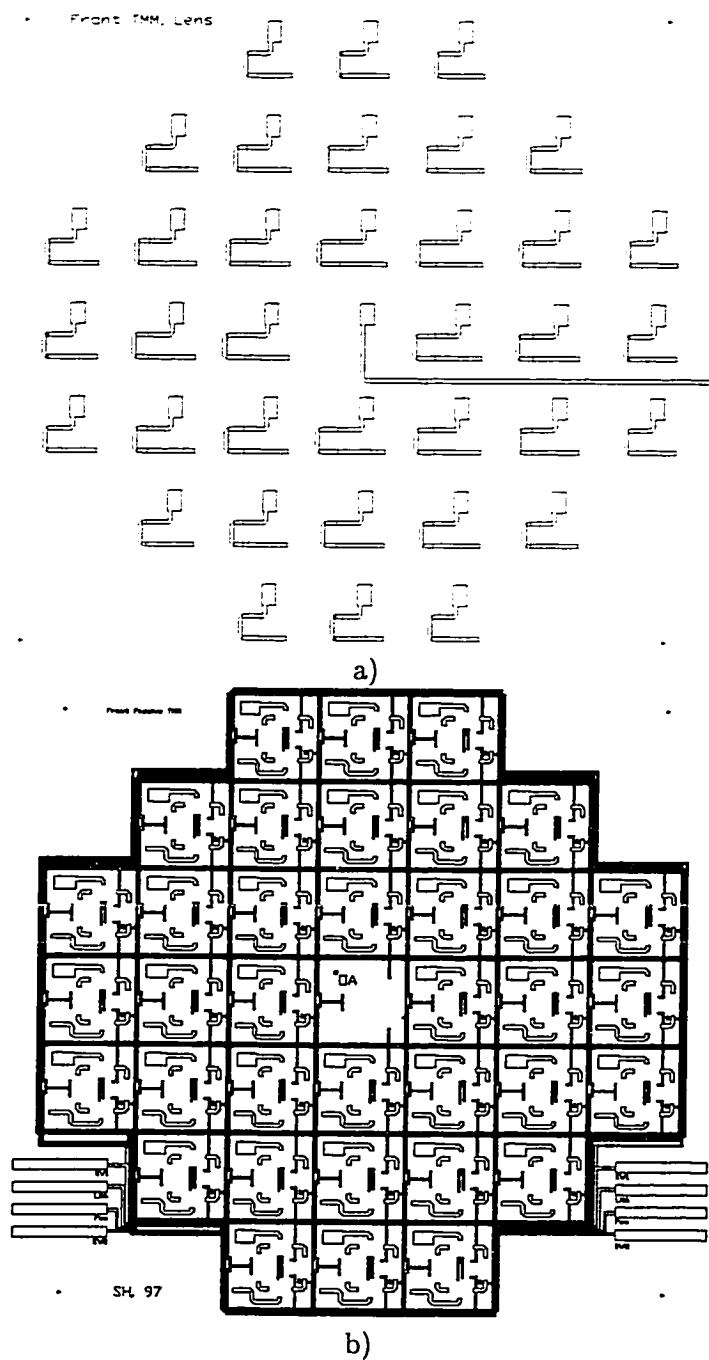


Figure 4.6. Layout of the a) feed and b) front side of the 36-element *Ka*-band transmit/receive lens amplifier array. The center 20 elements in the array are populated.

rotated 90 degrees, and the passive lens array inserted. The absolute gain plotted in Figure 4.7, shows a 2.7-dB loss at 28.8 GHz. A metallic mirror is next inserted at half the focal distance, and the patch antenna in the center of the array is used as a feed antenna. The absolute gain for this feed is about 0.2 dB at 28.8 GHz. The feed loss of this system is reduced, because the signals reflected from the array (due to a 30 % aperture efficiency) are reflected back by the mirror. The reduced bandwidth of this system is probably due to the standing waves between the mirror and the array. By increasing the aperture efficiency of the array, this effect can be reduced. The directive gain of the WR-28 waveguide feed is estimated to be 4.1 dB [62]. The measured antenna gains for the passive lens with a waveguide and a folded patch feed are 1.4 dB and 4.3 dB, respectively. The simulated directivity of a uniformly illuminated 36-element array is 22.8 dB. If an efficiency of 70 % is assumed for the patch antennas, the total feed loss becomes 19.9 dB with the waveguide feed. Simulations predicted about 15 dB feed loss for the waveguide fed lens. The difference of about 5 dB can be due to coupling in the antenna arrays, increased loss in the slot couplers due to a small air gap between the two substrates, and increased loss in the patch antennas and microstrip lines.

Similarly, the absolute gain for the active 20-element array is measured with an open WR-28 waveguide in both transmitting and receiving modes. In transmit mode, the absolute gain is measured with 5, 8, 11 and 17 elements populated as shown in Figure 4.8. An absolute gain of 7 dB is measured in transmit mode at 28.3 GHz with 17 elements populated. A 3-dB gain reduction is seen when the the array temperature increases to a maximum of around 108° C without air-cooling at room temperature and with the optimum bias point. The optimum bias point in transmit mode is:  $V_{power}=4$  V;  $I_{power}=2.22$  A; and  $I_{diodes}=300$  mA. The 3-dB bandwidth in transmit mode is about 300 MHz. Only 17 of the 20 transmit amplifiers operate, because three transmit amplifiers failed during fabrication and were disconnected.

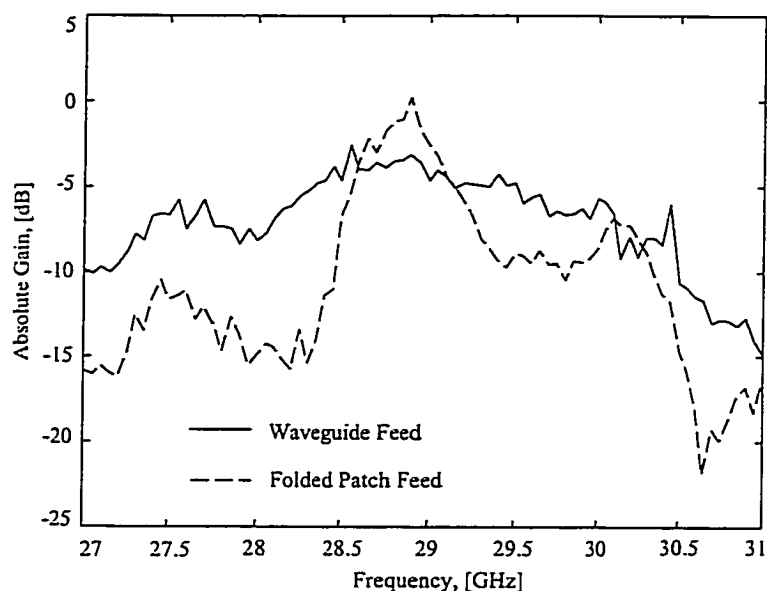


Figure 4.7. Measured absolute gain for the passive 36-element array fed from an open WR-28 waveguide and a folded patch antenna feed as indicated in Figure 4.1.

Assuming a 70 % radiation efficiency for the patches, a 1-dB insertion loss for the switches, and a saturated output power of 18.5 dBm from the transmit amplifiers, a total radiated power of 0.7 W can be estimated. The expected effective radiated power (EIRP) of this array is 70 Watts. A TWT amplifier with sufficient output power to saturate the array for an EIRP measurement of this array is ordered.

In receive mode, the absolute gain is measured with 5, 8, 11 and 20 elements populated as shown in Figure 4.9. An absolute gain of -2 dB is measured in receive mode at 28.5 GHz with 20 elements populated. The LNAs used in the array are low-gain units not initially intended for sale by Alpha. The relatively low absolute gain in receive mode can be due to a lower than expected amplifier gain. The 9-dB difference between the transmit and receive mode gain indicates an average amplifier gain of about 10 dB for the LNAs, if a 19-dB amplifier gain is assumed for the transmit MMICs. The optimum bias point in receive mode is:  $V_{power}=4$  V;  $I_{power}=450$  mA; and  $I_{diodes}=300$  mA. The 3-dB bandwidth in receive mode is about 750 MHz. Equipment for noise-figure measurements at *Ka*-band is not available at



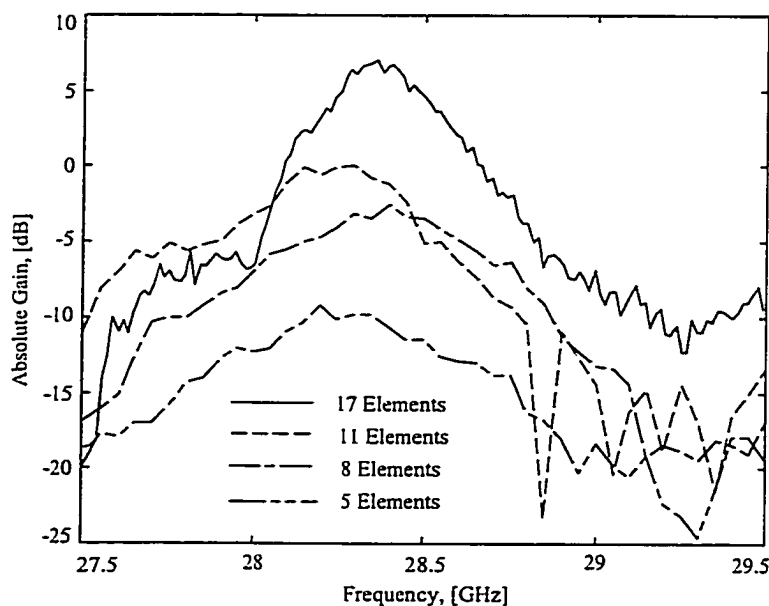


Figure 4.8. Measured absolute gain for the *Ka*-band array in transmit mode versus number of elements populated. The lens array is fed from an open WR-28 waveguide section located at the focal distance. Averaging (5) is used with 5, 8 and 11 elements populated.

this point. Schoenberg *et al.* [13] showed that the noise figure of a lens amplifier array is only slightly higher than the noise figure of a single array element, because the noise contributed by the individual amplifiers in the array are uncorrelated. The noise figure of the receive amplifiers is about 2.8 dB.

If a directive gain of 4.1 dB is estimated for the open waveguide, the measured antenna gains can be plotted as shown in Figure 4.10 with 17 elements in transmit mode and 20 elements in receive mode. The maximum antenna gain in transmitting and receiving modes are 11.1 dB and 2.1 dB, respectively. The measured antenna gains with a folded feed are plotted in Figure 4.11. The maximum antenna gains are about the same for this feed, but the bandwidths are slightly lower as expected.

The E- and H-plane radiation patterns are estimated with a simple experimental set-up on an optical table and enclosed with absorbing material in transmit

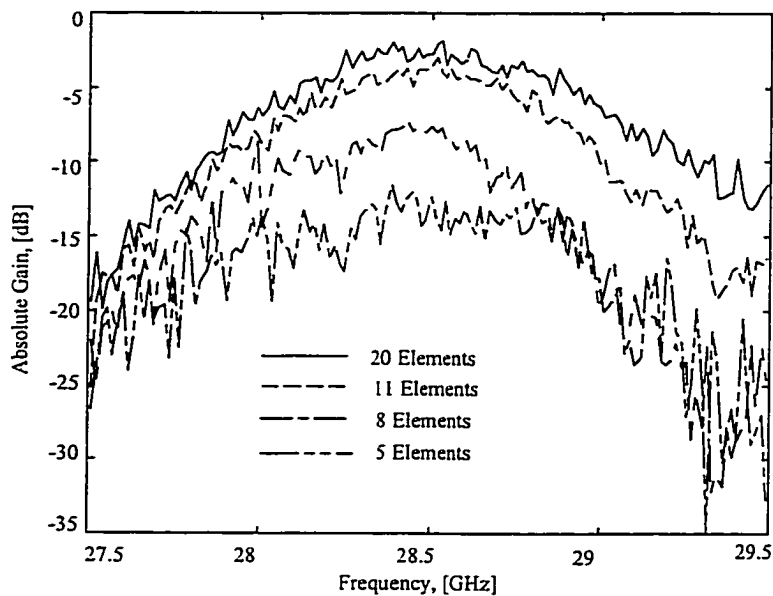


Figure 4.9. Measured absolute gain for the *Ka*-band array in receive mode versus number of elements populated. The lens array is fed from an open waveguide section located at the focal distance.

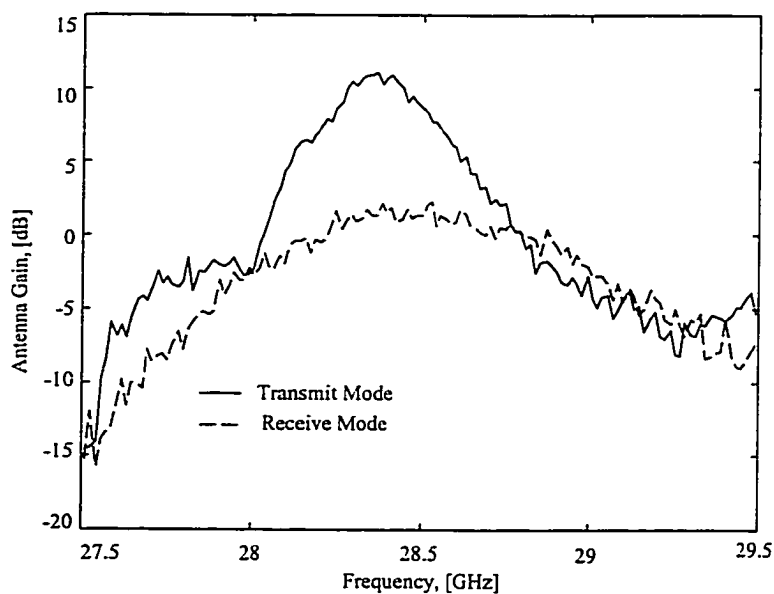


Figure 4.10. Measured antenna gains for the *Ka*-band array in transmitting and receiving modes. The lens array is fed from an open waveguide section located at the focal distance.

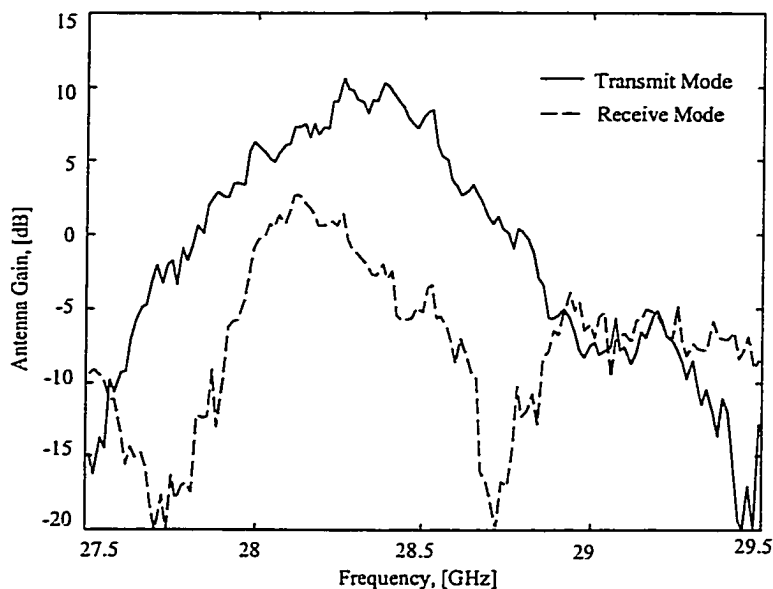


Figure 4.11. Measured antenna gains for the *Ka*-band array in transmitting and receiving modes. The lens array is fed from a patch antenna located in the center of the feed-side array. A metallic mirror is located at half the focal distance in front of the feed element as indicated in Figure 4.1.

mode at 28.3 GHz as plotted in Figure 4.12. The patterns show a main lobe with about  $15^\circ$  beamwidth in the broadside direction as expected from the simulations. The relatively high side-lobe levels can be due to a less uniform phase and amplitude distribution across the array as well as multipath reflections in the experimental set-up. A phase error can be due to unequal bond-wire lengths from the microstrip lines to the MMICs in the unit cells. A maximum path length difference of about 0.5 mm (18 degrees) between the elements seem possible. Two bond wires in parallel are used for each connection to reduce this error as well as the series inductance of the wires, and improve the reliability of the lens array. The measured cross-polarized signal power is about -10 dB relative to the main lobe.

To see how the performance of a lens amplifier array degrades when devices fail, the radiation pattern of the 36-element array was calculated with 0, 4 (10%) and 10 (30%) elements removed. The results plotted in Figure 4.13, show graceful degradation of these arrays. With 30% of the elements removed, the side-lobe levels

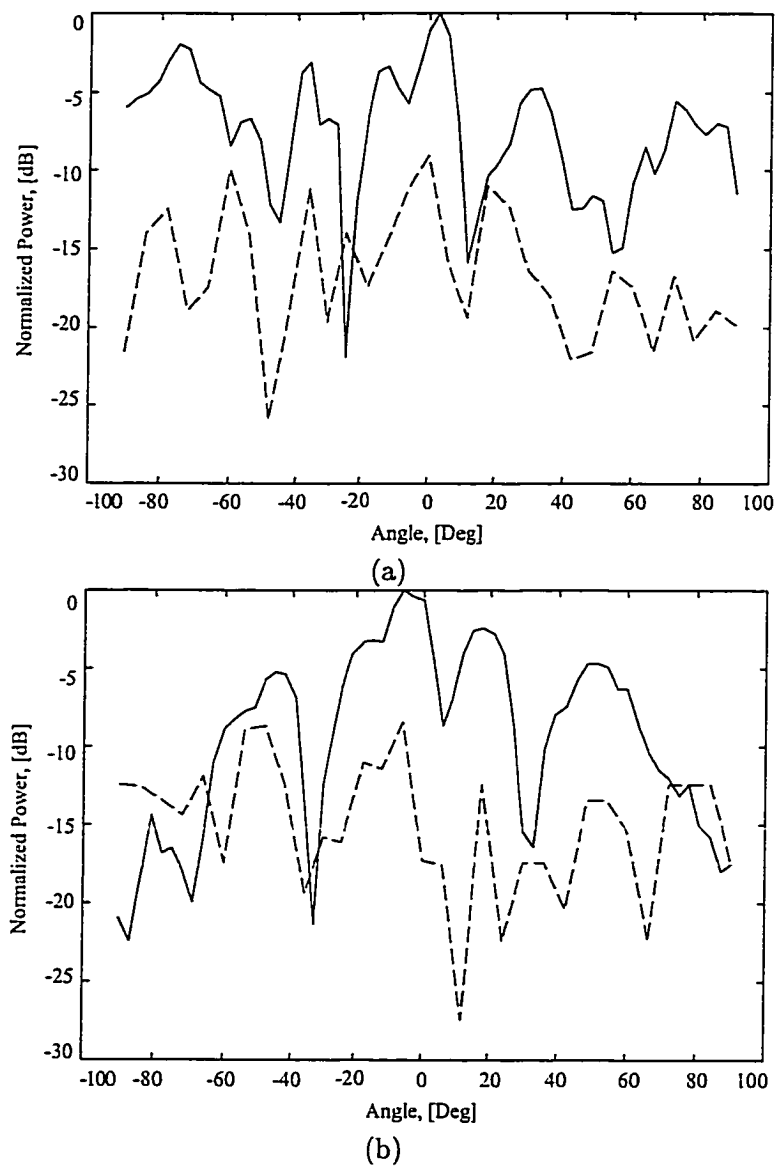


Figure 4.12. (a) Measured co-polarized (—) and cross-polarized (---) E-plane radiation pattern for the transmit amplifier at 28.3 GHz. (b) Measured co-polarized (—) and cross-polarized (---) H-plane radiation pattern for the transmit amplifier at 28.3 GHz.

increase and the broadside directivity decreases by about -3 dB. The beamwidth does not change significantly. Power loss due to increased feed loss of the array is not included in the simulations.

The DC power supplied to the 17 transmit amplifiers at the optimum bias point for gain is about 9 W. For maximum output power, a higher bias point corresponding to a DC power of 15 W can be used. Most of this power is dissipated in the form of heat. The temperature profile of the feed side substrate is measured for the lower bias point with and without air cooling from a desk-top fan, Figure 4.14. The maximum temperature with and without the fan is 57° C and 108° C, respectively.

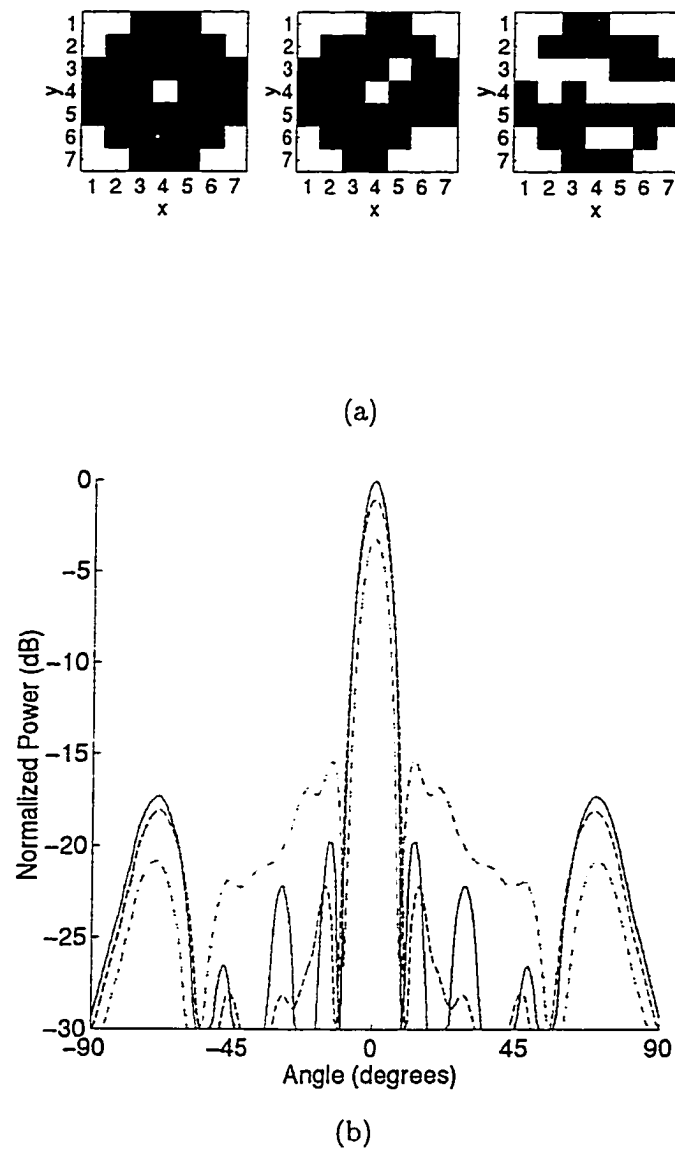


Figure 4.13. (a) Layout of the 36-element array with 0, 4 and 10 elements removed. (b) Simulated E-plane radiation pattern for the three different cases are shown in solid, dashed, and dashed-dotted lines, respectively. The patterns were calculated using the measured pattern of a single patch antenna.

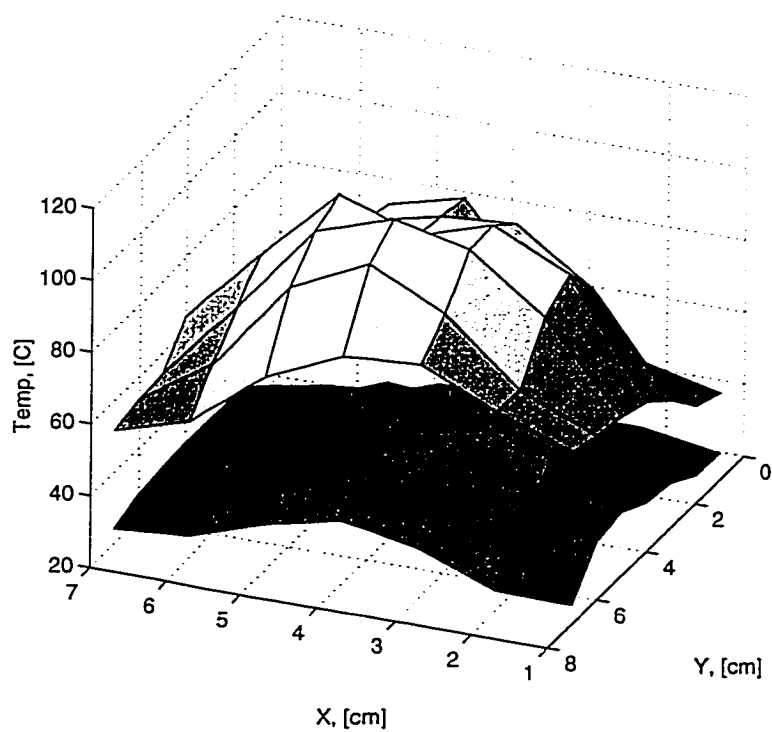


Figure 4.14. Measured temperature profile of the  $Ka$ -band array in transmit mode with and without air cooling. The DC bias supplied to the transmit amplifiers is  $V_{power}=4\text{ V}$ ,  $I_{power}=2.25\text{ A}$ .

## CHAPTER 5

### A QUASI-OPTICAL ISOLATOR

#### 5.1 Motivation

Quasi-optical active grids for power combining were developed with high-power millimeter-wave solid-state transmitters in mind. In a quasi-optical transmitter, the output is a quasi-optical power amplifier. Most quasi-optical amplifiers to date are linearly polarized, with the input and output antennas polarized orthogonally to each other to provide isolation. To protect the amplifier against high-level reflections, an external isolator can be used. In this chapter a quasi-optical isolator is presented. The isolator is designed to improve the isolation and stability of a quasi-optical amplifier and provide additional functions such as tuning and linear-to-circular polarization conversion.

The isolator, shown in Figure 5.1, consists of multiple loaded gratings and is cascadable with a quasi-optical amplifier. A system based on the same principle of operation, consisting of a meander-line polarizer backed by a metallic ground plane, was designed for reducing radar cross section (RCS) [81]. A similar quasi-optical circular polarization duplexer was presented in [82].

In Figure 5.1, the vertically polarized output wave from a quasi-optical amplifier is first incident on a pair of grids, which do not introduce any significant transmission loss. Both grids consist of horizontal printed strips, and the second one is in addition loaded with  $390\text{-}\Omega$  chip resistors. The vertically polarized wave then passes through a linear-to-circular polarization converter, and is right-hand



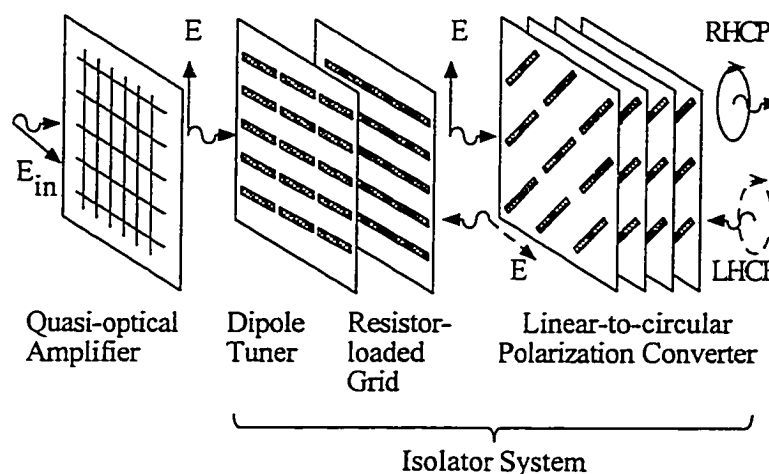


Figure 5.1. The isolator system consists of a linear-to-circular polarization converter and an absorbing surface. Transmitted waves are given by solid lines and reflected waves by dashed lines.

circularly polarized at the output. In the event of a reflection, e.g. the transmitter facing a large conductive object, the right-hand circularly polarized wave reflects back towards the transmitter as a left-hand circularly polarized wave. The left-hand circularly polarized wave becomes horizontally polarized upon passing through the polarization converter, and is then absorbed in the resistor-loaded grid.

It is possible to view the linear-to-circular polarization converter as a four-port device by considering the horizontal and vertical polarizations as separate ports at the input and output. In this case, since the horizontally and vertically polarized waves have half the power of the input wave and are  $90^\circ$  out of phase, this device can technically be considered a 3-dB  $90^\circ$  hybrid coupler. However, the ports at the output are actually coupled together to form a circularly polarized wave, and the horizontally polarized port at the input is terminated by the absorbing surface, so effectively this device has only one input and one output port. With the above properties in mind, we call the device in Figure 5.1 an isolator.

## 5.2 Design

The linear-to-circular polarization converter described in detail in [83] operates at around 9 GHz, so the isolator is designed for that range. A full-wave analysis program developed at the University of Colorado was used for the design [83]. The absorbing surface consists of a resistively loaded grid and a dipole tuner grid separated by  $\lambda/4$  of air. The resistive grid has a period of 10 mm and consists of 9-mm-long thin metallic strips separated by 1-mm gaps. Lumped 390- $\Omega$  chip resistors are soldered across the gaps. The dipole tuner grid consists of 15-mm-long dipoles separated by 7 mm, and periodically spaced 15 mm apart. Both grids are fabricated on 0.79-mm thick substrates with  $\epsilon_r = 2.17$ .

For the horizontal polarization, the dipole tuner grid can be interpreted as a transmission-line short at the design frequency. Because the two grids are separated by  $\lambda/4$ , the short can be represented as an open circuit at the plane of the resistive grid. The resistive grid can then be matched to the free-space impedance of 377  $\Omega$ , minimizing transmission and reflection of the horizontally polarized wave at the design frequency.

The linear-to-circular polarization converter consists of four inductively loaded dipole grids, as shown in Figure 5.1. The dipoles are 10 mm long and periodically spaced 13 mm apart. A 100-pF chip capacitor with a measured 0.7-nH lead inductance is soldered across each of the 1-mm gaps. Notice that the inductance is dominating the reactance of these capacitors at X-band. The lead inductance was included in the simulations. Each grid contains an array of dipoles oriented 45° with respect to a vertically polarized incident plane wave. The field component parallel to the dipoles is phase-shifted 90° relative to the orthogonal component, resulting in a circularly polarized transmitted wave. To achieve low transmission loss for both field components, four identical grids spaced 5.5 mm apart are used. This linear-to-circular polarization converter has a measured axial ratio of 1.3 dB and a 1.1 dB

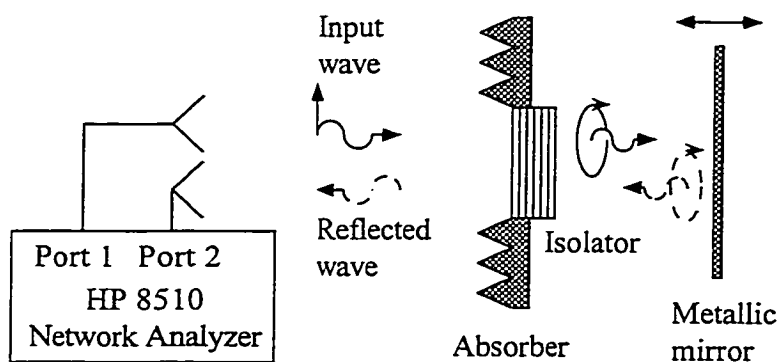


Figure 5.2. Experimental set-up of the isolator system. Two X-band horns are connected to ports 1 and 2 of a network analyzer. The isolator system is placed in the far field of the horns in the plane of an absorbing aperture. A metallic mirror is used as a variable load behind the isolator system.

transmission loss at 8.4 GHz [83].

### 5.3 Experiment

To characterize the isolator performance, two X-band horns are placed side-by-side as shown in Figure 5.2. One of the horns provides the incident vertically polarized wave from port 1 of an HP 8510 network analyzer. The other horn is connected to port 2 and is used to measure either the co-polarized or cross-polarized signal reflected through the isolator. The isolator system is inserted at the plane of an absorbing aperture in the far field of the horn antennas. A metallic mirror is used as a variable load behind the linear-to-circular polarization converter. Measurements of  $S_{21}$  are made for a range of mirror positions.

First, both the transmit and receive antennas were vertically polarized and the metallic mirror was located at the plane of the absorber. Measurements of  $S_{21}$  were obtained as the mirror was translated. The isolator system was then inserted and  $S_{21}$  measured for a range of mirror positions. Finally, the receive horn was horizontally polarized, and the isolator measurement was repeated for the same range of mirror positions. The maximum reflected powers were compared for a range of

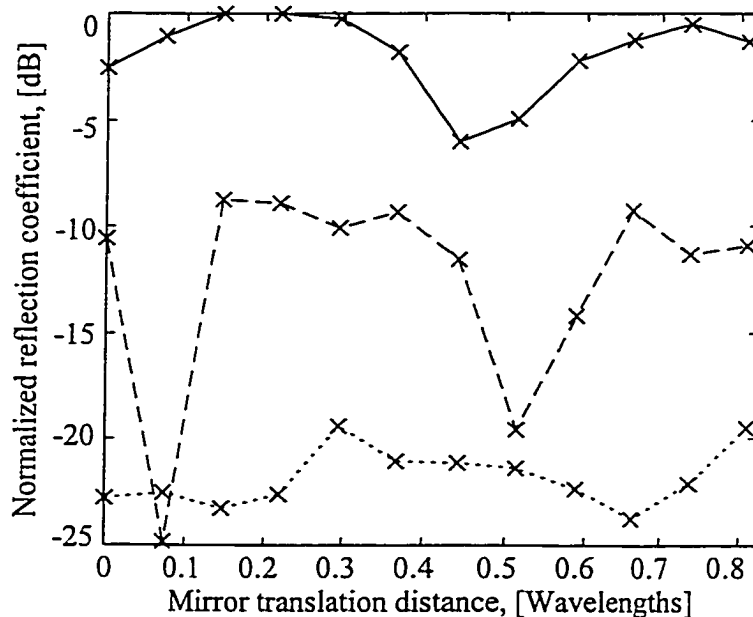


Figure 5.3. Measurement of the quasi-optical isolator at 8.83 GHz, normalized to the reflection from a metallic mirror as the mirror is translated. Co-polarized reflected signal (dashed line), cross-polarized signal (dotted line), and co-polarized signal with mirror only (solid line) are plotted.

frequencies.

The best isolation was found at 8.83 GHz, where the linear-to-circular polarization converter has a measured axial ratio of 2.5 dB and a transmission loss of 1.1 dB. The co-polarized and cross-polarized reflected signals, normalized to the maximum reflected signal when the isolator is replaced by a mirror, are plotted in Figure 5.3. At 8.83 GHz, the co-polarized and cross-polarized isolation for the maximum reflected signal are 9 dB and 19 dB, respectively.

## CHAPTER 6

### A QUASI-OPTICAL BPSK MODULATOR

#### 6.1 Motivation

To obtain a complete quasi-optical transceiver front end, a quasi-optical modulator is an essential component. Digital phase modulation is a widely used method in today's communication systems [84, 85, 86]. An  $X$ -band quasi-optical transmission-mode phase modulator is presented. The BPSK modulator uses  $p$ - $i$ - $n$  diode loaded grids to obtain digital phase shifts of  $0^\circ$  and  $90^\circ$ . It is suitable for cascading with other quasi-optical components. Three digital modulators can be stacked to form QPSK modulation ( $0^\circ$ ,  $90^\circ$ ,  $180^\circ$  and  $270^\circ$ ).

#### 6.2 Design

The modulator consists of two cascaded grids. Each grid is a printed  $10 \times 10$  array, with a period of one third of the free-space wavelength, and loaded with  $p$ - $i$ - $n$  diodes. Each unit cell of the grid contains two diodes, oppositely oriented with respect to the horizontal bias lines, Figure 6.1. The diodes are connected to vertical lines of different widths, which represent different reactive loading to an incoming

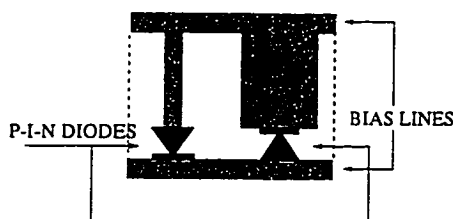


Figure 6.1: Quasi-optical transmission-type BPSK grid modulator.

vertically polarized plane wave. When one of the diodes is forward-biased and the other is reverse-biased, the phase change of the wave transmitted through the grid is much smaller than when the diodes are oppositely biased. Away from resonance, when the transmission loss of a single grid is low, the phase change is also small, so a single grid is not useful for a digital quadrature phase modulator, where  $90^\circ$  phase steps are required. In order to achieve low transmission loss with simultaneous large phase variation between the two states, a cascade of two grids is used. Effectively, this achieves impedance matching to the incoming plane wave. Two grids with unit cells as shown in Figure 6.1 have been fabricated with a period of 10 mm, and were populated with HP HSMP-3892 surface-mount *p-i-n* diodes. A full-wave analysis program MPORT was used for the design [87].

### 6.3 Experiment

An HP8510 network analyzer was used for the grid modulator measurements. The grids were placed in the far field of the transmitting and receiving horn antennas connected to the two ports of the network analyzer. An absorbing sheet was placed around the grid to minimize diffraction. A response calibration was performed without the grid and with the absorbing aperture in place. This sets the reference plane at the surface of the grid.

The phase of the transmission coefficient was measured for the two bias states. The grids exhibit a slightly lower operating frequency than designed, probably due to an underestimated diode package inductance in the model obtained from the manufacturer. This also resulted in relatively high transmission loss of about 5 dB, while the simulations predicted less than 1 dB at 10 GHz. At 9.1 GHz, a  $90^\circ$  relative phase shift was measured with less than 1 dB of relative amplitude change between the two phase states. Three such modulators can be cascaded for QPSK modulation. The bandwidth is shown to be around 5%, as shown in the measured

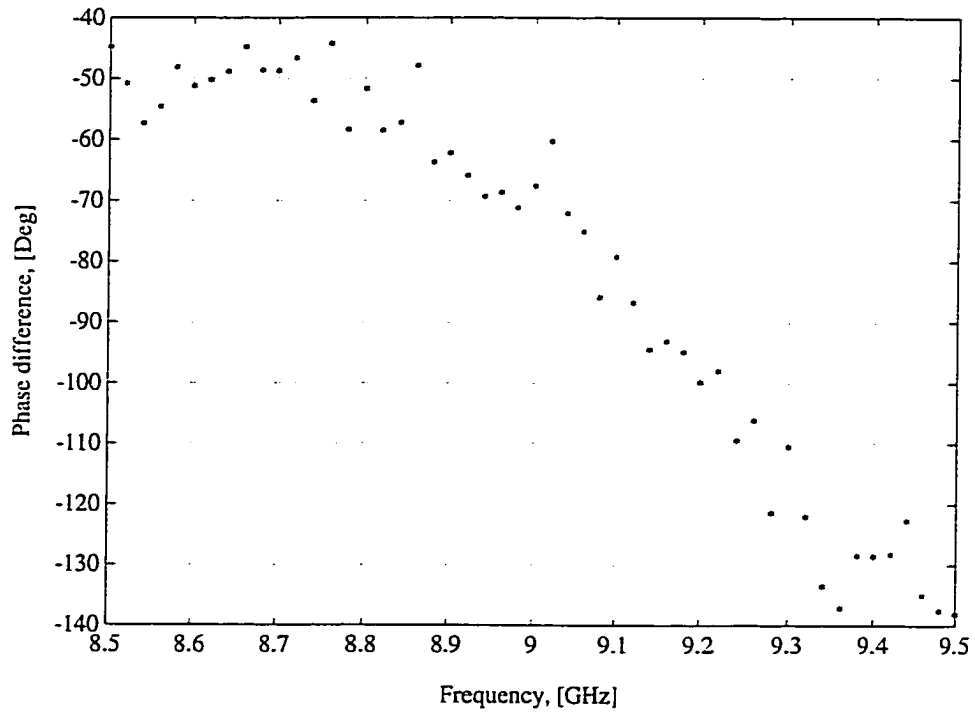


Figure 6.2. Measured phase shift for the BPSK quasi-optical transmission-type grid modulator.

results in Figure 6.2 and 6.3. In conclusion, this cascade of two  $p-i-n$  diode-loaded grids performs  $90^\circ$  electronically variable relative phase shift of a wave in transmission.

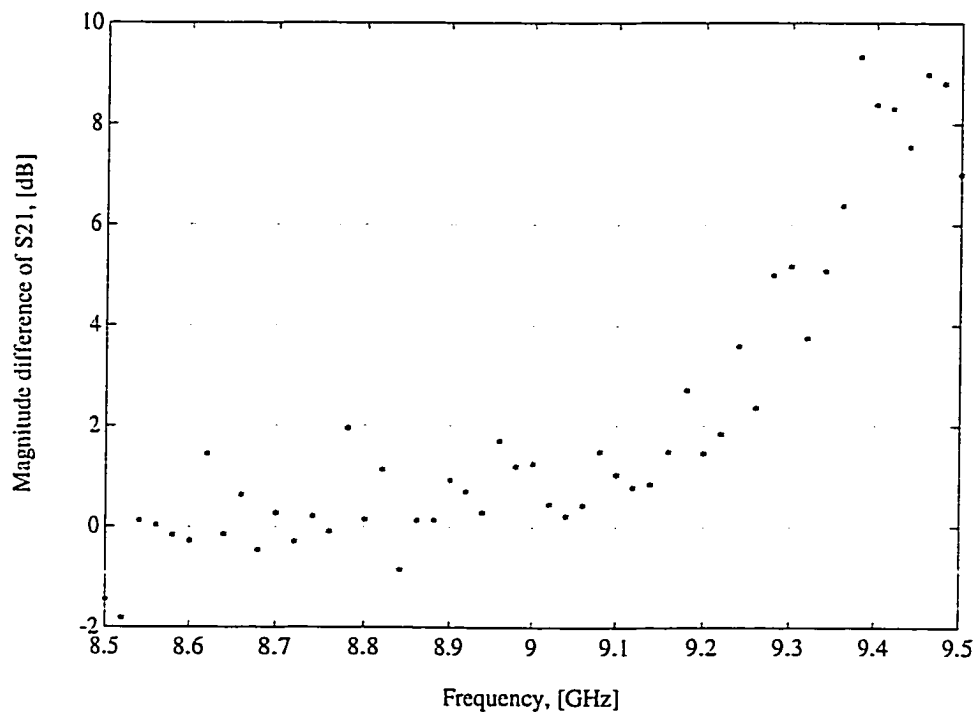


Figure 6.3. Measured relative amplitude for the BPSK quasi-optical transmission-type grid modulator.



## CHAPTER 7

### A QUASI-OPTICAL ANGLE DIVERSITY RECEIVER

By locating several receivers at different locations on the focal surface behind a lens amplifier array, angle diversity reception can be achieved. Signals incident on the lens array from different angles are thus received by different receivers on the focal surface. Signal processing can then be performed on these signals to improve the signal-to-noise ratio of the receiver. This technique can be useful for eliminating multipath fading nulls in wireless communications, since the probability of simultaneous fading at several incident angles is low [88]. As an example, in a Rayleigh channel and a BPSK receiver with an order of diversity equal to  $N$ , the probability of error  $P_e$  for a given average signal-to-noise ratio ( $\overline{SNR}$ ) per channel is given by [89]

$$P_e \approx \left( \frac{1}{4\overline{SNR}} \right)^N \binom{2N-1}{N}, \quad (7.1)$$

assuming a sufficiently large  $\overline{SNR}$  ( $> 10$  dB), and a mutually statistically independent fading of the  $N$  channels. For a level of diversity equal to three, the probability of error decrease as  $P_e \propto \left( \frac{1}{\overline{SNR}} \right)^3$ . For a similar receiver without diversity, the probability of error is  $P_e \propto \left( \frac{1}{\overline{SNR}} \right)$ .

The X-band 24-element lens amplifier array presented in [13] was used for this application. This lens amplifier array was not designed for low-noise and exhibits a noise figure of 3.4 dB. The measured 3-dB beamwidth of this lens is approximately

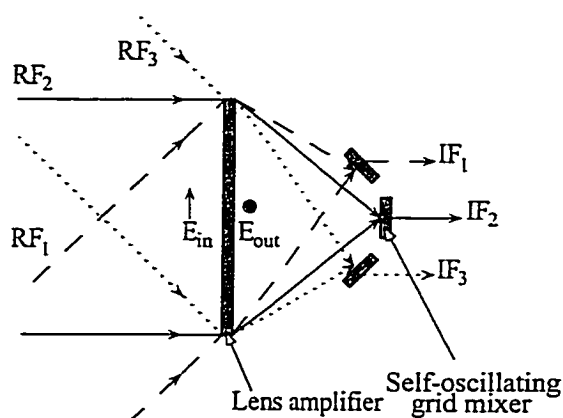


Figure 7.1. A quasi-optical angle diversity receiver. Three self-oscillating grid mixers located on the focal surface behind a lens amplifier array are used to independently receive signals incident from three different angles.

$11^\circ$ , and the side-lobe levels are below 10 dB. The array can be steered to  $30^\circ$  without introducing significant grating lobes. The 10-dB beamwidth is about  $25^\circ$ . By locating receivers at  $-30^\circ$ ,  $0^\circ$  and  $30^\circ$  locations as shown in Figure 7.1, signals are thus received with less than 10 dB interference.

Three  $C$ -band quasi-optical grid oscillators presented in [27] were used as sub-harmonic self-oscillating mixers where the second harmonic is used for the LO. The IF signal can then be detected on the bias-lines of the oscillator. While other mixers could be used for this application, a grid oscillator was used to demonstrate a quasi-optical receiver. A 600 MHz IF signal outside the injection locking bandwidth of the oscillator was used in this application.

The measured IF powers from three different mixers are shown in Figure 7.2 as the incidence angle of the RF signal is varied. Signals incident from the three different angles are isolated by about 10 dB. As expected from the beam-steering measurements, the IF power from each mixer are comparable to the RF powers received at these angles, Figure 7.3. This angle preserving property of a lens amplifier array was also utilized in the multi-user frequency reuse application presented earlier in Chapter 3.

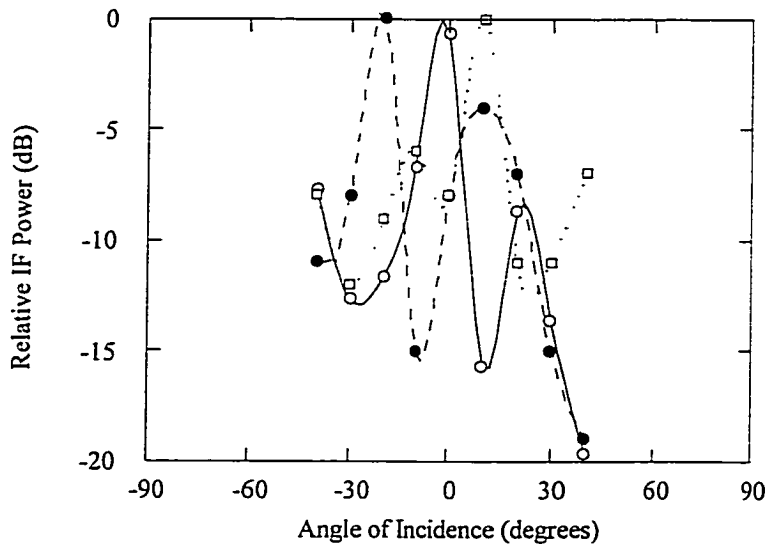


Figure 7.2. Measured IF power levels received by three self-oscillating grid mixers located at  $-30^\circ$ ,  $0^\circ$  and  $30^\circ$  on the focal surface behind a lens amplifier array. The IF frequency is 600 MHz in this application.

While this simple demonstration only used three receivers located on the horizontal focal arch of the lens, more receivers can be located on the focal surface for higher order of diversity. A larger lens with a narrower main beam can be used to increase the number of receiver locations on the focal surface. The lens array can also be designed for lower side-lobe levels to reduce the interference between the incident signals.

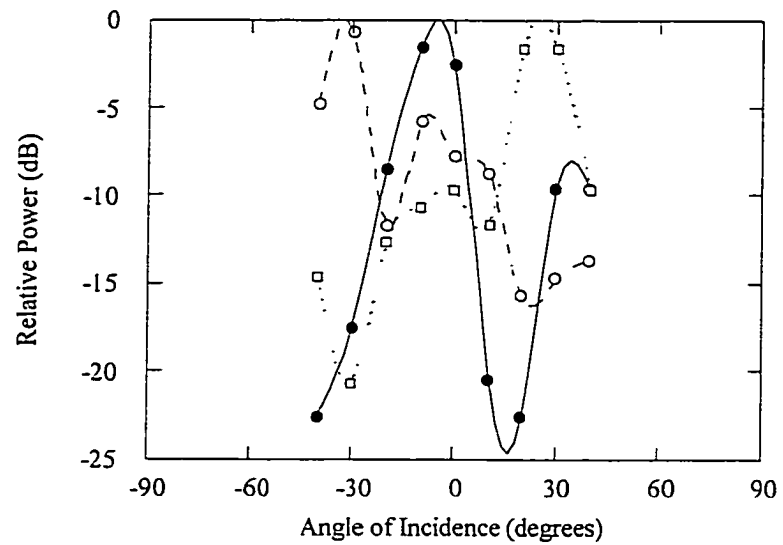


Figure 7.3. Measured RF power levels received by three E-plane horn antennas located at  $-30^\circ$ ,  $0^\circ$  and  $30^\circ$  on the focal surface behind a lens amplifier array.

## CHAPTER 8

### CONCLUSIONS AND FUTURE WORK

#### 8.1 Conclusions

The main goal of this thesis has been to design and demonstrate quasi-optical microwave and millimeter-wave transmit/receive lens amplifier arrays. Several other quasi-optical components for transceiver front-ends are also presented. Initial designs were made at *X*-band to ease fabrication and measurements as well as reduce the cost of devices. The *X*-band T/R module consists of three quasi-optical components: a BPSK modulator; an isolator; and a transmit/receive lens amplifier array. A final transmit/receive lens amplifier design was demonstrated at *Ka*-band.

The feed losses of lens amplifier arrays were investigated in Chapter 2. Several passive lens arrays operating at *X*-band were fabricated and tested to verify the simulations. The design and analysis of lens arrays were also discussed.

Both transmit and receive lens amplifier front-ends have been developed to increase the effective radiated power of a transmitter or to increase the dynamic range of a receiver. However, to form a quasi-optical transceiver, a transmit/receive lens amplifier is a necessary component. A 24-element *X*-band transmit/receive lens amplifier array using *p-i-n* diode SPDT switches to switch between transmit and receive amplifiers is demonstrated in Chapter 3. The antenna gains in transmit and receive mode at 10.2 GHz are 5 dB and 8.5 dB, respectively. The transmit/receive lens amplifier front-end was used to demonstrate several applications: (1) a quasi-optical T/R module; (2) a quasi-optical AM receiver; (3) significant multipath fading

reduction; (4) a multi-user with frequency reuse FSK data link.

Quasi-optical power combining was initially intended for obtaining higher power levels in the millimeter-wave spectrum where the output power from solid-state devices is limited. A transmit/receive lens amplifier array operating at *Ka*-band was developed and tested (Chapter 4) to demonstrate a quasi-optical millimeter-wave transceiver front-end. A hybrid design with MMIC switches and amplifiers in each unit cell was used. The 20-element active lens array can be fed with a folded feed for a compact design. Antenna gains of 7 dB and 2.1 dB are seen in transmit and receive modes at 28.3 GHz. An estimated output power of 0.6 W and an EIRP of 60 W is expected in

The quasi-optical isolator demonstrated in Chapter 5 consists of several cascaded grids loaded with passive elements. It can provide protection against high-level reflected signals as well as circular polarization at the output of a high-power linearly-polarized quasi-optical transmitter. At 8.83 GHz, the co-polarized and cross-polarized isolation for the maximum reflected signal is 9 dB and 19 dB, respectively. The insertion loss and axial ratio of the linear-to-circular polarization converter is 1.1 dB and 2.5 dB at this frequency.

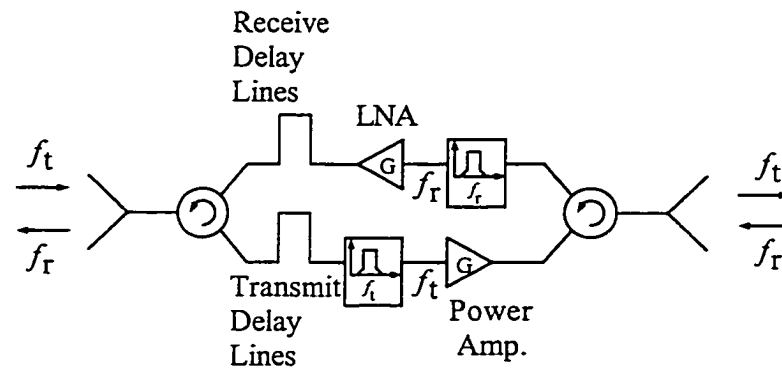
A quasi-optical BPSK modulator consisting of two grids loaded with *p-i-n* diodes was demonstrated with  $0^\circ$  and  $90^\circ$  of digital phase shifts at 9.1 GHz in Chapter 6. The modulator operates in transmission and can be cascaded with a quasi-optical amplifier array.

Finally, in Chapter 7, a simple experiment is presented to demonstrate how a lens amplifier array can be used for angle diversity reception.

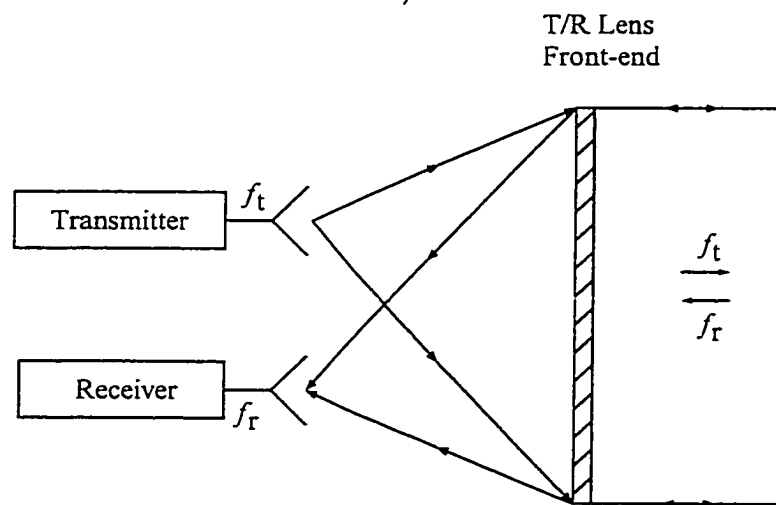
## 8.2 Future work

### 8.2.1 Quasi-optical T/R lens front-ends

Both T/R modules presented in this thesis use SPDT switches with *p-i-n* diodes to electronically switch between transmit and receive operation. To achieve higher switching speeds, optically addressed switches can replace these electronic switches. While the lens amplifiers presented here can be used for TDMA communications or radar systems, many communication systems require full duplex operation. It is therefore of interest to develop a simultaneous bi-directional lens amplifier array without using switches to isolate the amplifiers. To provide isolation between the transmit and receive amplifiers, orthogonal polarization or frequency separation of the transmit and receive signals can be used. In satellite communications, frequency separation of at least 10% is often used for the up and down links. In the Iridium system, the up link is at 29.1-29.3 GHz and the down link is at 19.4-19.6 GHz. By separating the transmit and receive frequencies, bandpass filters (diplexers) can be used to provide isolation. Another possibility is to replace the switches with surface mount circulators presently available at *X*-band. A schematic of a unit cell for a full duplex transmit/receive lens array with frequency separation is shown in Figure 8.1. High isolation of the diplexer is of importance in a communication system not only to protect the receiver, but also to reduce the out-of-band noise at the receiver leaking from the transmitter. Typical isolation needed in cellular systems is between 55 dB for low power levels (hundreds of watts) to 90 dB in kilowatt transmitters. In PCS that uses CDMA, about 55 dB isolation is required for the base-to-mobile frequency of 1.93-1.99 GHz and mobile-to-base of 1.85-1.9 GHz. In TDMA systems such as GSM, switching in time between transmit and receive is used, and there is no need for high isolation diplexers. By including separate delay lines for the transmitted and received signals, the transmitter and receiver can be located at separate locations behind the lens array as indicated in Figure 8.1.



a)



b)

Figure 8.1. a) Schematic of a unit cell for a full duplex transmit/receive lens amplifier array. b) Example of a full duplex transmit/receive lens amplifier front-end.



An interesting quasi-optical diplexer with -75 dB isolation was presented by Ramsay *et al.* [90]. This system is based on the same principle of operation as the isolator presented here. By replacing the absorbing surface with a polarizer, oriented at a 45-degree angle with respect to the optical axis, the incident signals can be refelected to a receiver located orthogonal to and away from the optical axis.

The thermal issues of high-power millimeter-wave arrays must be addressed before a high-power transmitter can be developed. A 3-dB gain reduction due to heat was seen for the *Ka*-band lens array presented in Chapter 4. Several design variables such as choice of substrate material, layout of the circuit, use of external heat sinks and use of high-efficiency amplifiers can reduce the surface temperature of a quasi-optical array.

### 8.2.2 Retrodirective Arrays

In many applications such as ID-tags and tracking systems, a retrodirective array can modulate and return an incoming signal to a transceiver. Existing retrodirective phased arrays use transmission lines to connect each element in the array to the element directly across from the center of the array [91]. For large arrays the number of transmission lines crossing each other become very large and complicated to fabricate. By placing a metallic mirror on the focal surface of a passive lens array, the lens would receive and reflect back incoming signals in the direction of incidence. Modulation of the reflected signals can be done in the array elements, or by placing many active antennas on the focal surface. A simultaneous bi-directional lens amplifier can be used to amplify the reflected signals.

### 8.2.3 High-speed Wireless Data Link

While a single millimeter-wave transmit/receive front-end is presented here, a second array can be fabricated to demonstrate a quasi-optical data-link. To form

a complete quasi-optical transceiver at millimeter-waves, a modulator and isolator similar to the *X*-band versions presented here can be scaled to millimeter-wave frequencies.

#### 8.2.4 Quasi-optical Angle Diversity Receiver

While a simple angle diversity receiver using a lens amplifier array was demonstrated in Chapter 7, it remains to investigate the optimum detector locations and lens design for this application. A theoretical description as well as an experimental verification of this receiver system in a multipath environment is presently investigated at the University of Colorado [92].

## BIBLIOGRAPHY

- [1] S. J. Gizinski III and J. C. Cardos, "High data rate wireless communications," *Microwave J.*, vol. 39, pp. 102-122, Oct. 1996.
- [2] D. Kraus, **Radio Astronomy**. McGraw-Hill, 1966.
- [3] Y. Takimoto and M. Kotaki, "Recent development of mm-wave applications in japan," *Microwave J.*, vol. 39, pp. 214-226, May 1996.
- [4] E. A. Ulbrich Jr. and D. Bryden, "A mm-wave, wireless local area network for use inside an aircraft," *Microwave J.*, vol. 40, pp. 172-175, Sept. 1997.
- [5] M. Russell, A. Crain, A. Curran, R. Campbell, C. Drubin, and W. Miccioli, "Millimeter-wave radar sensor for automotive intelligent cruise control (ICC)," *IEEE Trans. Microwave Theory Tech.*, vol. 45, pp. 2444-2453, Dec. 1997.
- [6] G. Kantorowicz and P. Palluel, "Backward wave oscillators," in *Infrared and Millimeter Waves*, vol. 1, ch. 4, New York: Academic Press, 1979.
- [7] Bierman, "Microwave tube design efforts yield steady performance improvements," *Microwave J.*, vol. 31, pp. 52-73, June 1988.
- [8] H. Hieslmair and Others, "State of the art of solid-state and tube transmitters," *Microwave J.*, vol. 26, pp. 46-48, Oct. 1983.
- [9] W. Hansen, "US TWTs from 1 to 100 GHz," **State of the Art Reference Supplement to Microwave J.**, vol. 32, pp. 179-193, Sept. 1989.

- [10] K. J. Slegler, R. H. Abrams, and R. K. Parker, "Trends in solid-state microwave and millimeter-wave technology," **IEEE MMT-S Newsletter**, pp. 11-15, Fall 1990.
  
- [11] Y. C. Shih and H. J. Kuno, "Solid-state sources from 1 to 100 GHz," **State of the Art Reference Supplement to Microwave J.**, vol. 32, pp. 145-161, Sept. 1989.
  
- [12] C. A. Liechti, "High-speed transistors: Directions for the 1990s," **State of the Art Reference Supplement to Microwave J.**, vol. 32, pp. 165-177, Sept. 1989.
  
- [13] J. S. H. Schoenberg, **Quasi-Optical Constrained Lens Amplifiers**. PhD thesis, Univ. of Colorado, Boulder, CO, 1995.
  
- [14] R. A. York and Z. B. Popović, **Active and quasi-optical arrays for solid-state power combining**. New York: John Wiley & Sons, Inc., 1997.
  
- [15] K. J. Russel, "Microwave power combining techniques," **IEEE Trans. Microwave Theory Tech.**, vol. 27, pp. 472-478, May 1979.
  
- [16] J. A. Navarro and K. Chang, **Integrated Active Antennas and Spatial Power Combining**. New York: John Wiley & Sons, Inc., 1996.
  
- [17] D. Staiman, M. E. Breese, and W. T. Patton, "New technique for combining solid-state sources," **IEEE J. Solid-State Circuits**, vol. SC-3, pp. 238-243, Sept. 1968.
  
- [18] M. F. Durkin *et al.*, "35 GHz active aperture," **IEEE MTT-S Int. Microwave Symp. Dig.**, pp. 425-427, Jun. 1981.
  
- [19] J. W. Mink, "Quasi-optical power combining of solid-state millimeter-wave sources," **IEEE Trans. Microwave Theory Tech.**, vol. MTT-34, pp. 273-279, Feb. 1986.

- [20] J. Birkeland and T. Itoh, "FET-based planar circuits for quasi-optical sources and transceivers," **IEEE Trans. Microwave Theory Tech.**, vol. 37, pp. 1452–1459, Sept. 1989.
- [21] S. T. Chew and T. Itoh, "A  $2 \times 2$  beam-switching active antenna array," **IEEE MTT-S Int. Microwave Symp. Dig.**, pp. 925–928, June 1995.
- [22] R. Flynt, L. Fan, J. Navarro, and K. Chang, "Low cost and compact active integrated antenna transceiver for system applications," **IEEE MTT-S Int. Microwave Symp. Dig.**, pp. 953–956, Jun. 1995.
- [23] M. J. Cryan, P. Hall, S. H. Tsang, and J. Sha, "Integrated active antenna with full duplex operation," **IEEE Trans. Microwave Theory Tech.**, vol. 45, pp. 1742–1748, Oct. 1997.
- [24] A. Mehrotra, **Cellular Radio Performance Engineering**, pp. 177–235. Artech House, 1994.
- [25] H. H. Meinel, "Automotive radars," **Workshop: 1997 IEEE / MTT-S Int. Microwave Symp.**, June 1997.
- [26] R. M. Weikle II, M. Kim, J. B. Hacker, M. P. DeLisio, Z. B. Popović, and D. B. Rutledge, "Transistor oscillator and amplifier grids," **Proc. IEEE**, vol. 80, pp. 1800–1809, Nov. 1992.
- [27] W. A. Shiroma, **Cascaded Active and Passive Grids for Quasi-Optical Front Ends**. PhD thesis, Univ. of Colorado, Boulder, CO, 1996.
- [28] R. A. York, "Quasi-optical power-combining techniques," in **Millimeter and Microwave Engineering for Communications and Radar** (J. C. Wiltse, ed.), vol. CR54 of **Critical Reviews of Optical Science and Technology**, pp. 63–97, Bellingham, Washington: SPIE Optical Engineering Press, 1994.
- [29] M. Kim, J. J. Rosenberg, R. Smith, R. M. Weikle II, J. B. Hacker, M. De Lisio, and D. B. Rutledge, "A grid amplifier," **IEEE Microwave and Guided Wave Let.**, vol. 1, pp. 322–324, Nov. 1991.

- [30] M. Kim, E. A. Sovero, J. B. Hacker, M. P. De Lisio, J. C. Chiao, S. J. Li, D. R. Gagnon, J. J. Rosenberg, and D. B. Rutledge, "A 100-element HBT grid amplifier," *IEEE Trans. Microwave Theory Tech.*, vol. 41, pp. 1762–1771, Oct. 1993.
- [31] N. Sheth, T. Ivanov, A. Balasubramaniyan, and A. Mortazawi, "A nine HEMT spatial amplifier," *IEEE MTT-S Int. Microwave Symp. Dig.*, vol. 2, pp. 1239–1242, Jun. 1994.
- [32] J. Schoenberg, T. Mader, B. Shaw, and Z. B. Popović, "Quasi-optical antenna array amplifiers," *IEEE MTT-S Int. Microwave Symp. Dig.*, vol. 2, pp. 605–608, Jun. 1995.
- [33] J. Hubert, J. Schoenberg, and Z. B. Popović, "High-power hybrid quasi-optical  $K\alpha$ -band amplifier design," *IEEE MTT-S Int. Microwave Symp. Dig.*, vol. 2, pp. 585–588, May 1995.
- [34] T. B. Mader, **Quasi-Optical Class-E Power Amplifiers**. PhD thesis, Univ. of Colorado, Boulder, CO, 1995.
- [35] J. Schoenberg, S. C. Bundy, and Z. B. Popović, "Two-level power combining using a lens amplifier," *IEEE Trans. Microwave Theory Tech.*, vol. 42, pp. 2480–2485, Dec. 1994.
- [36] M. Marković, **Quasi-Optical Modulators and Broadband High-Efficiency Amplifiers**. PhD thesis, Univ. of Colorado, Boulder, CO, 1997.
- [37] J. Dixon, G. O'Dell, J. Schoenberg, S. Duncan, and Z. Popović, "60 GHz monolithic active antenna array," in *1997 IEEE Int. Antennas and Prop. Symp. Digest*, vol. 1, (Montreal, Canada), pp. 38–41, July 1997.
- [38] M. P. DeLisio, S. W. Duncan, D.-W. Tu, S. Weinreb, C.-M. Liu, and D. B. Rutledge, "A 44–60 GHz monolithic pHEMT grid amplifier," *IEEE MTT-S Int. Microwave Symp. Dig.*, vol. 2, pp. 1127–1130, June 1996.

- [39] E. A. Sovero, Y. Kwon, D. S. Deakin, A. L. Sailer, and J. A. Higgins, "A PHEMT based monolithic plane wave amplifier for 42 GHz," **IEEE MTT-S Int. Microwave Symp. Dig.**, vol. 2, pp. 1111–1114, June 1996.
- [40] A. Alexanian, H.-S. Tsai, and R. A. York, "Quasi-optical traveling wave amplifiers," **IEEE MTT-S Int. Microwave Symp. Dig.**, vol. 2, pp. 1115–1118, June 1996.
- [41] J. Schoenberg, T. Mader, B. Shaw, and Z. B. Popović, "Quasi-optical antenna array amplifiers," in **1995 IEEE MTT-S Int. Microwave Symp. Dig.**, (Orlando, FL), pp. 605–608, May 1995.
- [42] A. R. Perkons and T. Itoh, "TE surface wave power combining by a planar 10-element active lens amplifier," **IEEE MTT-S Int. Microwave Symp. Dig.**, vol. 2, pp. 691–694, Jun. 1997.
- [43] S. Ortiz, T. Ivanov, and A. Mortazawi, "A transmit-receive spatial amplifier array," **IEEE MTT-S Int. Microwave Symp. Dig.**, vol. 2, pp. 679–682, Jun. 1997.
- [44] S. Hollung, A. E. Cox, and Z. B. Popović, "A quasi-optical bi-directional lens amplifier," **IEEE Trans. Microwave Theory Tech.**, vol. 47, pp. 2352–2357, Dec. 1997.
- [45] M. Marković, S. Hollung, and Z. B. Popović, "Quasi-optical phase modulators," in **1996 IEEE MTT-S Int. Microwave Symp. Dig.**, (San Francisco, CA), pp. 1247–1250, June 1996.
- [46] S. Hollung, W. Shiroma, M. Marković, and Z. B. Popović, "A quasi-optical isolator," **IEEE Microwave and Guided Wave Let.**, vol. 6, pp. 205–206, May 1996.
- [47] V. D. Hwang and T. Itoh, "Quasi-optical HEMT and MESFET self-oscillating mixers," **IEEE Trans. Microwave Theory Tech.**, vol. 36, pp. 1701–1705, Dec. 1988.

- [48] J. B. Hacker, R. M. Weikle II, M. Kim, M. De Lisio, and D. B. Rutledge, "A 100-element planar schottky diode grid mixer," **IEEE Trans. Microwave Theory Tech.**, vol. 40, pp. 557-562, Mar. 1992.
- [49] W. A. Shiroma, E. W. Bryerton, S. Hollung, and Z. B. Popović, "A quasi-optical receiver with angle diversity," in **1996 IEEE MTT-S Int. Microwave Symp. Dig.**, (San Francisco, CA), pp. 1131-1134, June 1996.
- [50] J. B. Hacker and R. M. Weikle II, **Quasi-optical grid arrays**, pp. 249-324. New York: Wiley, 1995.
- [51] A. A. M. Saleh, "An adjustable quasi-optical bandpass filter - part i: theory and design formulas," **IEEE Trans. Microwave Theory Tech.**, vol. 22, pp. 728-739, Jul. 1974.
- [52] H.-X. Liu, L. B. Sjogren, C. W. Domier, N. C. Luhmann Jr., D. L. Sivco, and A. Y. Cho, "Monolithic quasi-optical frequency tripler array with 5-W output power at 99 GHz," **IEEE Electron. Device Lett.**, vol. 14, pp. 329-331, July 1993.
- [53] C. F. Jou, W. W. Lam, H. Z. Chen, K. S. Stolt, N. C. Luhmann Jr., and D. B. Rutledge, "Millimeter-wave diode-grid frequency doubler," **IEEE Trans. Microwave Theory Tech.**, vol. 36, pp. 1507-1514, Nov. 1988.
- [54] A. Moussessian, M. C. Wanke, Y. Li, J.-C. Chiao, F. A. Hegmann, S. J. Allen, T. W. Crowe, and D. B. Rutledge, "A terahertz grid frequency doubler," **IEEE MTT-S Int. Microwave Symp. Dig.**, vol. 2, pp. 683-686, Jun. 1997.
- [55] K. D. Stephan, F. H. Spooner, and P. F. Goldsmith, "Quasi-optical millimeter-wave hybrid and monolithic PIN-diode switches," **IEEE Trans. Microwave Theory Tech.**, vol. 41, pp. 1791-1798, Oct. 1993.
- [56] K. D. Stephan and P. F. Goldsmith, "W-band quasioptical integrated PIN diode switch," in **1992 IEEE MTT-S Int. Microwave Symp. Dig.**, (Albuquerque, NM), pp. 591-594, 1992.



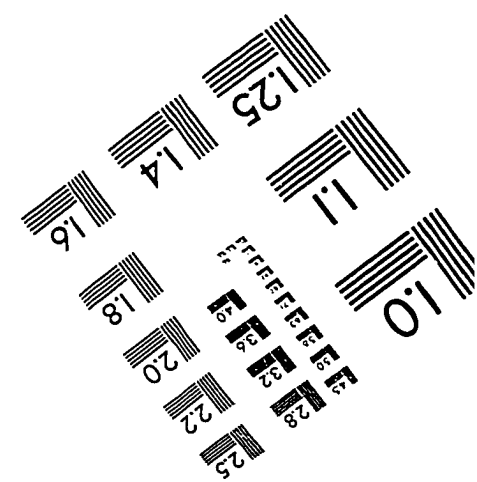
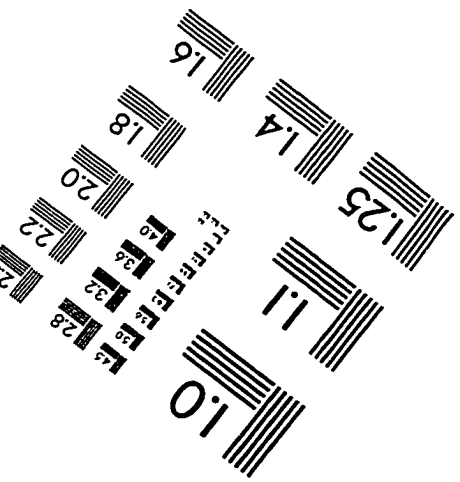
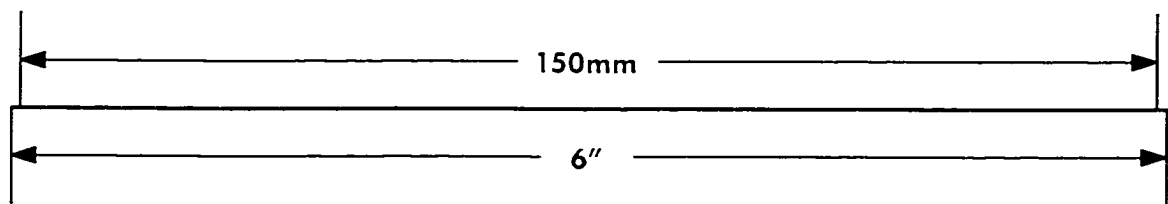
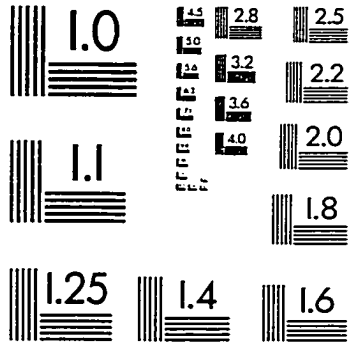
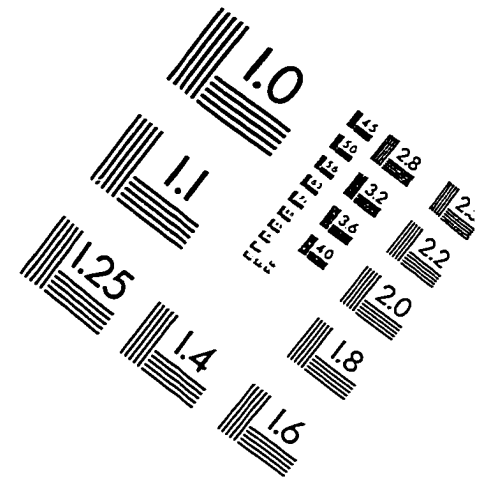
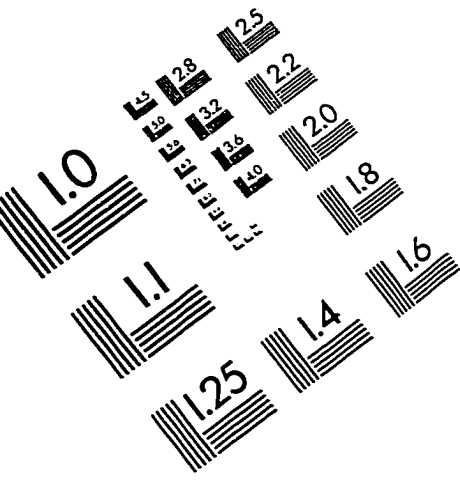
- [57] W. W. Lam, C. F. Jou, H. Z. Chen, K. S. Stolt, N. C. Luhmann Jr., and D. B. Rutledge, "Millimeter-wave diode-grid phase shifter," **IEEE Trans. Microwave Theory Tech.**, vol. 36, pp. 902-907, May 1988.
- [58] P. Lefleur, D. J. Roscoe, and M. Cuhaci, "A 20 GHz active integrated multilayer microstrip patch array for portable communication terminals," in **1997 IEEE Int. Antennas and Prop. Symp. Digest**, vol. 2, (Montreal, Canada), pp. 1260-1263, July 1997.
- [59] S. Kingsley and S. Quegan, **Understanding Radar Systems**, ch. 15. London: McGraw-Hill, 1992.
- [60] D. M. Pozar, **Microwave Engineering**, ch. 12.3, p. 681. New York: Addison-Wesley Publishing Comp., Inc., 1990.
- [61] T. Berg, "High-gain quasi-optical lens amplifier array," Master's thesis, Univ. of Colorado, Boulder, CO, 1997.
- [62] R. E. Collin, **Antennas and Radiowave Propagation**. New York: McGraw-Hill, 1985.
- [63] S. Cornbleet, **Microwave and geometrical optics**, ch. 3. New York: Academic Press, 1994.
- [64] H. Gent, "The bootlace aerial," **Royal Radar Establishment Journal**, pp. 47-57, Oct. 1957.
- [65] W. Rotman and R. Turner, "Wide angle microwave lens for line source applications," **IEEE Trans. Ant. and Prop.**, vol. AP-11, pp. 623-632, Nov. 1963.
- [66] J. Browne, "Rotman lens offers alternative to millimeter-wave antenna technologies," **Microwaves & RF**, vol. 35, p. 23, Dec. 1996.

- [67] J. B. L. Rao, "Multifocal three-dimensional bootlace lenses," **IEEE Trans. Ant. and Prop.**, vol. AP-30, pp. 1050–1056, Nov. 1982.
- [68] C. M. Rappaport and A. I. Zaghloul, "Optimized three-dimensional lenses for wide-angle scanning," **IEEE Trans. Ant. and Prop.**, vol. AP-33, pp. 1227–1236, Nov. 1985.
- [69] D. T. McGrath, "Planar three-dimensional constrained lenses," **IEEE Trans. Ant. and Prop.**, vol. 34, pp. 46–50, Jan. 1986.
- [70] D. C. O'Shea, **Elements of modern optical design**, ch. 7. New York: John Wiley & Sons, Inc., 1985.
- [71] C. A. Balanis, **Antenna Theory**, ch. 13, pp. 707–712. New York: Wiley, 1997.
- [72] T. Ivanov and A. Mortazawi, "Two stage double layer microstrip spatial amplifiers," **IEEE Trans. Microwave Theory Tech.**, vol. 2, pp. 589–592, June 1995.
- [73] H. S. Tsai, M. J. Rodwell, and R. A. York, "Planar amplifier array with improved bandwidth using folded-slots," **IEEE Microwave and Guided Wave Let.**, vol. 4, pp. 112–114, Apr. 1994.
- [74] P. Bhartia, K. V. S. Rao, and R. S. Tomar, **Millimeter-wave microstrip and printed circuit antennas**, ch. 3, p. 51. Boston: Artech House, 1991.
- [75] T. B. Mader, M. Marković, E. Bryerton, M. Forman, and Z. B. Popović, "Analysis and design of class-E microwave power amplifiers," **submitted to IEEE Trans. Microwave Theory Tech.**, Jan. 1996.
- [76] J. Hubert, "High-power quasi-optical *Ka*-band amplifier arrays," **Int. Conf. on Infrared and Millimeter Waves**, pp. 145–146, Dec. 1995.

- [77] N. J. Koliás and R. C. Compton, "Thermal management for high-power active amplifier arrays," *IEEE Trans. Microwave Theory Tech.*, vol. 44, pp. 963–966, June 1995.
- [78] M. A. Gouker, "Toward standard figures-of-merit for spatial and quasi-optical power-combined arrays," *IEEE Trans. Microwave Theory Tech.*, vol. 43, pp. 1614–1617, July 1995.
- [79] W. C. Y. Lee, *Mobile communications design fundamentals*, ch. 3. New York: John Wiley & Sons, Inc., 1993.
- [80] K. C. Gupta, "CAD of active microstrip antennas and microstrip arrays," *1995 Asia-Pacific Microwave Conference Proceedings*, pp. 891–895, Dec. 1994.
- [81] E. Ongareau, A. Roussaud, E. Marouby, and J.-R. Levrel, "Radar cross-section reduction by polarization rotation," *Microwave and Opt. Technol. Lett.*, vol. 8, pp. 316–318, Apr. 1995.
- [82] N. Nakajima and R. Watanabe, "A quasioptical circuit technology for shortmillimeter wavelength multiplexers," *IEEE Trans. Microwave Theory Tech.*, vol. MTT-29, pp. 897–905, Sep. 1981.
- [83] W. A. Shiroma, S. C. Bundy, S. Hollung, B. D. Bauernfeind, and Z. B. Popović, "Cascaded active and passive quasi-optical grids," *IEEE Trans. Microwave Theory Tech.*, vol. 43, pp. 2904–2909, Dec. 1995.
- [84] Z. B. Popović, J. S. H. Schoenberg, T. Mader, W. A. Shiroma, S. Hollung, M. Marković, J. Dixon, and S. C. Bundy, "Quasi-optical components and subsystems for communications," *1995 Conf. Proc. of the Int. Symp. on Signals, Systems and Electronics*, pp. 93–98, Oct. 1995.
- [85] M. J. Vaughan, W. Wright, and R. C. Compton, "Active antenna elements for millimeter-wave cellular communications," *1995 Conf. Proc. of the Int. Symp. on Signals, Systems and Electronics*, pp. 9–12, Oct. 1995.

- [86] C. W. Pobanz, J. Lin, and T. Itoh, "Active integrated antennas for microwave wireless systems," **1995 Conf. Proc. of the Int. Symp. on Signals, Systems and Electronics**, pp. 1-4, Oct. 1995.
- [87] S. C. Bundy and Z. B. Popović, "A generalized analysis for grid oscillator design," **IEEE Trans. Microwave Theory Tech.**, vol. 42, pp. 2486-2491, Dec. 1994.
- [88] W. C. Jakes, **Microwave Mobile Communications**, p. 311. New York: John Wiley, 1974.
- [89] J. G. Proakis, **Digital Communications**, ch. 7, pp. 473-474. New York: McGraw-Hill, 1983.
- [90] J. F. Ramsay and W. F. Gunn, "A polarized mirror duplexer for use with a circularly polarized lens aerial," **Marconi Review**, vol. 18, pp. 29-36, 1955.
- [91] L. C. Van Atta, "Electromagnetic reflector." U.S. Patent # 2 908 002, Oct. 1959.
- [92] J. Vian. personal communication.

# IMAGE EVALUATION TEST TARGET (QA-3)



APPLIED IMAGE, Inc  
1653 East Main Street  
Rochester, NY 14609 USA  
Phone: 716/482-0300  
Fax: 716/288-5989

© 1993, Applied Image, Inc., All Rights Reserved